



**Hydraulics Research**  
Wallingford

---

# The Hydrodynamics of the Carousel

---

P Besley, BSc  
E A Delo, BSc, PhD, CEng, MICE, MIWEM

Report SR 239  
January 1990

**Published by**  
Hydraulics Research Limited  
Wallingford, Oxfordshire OX10 8BA. United Kingdom.  
Telephone: 0491 35381. Telex: 848552. FAX: 0491 32233

---

## ***Contract***

---

This report describes work funded by the Department of the Environment and Hydraulic Research Limited under Research contract PECD 7/6/110 for which the DoE nominated officer was Dr R P Thorogood. It is published on behalf of the Department of the Environment, but any opinions expressed are not necessarily those of the Department of the Environment. The report was compiled by Mr P Besley, under the supervision of Dr E A Delo in the Tidal Engineering Department of Hydraulics Research, Wallingford under the management of Mr M F C Thorn.

© Crown Copyright 1990

Published by the permission of the Controller of Her Majesty's Stationery Office.

---

## **Abstract**

---

A research programme has been undertaken by Hydraulics Research in conjunction with Polytechnic South West (PSW) to measure and predict the hydrodynamics of the HR Carousel flume. The project was funded jointly by the Science and Engineering Research Council, Hydraulics Research Limited and the Department of the Environment.

The aim of the work described in this report was (i) to measure the hydrodynamics of the Carousel, (ii) to apply the HARWELL-FLOW3D mathematical model to the flow in the Carousel, and (iii) to compare shear stress results derived from the Carousel and the mathematical model.

This successful study has increased the breadth and depth of knowledge of the hydrodynamics of the Carousel which has improved the reputation of the Carousel as a major and unique UK research facility. The study has enabled the Carousel to be more widely used for engineering research on cohesive sediments both by Hydraulics Research and by other UK research institutions.

The accuracy and scope of the engineering tests on cohesive sediment samples from sites around the world which are carried out by Hydraulics Research in the Carousel have been improved by the results of this study. The ability to predict the movement of cohesive sediment within coastal, estuarine or inland waters has a significant economical and ecological importance in the development of new engineering works and the maintenance of existing installations. The future viability of a proposed new port, for example, could largely depend on the cost of routine dredging necessary to sustain its accessibility to shipping. Many other schemes, such as the reclamation of intertidal flats, or the construction of flood protection structures or the laying of outfalls, also require a sound engineering appraisal of the likely changes in the patterns of sediment movement which will result after the scheme is built. Furthermore, the capability to predict the movement of cohesive sediment is crucial in the understanding of the distribution of certain pollutants, in particular heavy metals which are adsorbed on to clay and silt particles.

As yet, it is not possible to predict the behaviour of a cohesive sediment from its physical and chemical properties alone and the principal thrust of research has been to determine in the laboratory, for a given set of flow conditions, the behaviour of a sample of the cohesive sediment taken from the field.

The Carousel flume is an annular flume, with an outer diameter of 6m, a channel width of 0.4m and depth of 0.35m, and has a detachable roof 0.09m thick. The flume stands approximately 1.1m off the ground, supported by 12 brick pillars. The channel and the roof are constructed of fibre glass, with a 0.12m long perspex section in the channel for viewing. The roof fits into the channel, and floats on the fluid. Fluid motion in the Carousel flume is induced and continued by the drag between the roof and the fluid surface as the roof rotates.

Experiments were undertaken to measure all three velocity components (circumferential, vertical and radial) of the flow within the Carousel. PSW has applied the HARWELL-FLOW3D package to numerically model the turbulent flow of clean water in the Carousel. This data was compared with velocity

measurements within the flume and found to give good agreement for the primary flow field.

A new method of measuring bed shear stress in the Carousel was deployed using flush mounted hot wire anemometry probes. All stress measurements were made in clean water. The data retrieved by the shear stress probes was compared with shear stress data from the HARWELL-FLOW3D model and the correlation was found to be good.

The measured and predicted shear stress data was also compared with the depths of erosion across the width of the Carousel flume for a number of muds previously tested by Hydraulics Research. This indicated that the depths of erosion of the cohesive sediments closely reflected the applied bed shear stress within the Carousel.

The shear stress probes have not yet been used with cohesive sediment suspensions as they would be very susceptible to surface damage without a secondary polymer coating.

---

# Contents

---

	Page
<b>1. Introduction</b> .....	1
1.1 Scope of project .....	1
1.2 Description of erosion flume / operation and instrumentation .....	1
<b>2. Measured velocities</b> .....	3
2.1 Summary of 1984 findings .....	3
2.1.1 Work description .....	3
2.1.2 Velocity flow fields .....	3
2.1.3 Interpretation .....	3
2.2 Velocity measurements 1988 .....	4
2.2.1 Experimental arrangement .....	4
2.3 Discussion .....	4
<b>3. Velocity measurements predicted by the HARWELL-FLOW3D model</b> .....	6
3.1 Introduction .....	6
3.1.1 Mixing length hypothesis (MLH) .....	6
3.1.2 k- $\epsilon$ model .....	6
3.2 Results .....	7
<b>4. Bed shear stress measurements within the carousel</b> .....	7
4.1 Introduction .....	7
4.2 Description of shear stress probes and results .....	8
4.2.1 Description of equipment .....	8
4.2.2 Calibration .....	8
4.2.3 Scope of tests .....	9
4.2.4 Results .....	9
4.3 Near bed velocities .....	9
4.3.1 Experimental procedure .....	9
4.3.2 Results .....	10
4.4 Eroded mud profiles .....	11
4.4.1 Bed preparation .....	11
4.4.2 Test procedure .....	11
4.4.3 Bed profiles during each run .....	12
4.4.4 Mud profile\shear strength relationship .....	12

---

## Contents continued

---

	Page
<b>5. Predicted shear stress measurement</b> .....	13
5.1 PSW HARWELL-FLOW3D model .....	13
5.2 Results .....	13
5.2.1 Bed shear stress .....	13
5.2.2 Orientation of peak shear stress .....	14
5.2.3 Side wall shear-stress .....	14
<b>6. Conclusions</b> .....	15
<b>7. Acknowledgements</b> .....	15
<b>8. References</b> .....	16

### Tables

1. Relative magnitude of the velocity component ratio's
2. Measured bed shear stress values for a flow depth of 50m
3. Measured bed shear stress values for a flow depth of 100m
4. Measured bed shear stress values for a flow depth of 200m
5. Summary of near bed velocity data
6. Bed shear stress data calculated from the logarithmic parts of the velocity profiles
7. Summary of PSW numerically calculated bed shear stress results
8. Orientation and magnitude of bed shear stresses
9. A comparison of numerical and measured side wall shear stress data

### Figures

1. The carousel
2. Energy input calibration
3. Roof speed calibration
4. Filling and emptying system
5. The laser velocity meter
6. Cross-sectional velocity contours (adapted from SR33)
7. Generalised velocity contours and suggested route of secondary flow (adapted from SR33)
8. Roof speed versus cross sectional mean velocity
9. Velocity variation across the width
10. Plot showing horizontal velocity isovels for two roof rotation rates and a fluid depth of 0.1m.
11. Plot showing typical vertical velocity isovels for roof rotation rate indicated and a fluid depth of 0.1m.
12. Plot showing typical radial velocity isovels for roof rotation rates indicated and a fluid depth of 0.1m.
13. Flume cross sections showing typical vertical/radial velocity vector diagrams for a fluid depth of 0.1m and roof rotation rates indicated.
14. Typical PSW isovel pattern
15. Typical shear stress probe calibration curve.
16. Graph showing near bed velocity profiles for three cross-flume positions for varying lid rotation rates.

---

## **Contents continued**

---

### **Figures continued**

17. A comparison of shear stress measured by the probes and derived from near bed velocity profiles.
18. Bed shear stress values versus roof speed for three cross-flume positions. Stress values derived from laser velocity profiles.
19. Average bed shear stress values against roof speed.
- 20a. Graph showing typical erosion profiles across the flume for a number of lid rotation rates indicated.
- 20b. Graphs showing the relationship between depth of erosion and bed shear stresses predicted by the PSW numerical model.
21. A composite plot summarizing PSW bed shear stress results.
22. A sequence of graphs comparing carousel bed shear-stress data with PSW mathematical model results for a fluid depth of 0.1m and a number of roof rotation rates indicated.
23. Two graphs comparing carousel bed shear-stress data with PSW mathematical model results for a fluid depth of 0.05m and a number of roof rotation rates indicated.
24. Two graphs comparing carousel bed shear-stress data with PSW mathematical model results for a fluid depth of 0.2m and a number of roof rotation rates indicated.
25. Composite plot showing the magnitude and direction of the bed shear stress. Probe positions and carousel roof rotation rates are indicated.
26. Composite plots comparing laboratory with predicted numerical data for the direction and magnitude of the bed shear stress. Probe positions and roof rotation rates are indicated.
27. Graph comparing carousel side-wall shear-stress with PSW mathematical model for 0.1m fluid depth and probe heights indicated.
28. Graph comparing carousel side-wall shear-stress with PSW mathematical model for 0.02m probe height and fluid depth indicated.

### **Appendix**

1. Tables showing 1988 velocity results.



---

## **1. Introduction**

---

### **1.1 Scope of project**

This report describes part of a strategic research study undertaken by Hydraulics Research and Polytechnic South West (PSW). The project was funded jointly by the Science and Engineering Research Council, Hydraulics Research Limited and the Department of the Environment. The aim of the study was (i) to describe the hydrodynamics of the carousel, (ii) to compare shear stress results derived from the carousel and the mathematical model, (iii) to investigate the response of a cohesive sediment to fluid shear.

A new method of measuring shear stress has been developed which took the form of flush mounted hot wire anemometry probes. The shear stress data was supplemented with horizontal (circumferential), vertical and radial velocity measurements. All velocity and stress measurements were made in pure water. This data was also related to mud erosion rates within the carousel for a number of mud types. During the mud erosion experiments, velocity measurements could not be made due to cloud suspensions within the flume. To date the shear stress probes have not been used in mud experiments as they are very susceptible to damage. However, work is being carried out at PSW to determine the influence of a polymer coating on the "bare" probes. If successful, then the problem of damage due to the presence of mud may be overcome.

### **1.2 Description of erosion flume, operation and instrumentation**

The carousel flume (Fig 1) is an annular flume, with an outer diameter of 6m, a channel width of 0.4m and depth of 0.35m, and has a detachable roof 0.09m thick. The flume stands approximately 1.1m off the ground, supported by 12 brick pillars. The channel and the roof are constructed of fibre glass, with a 0.12m long perspex section in the channel for viewing. The roof fits into the channel, and floats on the fluid. Fluid motion in the carousel flume is induced and continued by the drag between the roof and the fluid surface as the roof rotates.

The driving mechanism for the roof consists of a DC torque motor with a drive wheel, which turns a horizontal plate around the central spindle. The drive arm is attached to this horizontal plate at one end and to the roof at the other end.

A strain gauge is used to measure the force applied to the roof of the carousel flume as it rotates. It consists of a spring and displacement transducer arrangement attached to the driving arm at the point of contact with the roof. The magnitude of the applied force is determined by the displacement transducer deflection, which is displayed on a chart recorder. The strain gauge is calibrated by applying known forces via a pulley system. Mean strain gauge readings were converted to applied force using a best fit calibration line and the results related to the roof rotation rate (see Fig 2).

The speed of the motor, and hence roof speed, is controlled by a micro computer. The motor speed can be set to an accuracy of 0.1% of the

maximum speed. A tachometer voltage was recorded for various motor speed control settings. The relationship between the two was found to be linear. A relationship was also obtained between the motor speed and the roof speed, by recording the number of revolutions per minute the roof made at various motor speed settings. The relationship obtained (see Fig 3) demonstrates a slight non-linearity of the control system. Figure 4 shows schematically the filling and emptying processes involved with the carousel.

Flow velocity components were measured using a Laser anemometry technique (see Fig 5) in pure water. The measurements were very accurate ( $\pm 1 \text{ mms}^{-2}$ ) and can be made at any point in the cross-section of the flume, through the perspex viewing section. The equipment comprises three parts:-

- (a) Laser optical unit.
- (b) Photomultiplier optical unit.
- (c) Electronic units.

The laser velocity meter operates by emitting two convergent beams in the same horizontal plane. The two beams intersect at some point in the flow. It is at this intersection point that the velocity component of the flow normal to the beam crossing is measured. The photomultiplier unit is focussed on the beams crossing point, and as the flow passes this point light is scattered from the two beams, doppler shifted in frequency by equal and opposite amounts. The difference is detected in a signal modulation, which is then converted by one of the electronic units into a voltage output which in turn is fed onto a chart recorder. From this the velocity can easily be calculated. Before measurements were taken the laser was accurately levelled.

The sampling system of the carousel consists of two port holes, one on each wall of the flume, 80mm above the floor. Through each of these port holes protrudes an 'L' shaped stainless steel sampling tube, which has an internal diameter of 2mm. The outer wall sampling tube has its entrance facing upstream and its elevation can be altered by rotating the outer portion of this tube across a scale corresponding to 0-100mm above the flume floor.

During bed erosion tests, fluid is continuously extracted from the carousel flume by a peristaltic pump and passed through a constant temperature water bath and a densitometer before being returned to the carousel flume. The densitometer works on the principle of determining the frequency of a thin vibrating glass tube through which the fluid is pumped and comparing this to the frequency of clean water pumped through a second densitometer. The readings obtained are analyzed and displayed on a chart recorder. Bottle samples of the fluid are taken from time to time and analyzed gravimetrically to maintain an accurate calibration. In this manner the suspended sediment concentration of the fluid in the carousel flume is measured continuously to within a few percent. Previous measurements by Burt and Game (Ref 1) have shown that the mean suspended solids concentration of the fluid in the carousel flume is very close to the suspended solids concentration at the centre of flow, certainly less than 5% difference.

---

## **2. Measured velocities**

---

### **2.1 Summary of 1984 findings**

#### *2.1.1 Work description*

The aim of this project was to commission the carousel flume and its equipment, and to study flow velocities within the flume.

#### *2.1.2 Velocity flow fields*

Velocities within the carousel can be split into three components. (i) The primary flow in a horizontal direction, (ii) a vertical component and (iii) a radial component.

A large number of exploratory experiments with clear water were carried out to find a physical system which minimised secondary flow effects. The best results were obtained when the water depth was about 100mm and the roof had a smooth surface. This condition was adopted as standard for the majority of further tests.

Point velocity measurements (horizontal component) were taken on a grid across the width of the flume and this data was used to plot isovels (lines of equal velocity). Figure 6 shows examples of the velocity profiles obtained for different roof speeds.

#### *2.1.3 Interpretation*

From figure 6 it can be seen that the isovel patterns are all very similar, displaying a sharp inward bend at a depth of 20 mm with the middle sections sloping upwards towards the outside and a gentle bend outward at an 80mm depth. Because these figures were so similar they were used to construct a generalised section (Fig 7). Each isovel value is displayed as a fraction of the cross section mean velocity.

In the cross section velocity profiles (Fig 6) there is evidence of a secondary flow system, at right angles to the horizontal component of the flow. This has been sketched in figure 7.

This secondary circulation is induced by the centrifugal force produced when the roof is rotated. The water on the surface is forced outward, when it reaches the outer wall it is deflected downward. After leaving the outer wall most of the flow passes on towards the inner side and back up to the surface, but some remains in this corner and sets up a smaller circulation cell. From this description and figure 7 it may appear that the circulation cell is completed. This is not the case because the longitudinal component of flow gives it a resulting helical motion along the flume.

The velocity measurements used to produce the isovels in figures 6 and 7 were also used to measure cross sectional mean horizontal velocities for each motor speed setting. The relationship is seen in figure 8, demonstrating that mean water speed is directly proportional to roof speed over most of the operating range. Thus, using the above relationship and figure 8, it is possible to predict

with reasonable accuracy the entire cross sectional flow field knowing only the roof speed.

The isovels in figures 6 and 7 give a rather misleading view of the flow field, emphasising the variation across the width. Figure 9 shows the variation across the width at several depths. Also shown is the roof speed normalised to cross sectional mean velocity. This figure clearly shows that the horizontal velocity distribution across the width of the flume is closely related to the variation in tangential roof speed due to radius.

## 2.2 Velocity measurements 1988

The 1984 findings showed a significant secondary flow within the carousel flume and it was therefore decided to quantify the vertical and radial velocity components using the laser doppler technique. Thus, a second set of data was collected consisting of horizontal, vertical and radial velocity components for a number of roof rotation rates and a fluid depth of 100mm. As the results are compared with data from section 2.1 a standard set of roof rotation rates was utilised. Roof rotation rates of 1, 1.5, 2 and 3.7rpm were used. These values corresponded to motor speed settings of 160, 240, 320 and 650 respectively (see Fig 3). Velocity measurements were taken on grids defined in Appendix A. Appendix A displays all the velocity data in a tabular form. The tables indicate the position of velocity measurement as a cross with the associated velocity value labelled beneath.

### 2.2.1 Experimental arrangement

**Horizontal velocity readings.** The laser was set up and used in a manner described previously. Positive values indicate flow in a clockwise direction around the flume.

**Vertical velocity readings.** These readings were made by rotating the laser beams through 90°. Positive values indicate a direction towards the flumes roof.

**Radial readings.** Due to technical difficulties the laser set up had to be altered for this experiment. One of the two laser beams was weakened and the photo-multiplier was positioned directly in line with this beam. A mirror was positioned beneath the flume tilted at an angle of 45° in order to redirect the laser beams into the fluid. The weakened beam was then directed back out of the flume after crossing the stronger beam via a dentist type angled mirror (glass area approximately 20mm by 20mm) supported on a shaft of 5mm diameter beneath the roof. The photo-multiplier was then positioned directly along the path of the weakened beam. Optical quality mirrors were used throughout. Positive values of radial velocities indicate flow towards the flume centre.

## 2.3 Discussion

Figure 10 illustrates two typical cross-sectional horizontal velocity contour plots. The form of both appear to be very similar. The upper graph illustrates a roof rotation of 1.5rpm, and the lower graph a roof rotation rate of 3.7rpm. Note the similar form to the previous results (see Fig 6) including the secondary flows close to the outer wall illustrated in all the graphs.

Comparing the horizontal results with section 2.1 (Fig 6) very little difference was seen in the velocity measurements at comparable lid rotation rates and depth of fluid. At low rotation rate (1rpm) the horizontal velocities were consistently 15% higher than the data presented in Appendix A. At a high rotation rate (3.7rpm) the results were consistently lower by 4%. For the other two rotation rates (1.5 and 2rpm) horizontal velocity measurements are very similar with differences of less than 1%.

In general the maximum horizontal velocity was at least a factor of 10 greater than the vertical and radial components. Maximum radial velocities were generally equal to the vertical (see table 1 for a summary of the data).

Figure 11 illustrates typical cross-sectional vertical velocity contour plots for the same roof rotation rates shown in figure 10. Little fluid movement can be seen towards the centre of the flume with a great deal of vertical flow at the flumes side walls. The flow direction is down at the outer wall and up at the inner wall which is as reported in section 2.1. An interesting phenomena shown in both plots is the large negative velocities close to the channel floor. This anomaly is hard to explain.

Figure 12 illustrates typical cross-sectional radial velocity contour plots for the same roof rotation rates shown in figure 10 and 11. Unfortunately, this data could only be collected for the bottom half of the flume. A flow at the bed towards the centre of the flume is clearly seen, and a return flow towards the outer wall will occur at the roof.

Figure 13 shows a typical radial/vertical vector diagram combining the data shown in figures 11 and 12. Thus the flow features described in figures 11 and 12 can be seen presented in another manner, enabling the secondary flow to be illustrated in two dimensions.

It is concluded from the above data that the secondary flow within the flume can be considered to be cork-screwed in nature, with the larger horizontal flow dominating the vertical and radial flows.

A test was performed to assess the effect the mirror (introduced to measure radial velocities) had on the horizontal and vertical velocities. The experiment was carried out by taking velocity readings at 40mm above the bed with the radial mirror 100mm from the outer face of the carousel. The results show that in a region 150mm away from the outside wall horizontal velocities were increased in magnitude. At the lowest speed setting, the effect was an approximate 40% increase in the velocities. However, there seemed to be little effect on vertical velocities and differences were within measuring tolerances.

In conclusion, comparing the results from section 2.1 and 2.2 the horizontal velocity component shows variation within a  $\pm 10\%$  range. Data previously reported in section 2.1 is shown in figure 6 and allows a direct comparison with the laboratory horizontal isovel plot shown in figure 10. The magnitude and the form of the isovel plots at all parts of the cross section show comparable values. This indicates the excellent repeatability of the horizontal velocity measurements. In addition results at a height of 20mm above the bed (section 4.3) compare well with the horizontal velocities in 2.1 and 2.2 for similar depth for all lid rotation speeds studied.

---

### **3. Velocity measurements predicted by the HARWELL-FLOW3D model**

---

#### **3.1 Introduction**

This section describes the work of Polytechnic South West (PSW). The aim was to numerically predict the velocity fields within the carousel. Numerical solutions are presented for the equations governing the flow of clear water in the carousel flume. The numerical results complement the physical data for flows of constant roof rotation rates. For a complete evaluation of PSW's work the reader is referred to references 5,6 and 7.

For clear water the fluid was considered to be incompressible and Newtonian, thus, the Navier-Stokes equations governed the fluid motion. A rotational Reynolds number was defined (Ref 5) based on the outer radius of the flume. The Reynolds number indicated the flow was turbulent for roof rotation rates > 1rpm.

Since the flow is turbulent at the roof rotational speeds used, the Navier-Stokes equations are averaged in the usual way, and an eddy-viscosity type of turbulence model is assumed. Reynolds stress terms are re-written in terms containing a turbulent viscosity. Thus, the final set of equations are of a similar form to the solutions for laminar flow.

Two turbulence models have been used which differ in the definition of turbulent viscosity.

##### **3.1.1 Mixing length hypothesis (MLH)**

This model assumes a shear rate dependent turbulent viscosity. The only unknowns in the equations are the mean velocity components, and an effective pressure.

##### **3.1.2 $k-\epsilon$ model**

This model introduces two further unknowns  $k$  and  $\epsilon$ , being the turbulence kinetic energy and dissipation respectively.

The  $k-\epsilon$  model is valid only for flows dominated by turbulent stresses. Special treatment is therefore required in solving for flows bounded by walls, since the viscous stresses become dominant in the near-wall region. The  $k-\epsilon$  model could be modified to apply to the low local Reynolds number region near the wall but this requires very fine grids and, consequently, large computing times. This is why wall functions are used.

HARWELL-FLOW3D, developed by UKAEA Harwell, uses an iterative process to calculate velocities using the above models. The solution was deemed to have converged when the moment coefficients changed by typically, less than 0.1% over a period of 250 iterations. Typically, convergence was achieved around 1500-2500 iterations.

## 3.2 Results

Both experimental and numerical results for the horizontal (primary) flows compare well. Horizontal velocity profiles for a range of lid rotation rates have been studied and the isovel distributions compare well for all cases (for a typical case see Fig 14).

Both the measured and predicted flow velocities illustrate a secondary flow involving vertical and radial velocity components. These flows are produced by the relative differential movement of the rotating lid. In experiments where a mud bed is present it would be expected the secondary flow would transfer eroded mud (in suspension) from the outer part of the flume to the inner, where deposition may take place due to the lower horizontal velocities.

The computed secondary flows were found to give important differences between the two turbulence models. The possible presence of a weak secondary eddy at the roof/inner wall boundary in the MLH model is an interesting phenomena. This eddy does not appear to be present in the laboratory results although a disturbance in the flow field can be seen. Unfortunately, experimental data is limited, so a definite answer as to the relative merits of the MLH and  $k-\epsilon$  models should be made with care. The shape of the streamlines from the MLH model certainly compare with the laboratory data better than the  $k-\epsilon$  data. The  $k-\epsilon$  flow pattern shows a relatively undisturbed rounded profile while the MLH programme illustrates distinct and duplicated kinks in isovels along the cross section similar to the laboratory flows.

---

## 4. *Bed shear stress measurements within the carousel*

---

### 4.1 Introduction

Four methods were employed for measuring the shear stress exerted by the fluid on the bed. The first method was simple and involved direct measurement of the energy input to the roof through the calibrated strain gauge. A number of different speeds of rotation of the roof were used. This method can only predict a mean bed shear stress.

The second and more complex way of determining the bed shear stress was by measurement of the near bed velocity profiles in the flume using laser doppler anemometry. The friction velocity at the bed was determined from a log-linear plot of height above bed and horizontal velocity. Velocities were determined at three sections across the width of the flume for different speeds of rotation of the roof. The bed shear stresses were then computed from the logarithmic portion of the velocity-depth profiles.

Thirdly, flush mounted shear stress probes were deployed to measure shear stress along the base and side walls of the flume.

Finally, the qualitative distribution of shear stress across the flume can be inferred from eroded profiles of muds. It was assumed that the shear strengths

of a mud bed increases with depth while being consistent across the width of the flume.

## 4.2 Description of shear stress probes and results

### 4.2.1 Description of equipment

A second perspex carousel viewing section was constructed by PSW to hold a number of shear stress probes both on the floor and on the side walls of the flume. The probes used the constant temperature hot wire anemometry technique. Each probe consisted of two thin electrically connected metallic strips mounted side by side on a perspex base. The strips were heated to approximately 30° C by an electrical current, the relative deflection of the connecting wire under stress produced a variation in output voltage, which was calibrated to shear stress and the results recorded.

The technique relies on the convective heat loss from the electrically heated probe to the surrounding water. The heat loss depends on the temperature and geometry of the sensor and on the fluid's velocity, temperature pressure, density and thermal properties. Assuming that only one of the fluid parameters was varied the heat loss was interpreted as a direct measure of the quantity in question, in this case shear stress. For a basic guide to the physics and electrical set up see reference 4.

Fluctuating fluid temperature was automatically compensated for using a temperature compensated bridge. Additionally, a note was taken of fluid temperatures during the experiments, and shear stress values measured corresponded well to the compensated values.

The deposition of impurities suspended in the flow onto the sensors dramatically altered their heat transfer properties. Ideally, if calibration is affected during an experiment the probe should be cleaned and re-calibrated.

In the flume, dissolved gases sometimes form bubbles on the sensor surface. This gas also modified the heat transport properties and should be removed. In extreme cases hot spots could occur which may damage the probe.

### 4.2.2 Calibration

A low turbulence flow of known velocity was used for calibration. The flow was produced in a purpose built calibration flume provided by PSW. The flume had a working section of 2m, possessing 10 manometers equally spaced down its length, which allowed accurate pressure measurement. The flume had a flow width of 100mm, depth of 4mm and was covered by a perspex lid. A number of flow conditions were studied by varying the input head. The maximum head used was 400mm. The repeatability of results under identical starting conditions were good.

Two shear stress probes were placed within the calibration flume, at one time. Ideally, the probes should have been placed at the same attitude as that for their use during an experiment. It was also necessary to use the leads used during the experiment as any change in the length or composition of the wire would affect its resistance. This in turn would affect the calibration of the probes. In conjunction with the problem described above, the Dantec logging

device containing the bridge balance circuitry proved very susceptible to vibration. It was therefore located in a position central to both the calibration flume and the carousel so it did not have to be moved in any way.

The calibration flume was provided with a relationship which described probe shear stress at given pressure heads. Each transducer was calibrated in the flume and a unique relationship was obtained between input head and output voltage of the transducer. This was then related to shear stress.

Each transducer had its own circuitry balanced prior to calibration. It was necessary to calibrate the transducers both before and after an experiment in the carousel as the calibration had a tendency to drift.

Figure 15 shows a typical calibration curve for one of the probes. The calibration has been carried out twice, once before (squares) and a second (triangles) after the experiment. The reader should be aware of the power law used, and assess the results accordingly.

#### *4.2.3 Scope of tests*

Initially, the bed shear stress profiles were defined for three depths of water and six roof rotation rates. Later the magnitude and direction of the shear stress was measured at two points across the tank, at distances of 0.03 and 0.2m away from the outer side wall. Finally wall shear stress measurements were taken for the same fluid depths at two probe positions 70 and 20mm above the bed.

#### *4.2.4 Results*

The first sets of data recovered were seriously affected by the problems described in section 4.2.1 and the almost random scatter of points was not acceptable. After the experimental procedure was improved and a greater familiarity with the equipment was established the experiments were run for a second time. A systematic approach was followed during the second set of experiments to study each aspect of the investigation in great detail. Very encouraging results have been acquired, which are discussed below.

All bed shear stress measurements are displayed in tabular form. Tables 2, 3 and 4 list data for three fluid depths 0.05, 0.1 and 0.2m respectively.

### **4.3 Near bed velocities**

In May/June 1986 laser measurements were undertaken to define the horizontal velocity component close to the bed. The aim of the experiment was to produce velocity profiles from close to the bottom of the flume to a height of 20mm above the floor. The magnitude of the bed shear stress was then calculated using these profiles.

#### *4.3.1 Experimental procedure*

Velocity measurements were taken at three positions across the channel: 120, 200 and 340mm from the outside edge of the flume. Data was collected at a number of heights within 20mm of the bottom. Horizontal velocity data is presented in table 5.

The following empirical relationship describes the variation of velocity with depth;

$$\frac{U}{U_*} = \frac{1}{k} \ln \frac{y}{y_0}$$

where

- U is the horizontal velocity component
- U<sub>\*</sub> is the shear velocity
- y is the distance above the bed
- y<sub>0</sub> is the intercept of the y axis and
- k = 0.4

The formula was converted into common logs, and a plot of horizontal velocity against the logarithm of height above the bed drawn. Figure 16 shows a composite semi logarithmic plot illustrating velocity profiles at the three cross-sections and for a number of different rotation rates. For a particular section and roof rotation rate the graph of velocity versus depth showed a near straight line. Thus values of U<sub>\*</sub> were calculated using the slope of the plots as follows:

$$U_* / 0.174 = dU / d(\log_{10} y)$$

Further, U<sub>\*</sub> is related to the bed shear stress

$$U_* = (\tau_0 / \rho)^{1/2}$$

where

- τ<sub>0</sub> is the bed shear stress
- ρ is the density of the fluid.

#### 4.3.2 Results

The horizontal velocity component of the flow increased towards both the outer wall and the top of the channel for a given rotation rate.

The later probe data shows a steady increase in the bed shear stress towards the outer side wall of the channel. Similarly, it was expected that the bed shear stress calculated from near bed velocities would show the same form. However, this was not the case. Figure 17 shows two typical shear stress profiles across the flume for roof rotation rates of 1.59 and 2.65rpm. Both measured and near bed velocity derived data are shown. The results for either side of the centre line of the flume compare well with the shear stress probe results. However, the centre line data show a continuous tendency to be rather larger than expected. An explanation for this effect has not been forthcoming.

A plot of bed shear stress against rpm is shown in figure 18, for the three cross stream positions studied. The average (1) bed shear stress across the width of the flume calculated from the near bed laser velocity data (Fig 18) is shown in Figure 19. Also plotted in Figure 19 is the shear stress on the wetted perimeter as given by the power input measured through the strain gauge (see Fig 2). These two curves show reasonable agreement and indicate a steady increase in bed shear stress with increasing speed of rotation of the roof. For

the purpose of estimating the bed shear stress during erosion tests the curve representing the average shear stress as calculated from the power input was used. However, it must be appreciated that the eroding fluid in an erosion test may have a high concentration of suspended solids and will not exhibit the same hydrodynamic behaviour as the clear water used in the calibration. Nevertheless, for the concentrations of suspended solids present in the carousel flume during an erosion test ( $\leq 4\text{kgm}^{-3}$ ), it is believed that this factor would not significantly affect the calculation of the erosion properties of the mud.

A mean geometrical bed shear stress was calculated from data derived from five probe positions across the flume, for measured and predicted data. The measured (average 2) and predicted results show good agreement. This data is plotted on Fig 19 (diamonds and triangles respectively). Comparing the mean shear stress results derived from near-bed velocities with the mean probe stresses, it can be seen in figure 19 that the plots show relatively good agreement. Note though, the gradient of the probe data appears to be greater than the data used previously. This indicates that at high roof rotation rates average bed shear stress values have been slightly under estimated in the past.

## **4.4 Eroded mud profiles**

### *4.4.1 Bed preparation*

To prepare a mud bed in the carousel flume, the mud is first mixed homogeneously in a mixing tank with a recirculating pump. The suspension is then pumped into the flume from the tank until the required depth of suspension in the flume is reached. The roof is lowered onto the suspension surface and the mud in suspension is allowed to deposit and consolidate. The period of consolidation is usually in the range of 2-5 days and the resulting bed has a thickness of 10-25mm. The depth of fluid above the bed is adjusted to be close to 100mm which corresponds to the depth of flow for which the bed shear stress measurements were made.

### *4.4.2 Test procedure*

An erosion test in the carousel flume comprises a number of discrete runs during which the speed of rotation of the roof (and hence the bed shear stress) is held constant. In a test there may be between 2-5 runs each lasting 60-200 minutes. The speed of the carousel flume is systematically increased for each successive run.

A run commences when the concentration of suspended solids is constant in the previous run. The speed of rotation of the roof is increased over a period of about 30 seconds to its new value. The concentration of suspended solids as measured continuously by the densitometer will at first increase rapidly (indicating a strong erosion), then more smoothly (modest erosion) and finally the concentration will remain nearly constant (no erosion). This pattern is reflected by the readings from the ultrasonic transducer which is mounted on the underside of the flume mid-way across its width. The change in the readings is directly proportional to the depth of erosion.

At the end of a run when erosion has stopped the actual depths of erosion at 20mm intervals across the width of the flume are determined using the ultrasonic transducer. The typical depth of erosion which is normally attained at the end of the test is about 5mm. If more mud is eroded then the high concentrations of suspended sediment begin to prevent the densitometer and ultrasonic depth transducer from functioning correctly. Furthermore, at the higher speeds of rotation the effects of secondary currents are greater and the differential depths of erosion across the flume become more pronounced.

The thickness of the mud bed in the carousel was measured from beneath the flume at the perspex viewing section by an ultrasonic transducer. This instrument displayed a peak signal which indicated the interface between the mud bed and the overlying fluid, this enabled the thickness of the bed to be determined to within 0.1mm. The transducer was calibrated through a fluid with a salinity similar to that in the mud bed. A moveable mounting device held the transducer in contact with the underside of the perspex section and was used to position the transducer at any point across the 0.4m width of the flume. In this way it was possible to obtain profiles of the bed and determine the depth of erosion at any time during the test.

#### 4.4.3 *Bed profiles during each run*

Figure 20a shows a sequence of bed profiles for Orwell river mud tested at a number of rotation rates during a single run. It can be seen in figure 20a that the rates of erosion are greatest near the outer edge of the tank where the shear stress is larger. It may be assumed that the shear strength of the mud is proportional to depth and so the eroded profiles illustrate the form of bed shear stress profiles across the flume.

#### 4.4.4 *Mud profile\shear strength relationship*

It was discovered that a power law of the form

$$\tau \propto D^{0.66}$$

fits the data well, where;

$\tau$  is the calculated bed shear stress and  
D is the depth of erosion.

The equation indicates a good correlation between measured erosion and calculated bed shear stress results. This is shown in figure 20b for two mud types studied. Unfortunately the roof rotation rates during the two types of experiments were not in general comparable. The readers attention is brought to some of the rotation rates that are. In the upper graph eroded mud profiles at 3.61 and 2.58rpm correlate well with the PSW data having rotation rates of 3.7 and 2.65rpm. Similarly, in the lower graph mud profiles at 3.65 and 2.59rpm correlate well with the PSW data having rotation rates of 3.7 and 2.65rpm. Note that other profiles and measurements lie in their expected sequences, ie both mud profiles and shear strength measurements increasing with roof rotation rate.

It is interesting to note the slight reduction in the depth of erosion at 0.05m from the outer edge of the flume. This reduction in the shear strength is not

in agreement with the numerical values provided by PSW which decreases very rapidly at approximately 0.01m from the outer wall. However, the shear stress probe measurements illustrate a similar trend to the erosion profiles.

---

## **5. Predicted shear stress**

---

### **5.1 PSW HARWELL-FLOW3D model**

The shear stress distribution along the bed of the flume was computed using the HARWELL-FLOW3D model. Simple bed stress distributions were produced for various roof speeds. Table 7 summarizes PSW bed shear stress results for three depths of fluid, 50, 100 and 200mm; seven rpm's; and, five cross stream positions.

### **5.2 Results**

It appears that the shear stress results were reasonably grid-independent. That is, the grid mesh size has no effect on the shear stress values calculated.

Figure 21 shows a composite plot of numerically calculated shear stress versus distance across the flume. The depth of flow is 100mm and roof rotation rates are shown. The figure illustrates steadily increasing values of the bed shear stress with distance away from the inner side wall for a given roof rotation rate. The rate of change in shear stress decreasing towards the outer wall. An increase in roof rotation rate causes a corresponding increase in bed shear stress.

The shear stress predicted by PSW very close (0.01m) away from the inner and outer walls decreases rapidly to zero at the walls. Hence, small changes in position gives rise to large changes in the bed shear stress.

#### **5.2.1 Bed shear stress**

Figure 22 shows a number of plots showing shear stress versus the distance across the carousel for a number of roof rotation rates with the PSW results superimposed. The fluid depth was 100mm for all experiments considered. The results include data from three separate runs for the same initial conditions. This indicates the improved repeatability of the laboratory experiments. The graph also shows the excellent correlation between the laboratory and numerical experiments for shear stress on the bed of the flume. It is interesting to note the drop in bed shear stress close to the outer side wall indicated by the laboratory experiments. This is not displayed in the numerical results where the shear stress continues to increase steadily to 0.01m from the outer wall. This drop in shear stress correlates with the reduced depths of erosion (see section 4.4.3) at a similar position for all the muds studied. It is suggested that this unexpected phenomena is caused by the hydrodynamics of the flume, and is possibly an effect caused by the secondary flows within the channel.

Figures 23 and 24 show graphs of predicted and probe measurements corresponding to shear stress for water depths of 50 and 200mm respectively. Note the reasonable correlation between the laboratory and numerical data.

These graphs illustrate a small decrease in the bed shear stress at a particular height for increased water depth for other variables remaining the same.

Some of the data points in figures 22, 23 and 24 still show the susceptibility of the probes to impurities within the channel. The erroneous points are attributed to air bubbles etc, interfering with the probes heat loss performance. These points could have been omitted but were left in to give completeness of data, they are seen as low readings at positions 2.8 and 3m across the flume for the second data set.

### *5.2.2 Orientation of peak shear stress*

PSW numerical prediction results showed that the maximum shear stress was deflected approximately  $10^\circ$  from the circumferential direction towards the centre of the carousel flume. In order to examine PSW's prediction a novel experimental technique was developed to measure direction and magnitude of the shear stress in the laboratory. The method used consisted of rotating the shear stress probes through known angles in their sockets. Table 8 summarizes probe data for three experiments at different rpm. Two probes were used for each experiment positioned at 0.2 and 0.03m away from the outer side wall. The probe angle is measured from the circumferential direction (0 degrees). A positive angle indicates a direction towards the centre of the flume, a negative angle indicates an angle towards the outer wall.

Figure 25 illustrates a composite plot showing direction and magnitude at three roof rotation rates and two cross-stream positions for a fluid depth of 100mm. It is quite clear that the maximum shear stress does not lie in a circumferential direction but deviated towards the carousel centre at an angle of approximately 10 degrees. The magnitude of the deflection and maximum shear stress varies little with distance towards the outside of the tank. A shear stress envelope can be drawn around each set of data points for constant roof rotation rates and the maximum shear stress defined.

Figures 26a, 26b and 26c compare laboratory and numerical data for various roof rotation rates. It is evident in every case that the shear stress values predicted by the numerical model for the 0.03m measuring point are far in excess of the laboratory data. Data for the flume's mid point compare favorably. For an excellent example see Fig. 26b.

### *5.2.3 Side wall shear-stress*

Two shear stress measuring points at heights of 20 and 70mm were used on the outer and inner side-walls. Table 9 compares inside and outside wall stresses for both laboratory and numerically modelled data. Figure 27 shows how the shear stress varies with increased lid rotation rate for a depth of 100mm and the two height cases. Again there is a good correlation between the laboratory and numerical model trends, although in this case it appears that the numerical model consistently calculates higher values of shear stress than the measured data. This is probably due to the difference in boundary conditions between the laboratory and the numerical models. It can be seen that the shear stress is greater towards the roof of the carousel for both wall positions presented also the shear stress is greater at the outer wall of the tank.

Figure 28 shows a similar graph to figure 27 but for fluid depths of 50 and 200mm. An interesting phenomena is seen in figures 27 and 28, in that, for a probe height of 0.02m the shear stress on the inner wall of the carousel remains relatively constant for the three depths studied. However, this is not the case for the shear stress data taken at the outer wall which shows a pronounced reduction in shear stress values with an increase in depth.

---

## **6. Conclusions**

---

It has been shown that laser velocity measurements within the carousel flume can be repeated and reproduced accurately over a wide range of roof rotation rates. PSW have mathematically determined the flow features using two models. The MLH model seems to reproduce the finer details better than the k- $\epsilon$  model.

The secondary flows within the flume were quantified, and show a corkscrew pattern. These flows will effect erosion and deposition rates in the flume.

Average bed shear stress data derived from logarithmic velocity profiles and shear stress probe measurements compared favorably.

Bed shear stress data measured in the carousel flume and PSW numerically predicted data show excellent agreement over the parameter range studied. Both numerical and laboratory results show the maximum shear stress values are orientated towards the inner side wall at an angle of between 10 to 15 degrees. The main difference between measured and predicted data is the drop in measured shear stress values close to the outer wall. The predicted results show a steady increase in shear stress values towards the outer wall, with a very sharp fall to zero within 0.01m of the outer wall. The measured values appear to be correct because a similar drop in shear stress is depicted by the mud bed profiles at a position of 0.025m away from the outer wall.

Wall stresses predicted by PSW appear to be greater than those measured within the flume, this is probably due to the difference in boundary conditions.

---

## **7. Acknowledgements**

---

The study was conducted by various members of the Tidal Engineering Department of Hydraulics Research over an eight year period. The deployment of the shear stress probes and the numerical modelling of the flow in the carousel was undertaken by Dr T E R Jones, Dr P James and Dr D Graham of Polytechnic South West.

---

## **8. References**

---

1. The Carousel: Commissioning of a circular flume for sediment transport research. Hydraulics Research Report SR 33, January 1985.
2. The behaviour of estuarine muds during tidal cycles: An experimental study and mathematical model. Hydraulics Research Report SR 138, February 1988.
3. Estuarine muds manual. Hydraulics Research Report SR 164, February 1988.
4. An elementary introduction to hot-wire and hot-film anemometry. Dantec.
5. Numerical modelling of turbulent water flow in the Hydraulics Research carousel flume. PSW Research Report MSOR-89-04.
6. Numerical evaluation of wall shear stresses in the Hydraulics Research Carousel flume for various depths of flume. PSW Research Report MSOR-89-09.
7. Numerical investigation into geometric modifications of the Hydraulics Research Carousel flume. PSW Research Report MSOR-89-10.

## ***Tables***



---

---

**Table 1 Relative magnitude of the velocity component ratio's**

---

Lid rotation rate (rpm)	Maximum z/w	Maximum r/w
1	0.1	0.1
1.5	0.09	0.09
2	0.09	0.09
3.7	0.04	0.01

*horizontal component w*

*vertical component z*

*radial component r*

**Table 2 Measured bed shear stress values for a flow depth of 50mm**

Date	Roof rot. rate (rpm)	Flow depth (mm)	Shear stress (Nm <sup>-2</sup> ) at given radius				
			2.63	2.71	2.8	2.89	2.97
16.11.89	1.06	50	0.092	0.009	0.041		0.081
	1.59	50	0.226	0.03	0.108		0.188
	2	50	0.384	0.05	0.205		0.304
	2.12	50	0.42	0.05	0.224		0.336
	2.65	50	0.649	0.087	0.356		0.497
	3.18	50	0.886	0.145	0.522		0.732
	3.7	50	1.332	0.197	0.726		1.001
14.11.89	1.06	50		0.032			0.034
	1.59	50		0.101			0.091
	2	50		0.173			0.169
	2.12	50		0.2			0.187
	2.65	50		0.325			0.32
	3.18	50		0.476			0.521
	3.7	50		0.657			0.68
10.11.89	1.06	50	0.012	0.024	0.052	0.062	
	1.59	50	0.06	0.062	0.13	0.141	
	2	50	0.105	0.126	0.236	0.241	
	2.12	50	0.117	0.138	0.269	0.263	
	2.65	50	0.208	0.222	0.394	0.413	
	3.18	50	0.314	0.338	0.609	0.594	
	3.7	50	0.428	0.465	0.828	0.765	

**Table 3 Measured bed shear stress values for a flow depth of 100mm**

Date	Roof rot. rate (rpm)	Flow depth (mm)	Shear stress (Nm <sup>-2</sup> ) at given radius				
			2.63	2.71	2.8	2.89	2.97
20.11.89	1.06	100	0.018	0.028	0.008	0.056	0.087
	1.59	100	0.052	0.056	0.023	0.149	0.211
	2	100	0.087	0.071	0.048	0.235	0.375
	2.12	100	0.105	0.074	0.05	0.254	0.428
	2.65	100	0.159	0.118	0.098	0.423	0.687
	3.18	100	0.246	0.185	0.129	0.627	0.988
	16.11.89	1.06	100	0.054	0.02	0.039	
	1.59	100	0.122	0.049	0.096		0.141
	2	100	0.209	0.077	0.176		0.222
	2.12	100	0.229	0.083	0.192		0.233
	2.65	100	0.362	0.126	0.316		0.366
	3.18	100	0.544	0.188	0.471		0.537
	3.7	100	0.768	0.256	0.624		0.72
15.11.89	1.06	100	0.018		0.01	0.05	0.075
	1.59	100	0.053		0.004	0.122	0.12
	2	100	0.086		0.011	0.213	0.254
	2.12	100	0.095		0.01	0.234	0.262
	2.65	100	0.162		0.017	0.363	0.4
	3.18	100	0.232		0.021	0.562	0.571
	3.7	100	0.318		0.028	0.764	0.808
14.11.89	1.06	100		0.039			0.02
	1.59	100		0.096			0.049
	2	100		0.161			0.087
	2.12	100		0.18			0.098
	2.65	100		0.304			0.178
	3.18	100		0.436			0.357
	3.7	100		0.596			0.478
10.11.89	1.06	100	0.023	0.026	0.037	0.05	
	1.59	100	0.073	0.065	0.112	0.127	
	2	100	0.131	0.121	0.198	0.192	
	2.12	100	0.136	0.132	0.22	0.223	
	2.65	100	0.225	0.216	0.344	0.344	
	3.18	100	0.317	0.324	0.529	0.501	
	3.7	100	0.447	0.444	0.726	0.687	

**Table 4 Measured bed shear stress values for a flow depth of 200mm**

Date	Roof rot. rate (rpm)	Flow depth (mm)	Shear stress (Nm <sup>-2</sup> ) at given radius				
			2.63	2.71	2.8	2.89	2.97
16.11.89	1.06	200	0.025	0.013	0.033		0.039
	1.59	200	0.064	0.043	0.083		0.088
	2	200	0.12	0.065	0.141		0.144
	2.12	200	0.123	0.075	0.153		0.173
	2.65	200	0.217	0.112	0.255		0.268
	3.18	200	0.314	0.167	0.381		0.374
	3.7	200	0.447	0.218	0.533		0.511
14.11.89	1.06	200		0.031			0.013
	1.59	200		0.076			0.032
	2	200		0.146			0.057
	2.12	200		0.17			0.062
	2.65	200		0.262			0.1
	3.18	200		0.381			0.18
	3.7	200		0.537			0.265
10.11.89	1.06	200	0.018	0.024	0.02	0.034	
	1.59	200	0.05	0.071	0.053	0.093	
	2	200	0.093	0.099	0.092	0.163	
	2.12	200	0.113	0.114	0.104	0.186	
	2.65	200	0.186	0.194	0.174	0.297	
	3.18	200	0.295	0.293	0.248	0.419	
	3.7	200	0.383	0.406	0.331	0.59	

**Table 5 Summary of near bed velocity data**

Roof rot. rate (rpm)	120mm from outside edge		Centre of flume 200mm from outside edge		340mm from outside edge	
	Height (mm)	Velocity (mms <sup>-1</sup> )	Height (mm)	Velocity (mms <sup>-1</sup> )	Height (mm)	Velocity (mms <sup>-1</sup> )
0.698	2	48	1.5	27	5	27
	3	45	4.0	51	10	43
	5	75	7.2	65	15	44
	7	82	9.0	73	20	47
	10	86	12.0	80		
	15	93	14.2	65		
	20	103				
1.304	2	134	1.5	82	5	90
	3	134	4.0	116	10	111
	5	158	7.2	140	15	115
	7	165	9.0	150	20	121
	10	172	12.0	162		
	15	182	14.2	162		
	20	189				
1.818	2	192	1.5	137	5	145
	3	192	4.0	170	10	162
	5	223	7.2	191	15	169
	7	237	9.0	210	20	175
	10	247	12.0	227		
	15	257	14.2	230		
	20	264				
2.857	2	292	1.5	225	5	229
	3	295	4.0	286	10	249
	5	343	7.2	314	15	270
	7	357	9.0	327	20	272
	10	370	12.0	348		
	15	393	14.2	356		
	20	405				
3.333			1.5	276		
			4.0	327		
			7.2	375		
			12.0	409		
			14.2	419		
3.75	2	394			5	310
	3	394			10	333
	5	451			15	357
	7	473			20	364
	10	494				
	15	515				
	20	532				

**Table 6** *Bed shear stress data calculated from the logarithmic parts of the velocity profiles*

Distance from outside wall (mm)	RPM	Cross sectional mean velocity from sr33 (mms <sup>-1</sup> )	Bed shear stress (Nm <sup>-2</sup> )
340	0.698	87	0.047
	1.304	162	0.088
	1.818	227	0.08
	2.857	355	0.186
	3.75	460	0.291
200	0.698	87	0.12
	1.304	162	0.21
	1.818	227	0.3
	2.857	355	0.54
	3.333	410	0.69
120	0.698	87	0.098
	1.304	162	0.107
	1.818	227	0.185
	2.857	355	0.409
	3.75	460	0.636

**Table 7 Summary of PSW numerically calculated bed shear stress results**

Flow angle normal

Radius (m)	Depth (mm)	Shear stress (Nm <sup>-2</sup> ) at given RPM						
		1.06	1.59	2.00	2.12	2.65	3.18	3.70
2.63	100	0.039	0.075	0.115		0.193	0.29	0.385
2.71	100	0.062	0.113	0.171		0.281	0.39	0.515
2.8	100	0.075	0.135	0.205		0.333	0.48	0.605
2.89	100	0.092	0.161	0.243		0.396	0.542	0.712
2.97	100	0.098	0.18	0.27		0.448	0.62	0.81
2.63	50				0.135			0.36
2.71	50				0.19			0.53
2.8	50				0.245			0.66
2.89	50				0.305			0.845
2.97	50				0.405			1.07
2.63	200				0.115			0.325
2.71	200				0.155			0.425
2.8	200				0.185			0.505
2.89	200				0.21			0.565
2.97	200				0.22			0.6

**Table 8 Orientation and magnitude of bed shear stresses**

Degrees	Shear stress (Nm <sup>-2</sup> )					
	RPM: 1.59 Radius(m): 2.8	1.59 2.97	2.65 2.8	2.65 2.97	3.7 2.8	3.7 2.97
0	0.114	0.112	0.336	0.349	0.682	0.693
5	0.12	0.107	0.34	0.384	0.704	0.666
10	0.116	0.1	0.341	0.377	0.68	0.699
15	0.128	0.096	0.347	0.355	0.691	0.701
20	0.121	0.097	0.34	0.377	0.689	0.7
25	0.129	0.099	0.337	0.353	0.663	0.687
30	0.121	0.098	0.326	0.34	0.672	0.675
60	0.097	0.065	0.251	0.24	0.499	0.489
90	0.062	0.047	0.138	0.145	0.27	0.282
-5	0.107	0.101	0.313	0.343	0.652	0.67
-10	0.116	0.095	0.298	0.297	0.654	0.673
-15	0.107	0.091	0.291	0.321	0.608	0.642
-20	0.092	0.092	0.274	0.334	0.567	0.636
-25	0.091	0.079	0.275	0.319	0.563	0.62
-30	0.085	0.072	0.243	0.277	0.497	0.578
-60	0.055	0.049	0.143	0.146	0.281	0.365
-90	0.057	0.047	0.12	0.157	0.256	0.312

**Table 9 A comparison of numerical and measured side wall shear stress data.**

RPM	Flow depth (mm)	Probe height (m)	Poly S.W. results		HR measurements	
			Inside stress (Nm <sup>-2</sup> )	Outside stress (Nm <sup>-2</sup> )	Inside stress (Nm <sup>-2</sup> )	Outside stress (Nm <sup>-2</sup> )
1.06	50	0.02			0.009	0.092
1.59	50	0.02			0.03	0.226
2	50	0.02			0.05	0.384
2.12	50	0.02	0.08	0.295	0.05	0.42
2.65	50	0.02			0.087	0.649
3.18	50	0.02			0.145	0.886
3.7	50	0.02	0.25	1.32	0.197	1.332
1.06	100	0.02	0.035	0.09	0.02	0.054
1.59	100	0.02	0.07	0.17	0.049	0.122
2	100	0.02	0.095	0.255	0.077	0.209
2.65	100	0.02	0.165	0.425	0.126	0.362
3.18	100	0.02	0.23	0.59	0.188	0.544
3.7	100	0.02	0.305	0.78	0.256	0.768
1.06	200	0.02			0.013	0.025
1.59	200	0.02			0.043	0.064
2	200	0.02			0.065	0.12
2.12	200	0.02	0.099	0.175	0.075	0.123
2.65	200	0.02			0.112	0.217
3.18	200	0.02			0.167	0.314
3.7	200	0.02	0.255	0.485	0.218	0.447
1.06	100	0.07	0.03	0.15	0.008	0.087
1.59	100	0.07	0.055	0.3	0.023	0.211
2	100	0.07	0.08	0.445	0.048	0.375
2.65	100	0.07	0.12	0.73	0.098	0.687
3.18	100	0.07	0.165	1	0.129	0.988
3.7	100	0.07	0.215	1.3	0.195	1.337



## ***Figures***



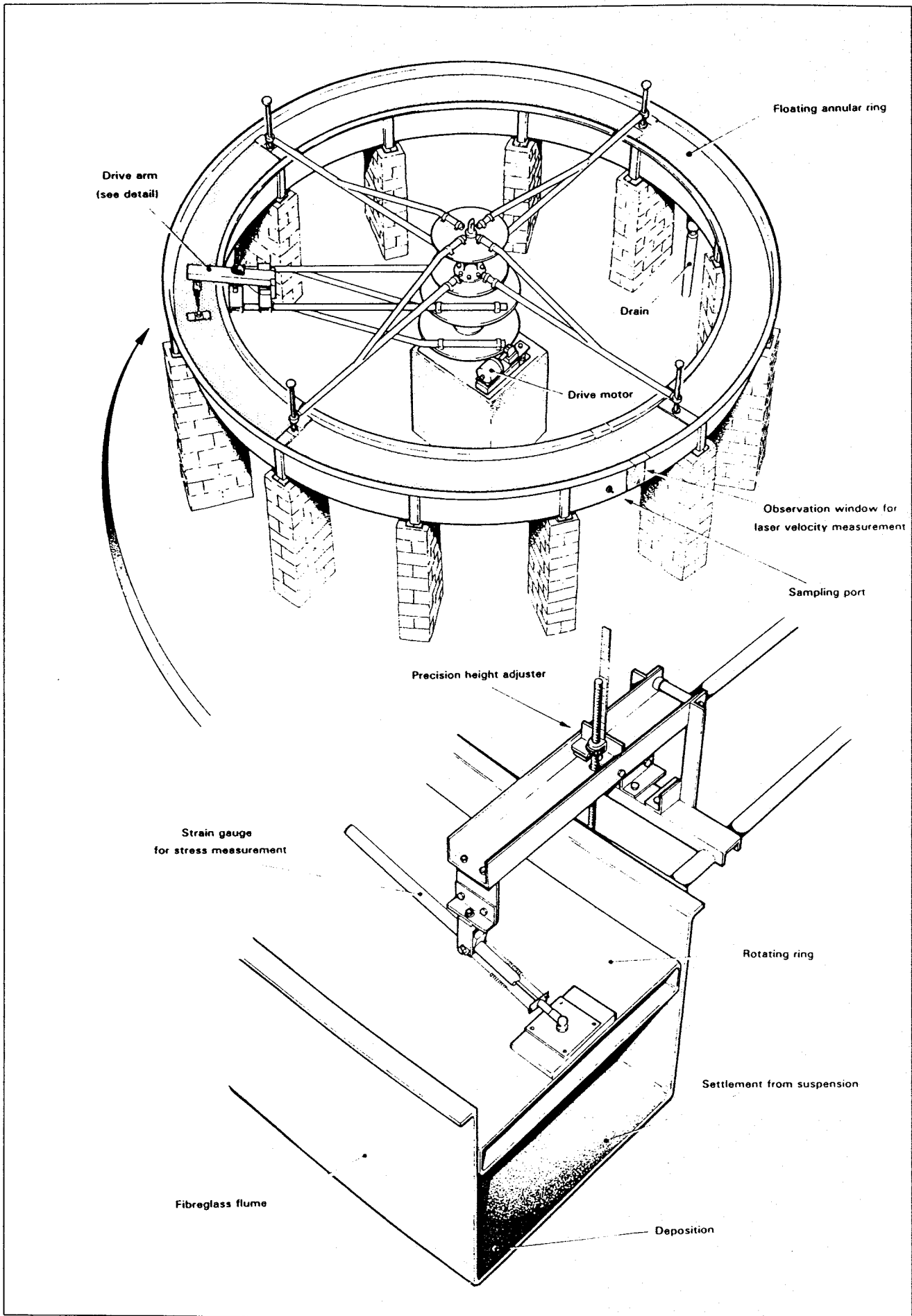


Fig 1 The carousel

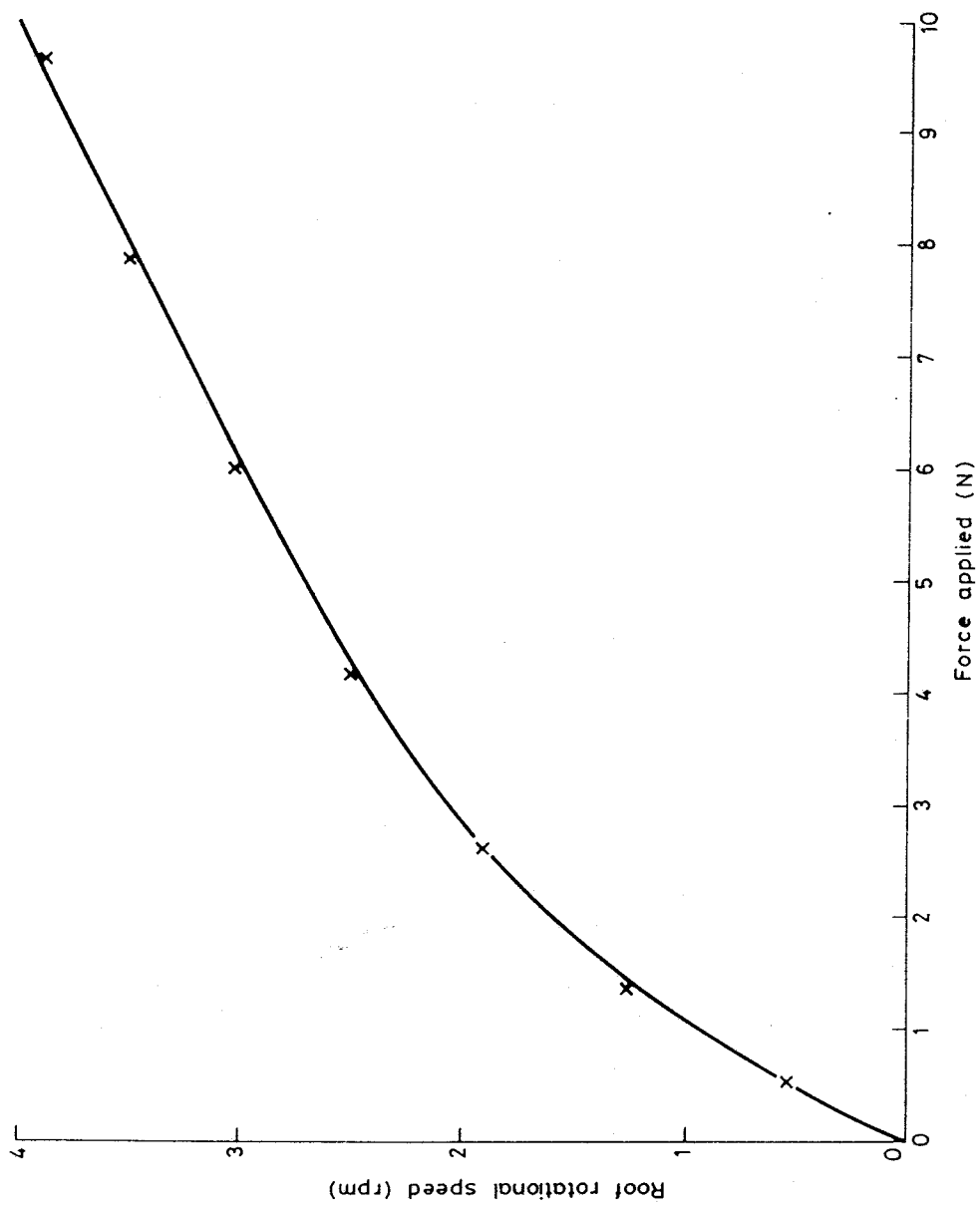


Fig 2 Energy input calibration

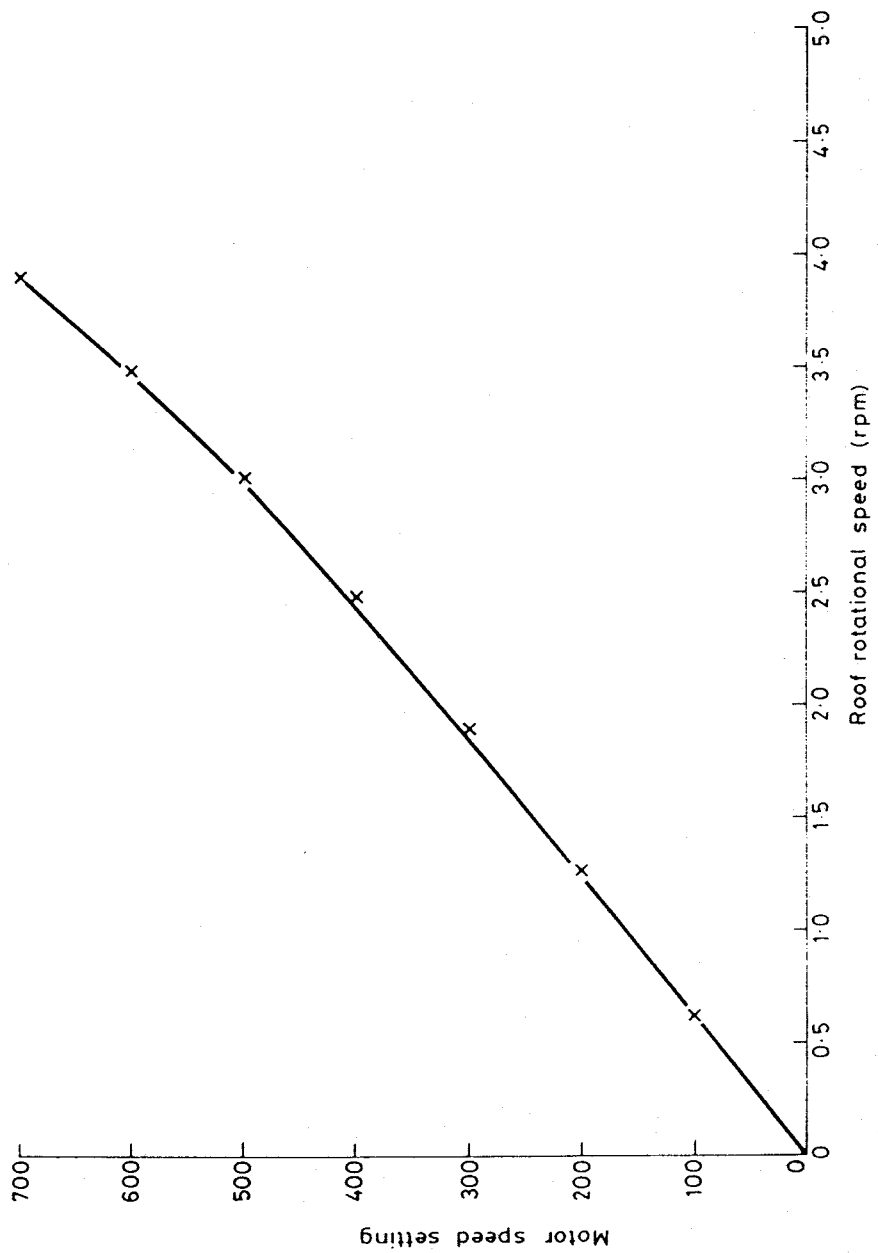


Fig 3 Roof speed calibration

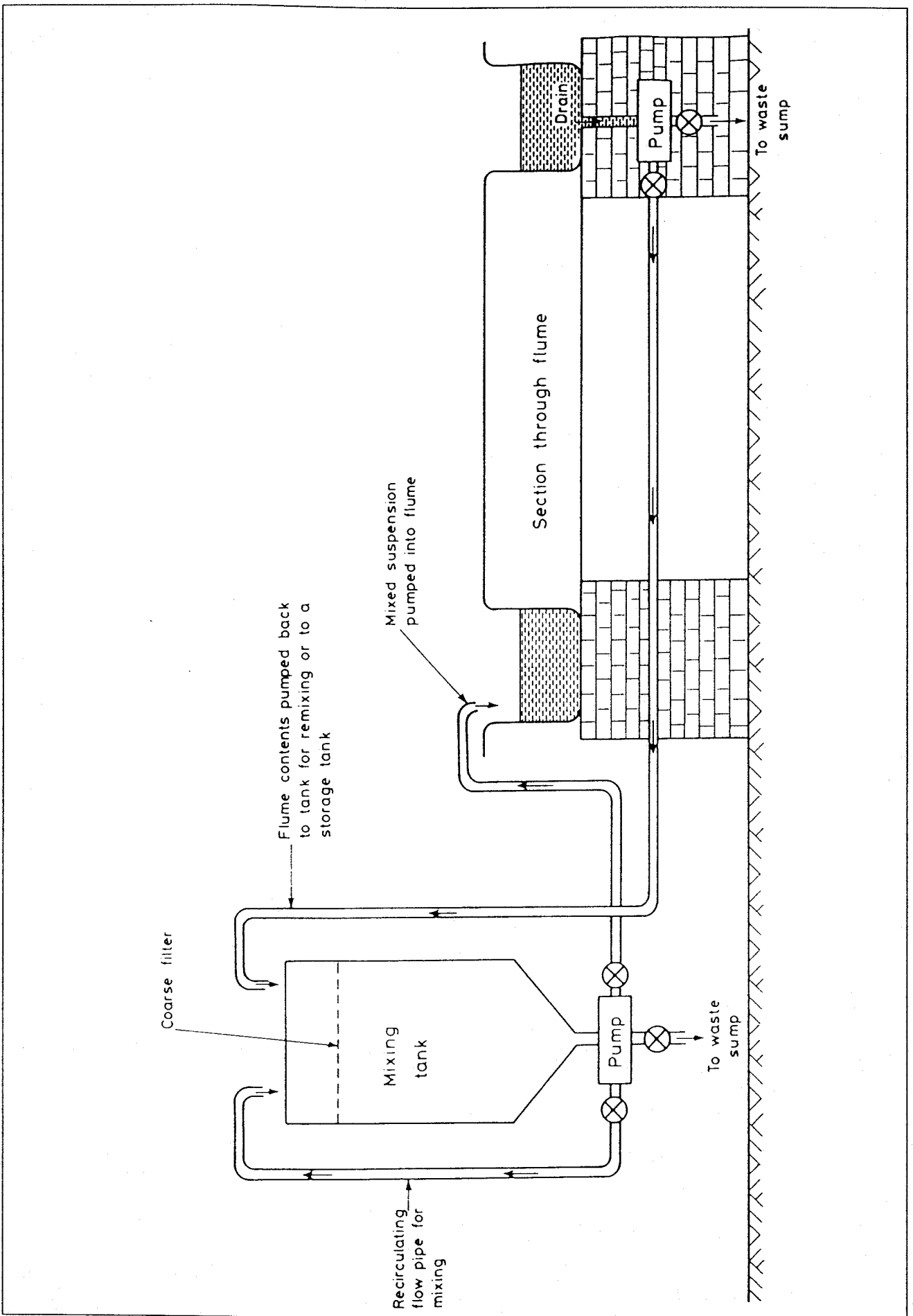
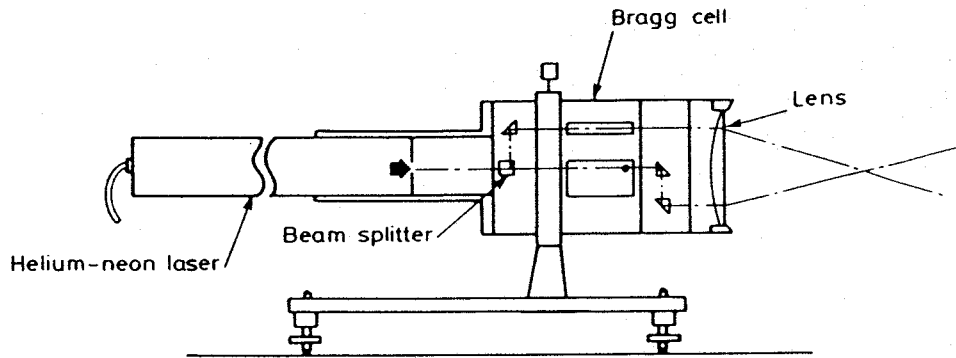
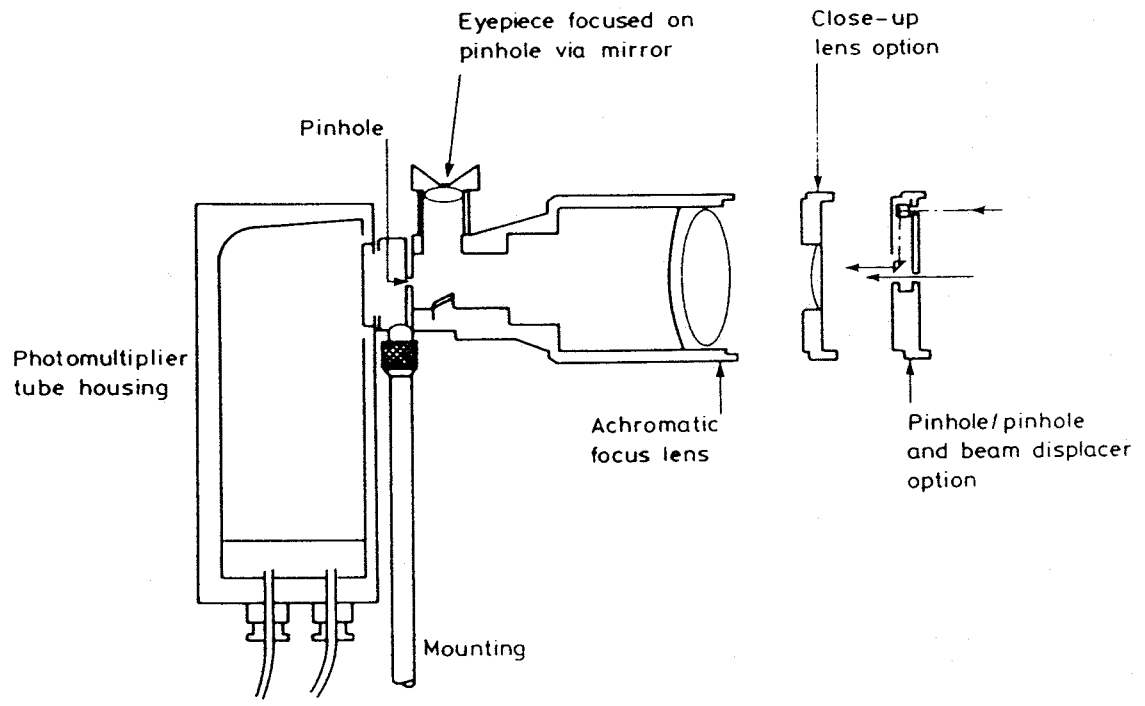


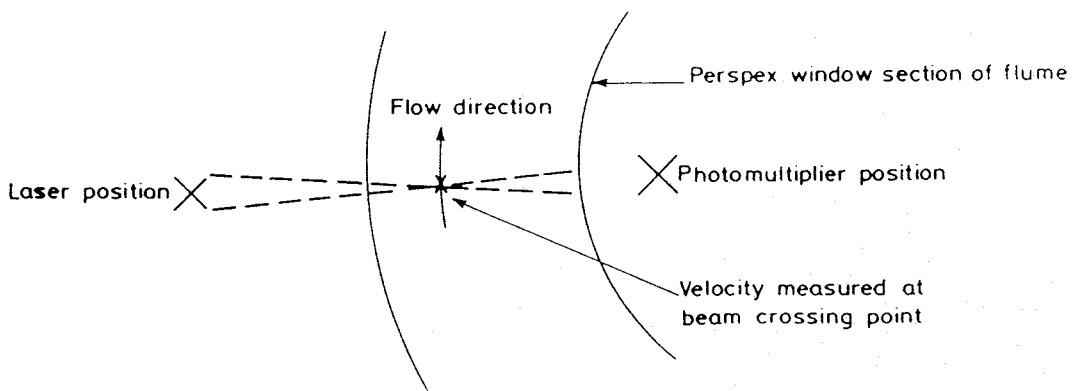
Fig 4 Filling and emptying system



(a) Laser optical unit



(b) Photomultiplier optical unit



(c) Velocity measuring position

Fig 5 The laser velocity meter

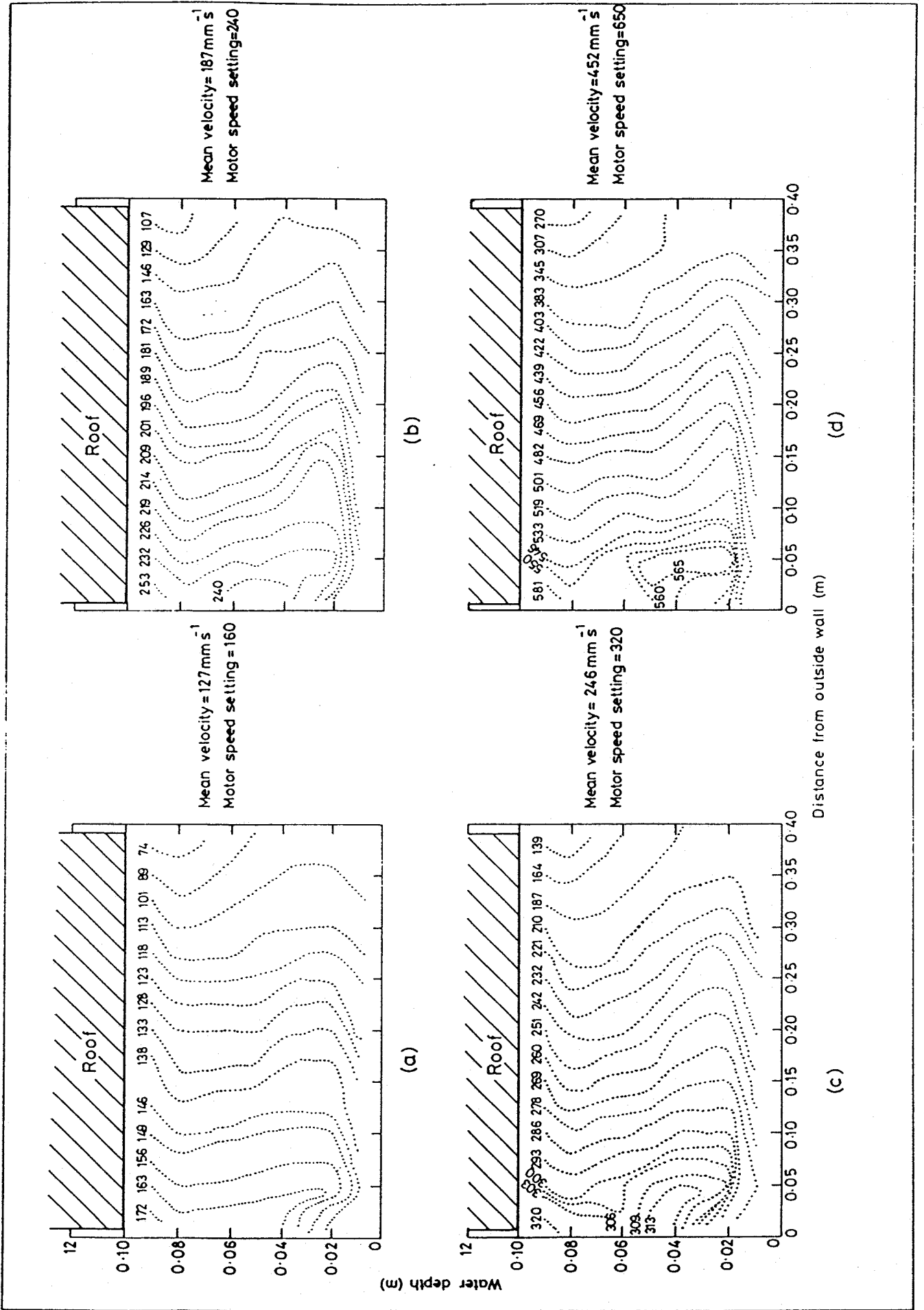
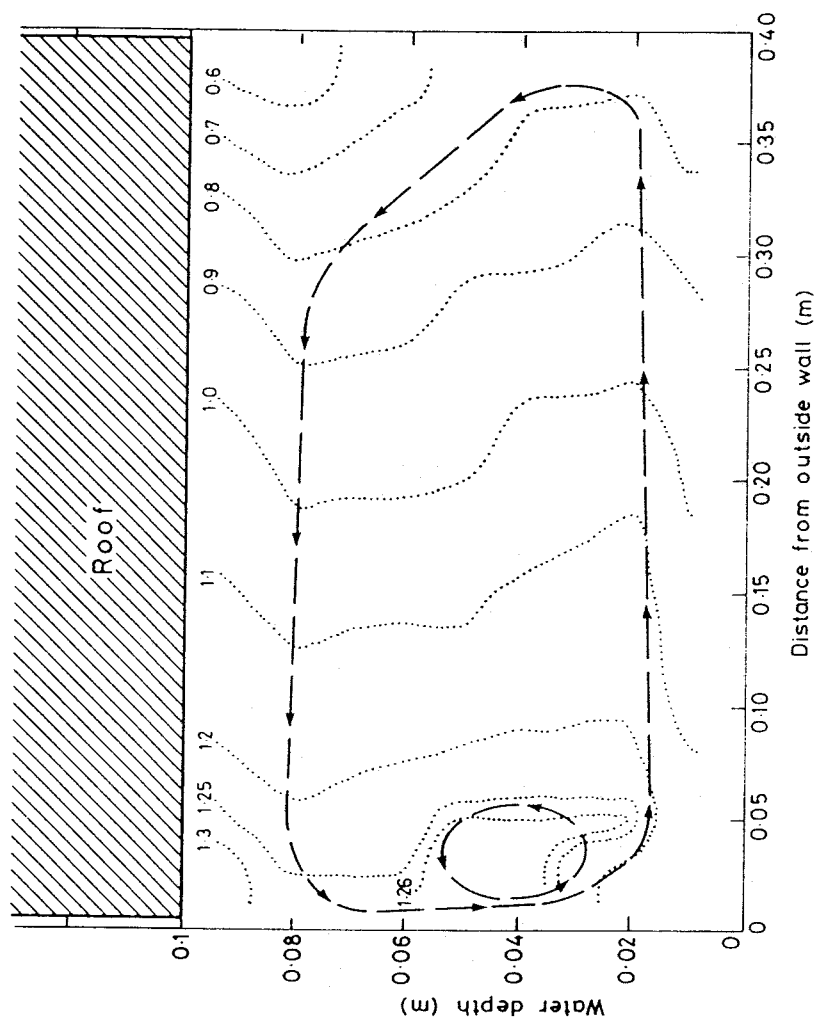


Fig 6 Cross-sectional velocity contours (adapted from SR33)



Note  
Direction of flow into  
page

Velocity contours  
normalised to cross-  
sectional mean velocity

.....  
Isovel (line of equal  
velocity)

---  
Suggested route of  
secondary flow

Fig 7

Generalised velocity contours and  
suggested route of secondary flow  
(adapted from SR33)

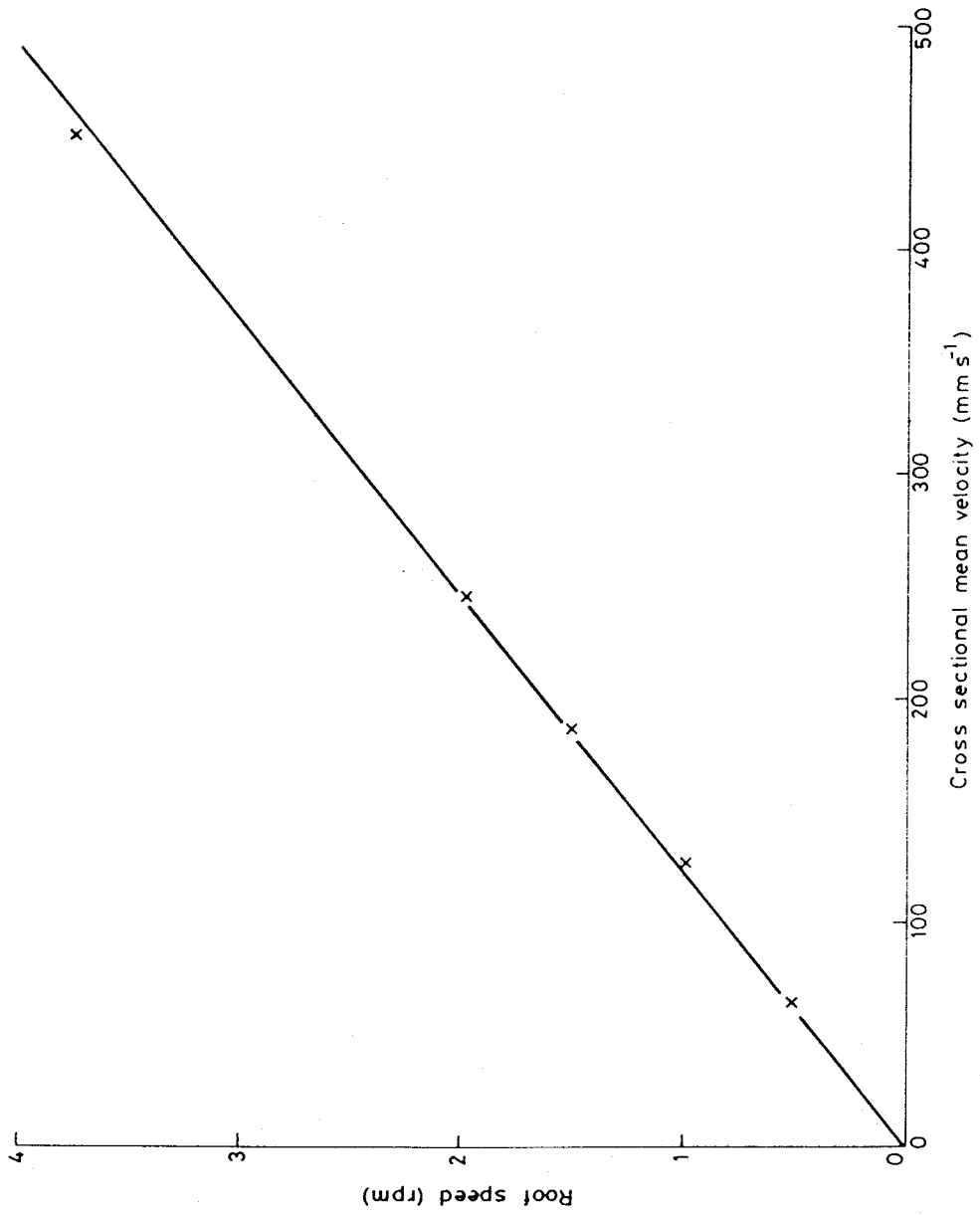


Fig 8 Roof speed versus cross-sectional mean velocity

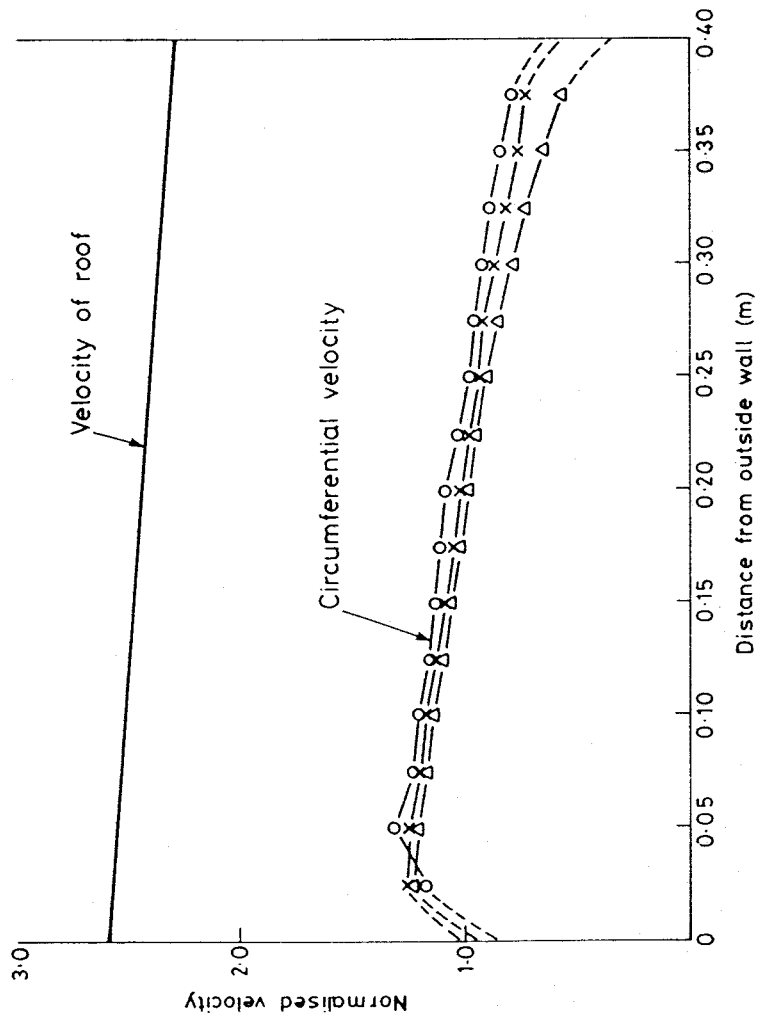


Fig 9 Velocity variation across the width

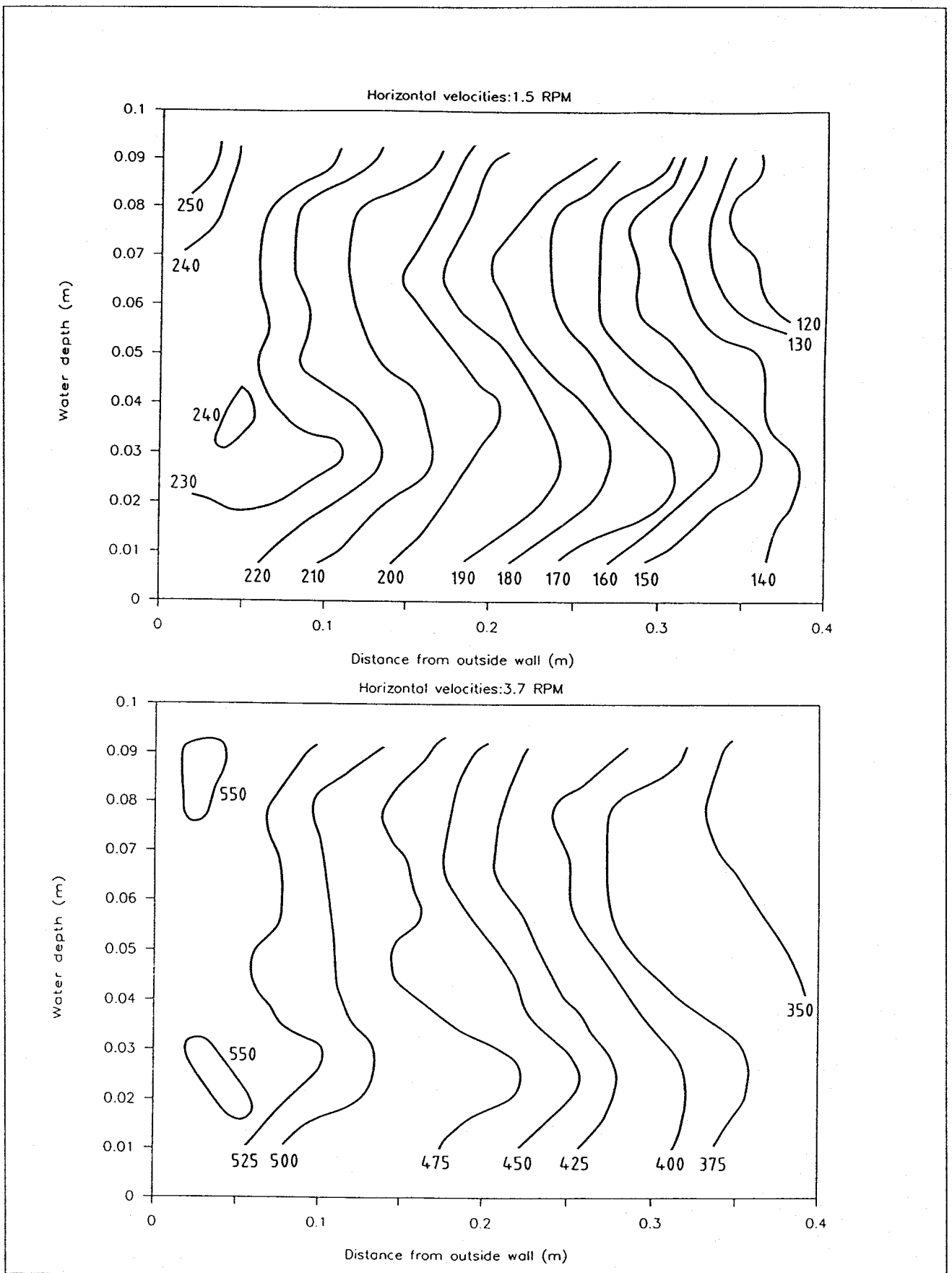


Fig 10 Plot showing horizontal velocity isovels for two roof rotation rates and a fluid depth of 0.1m.

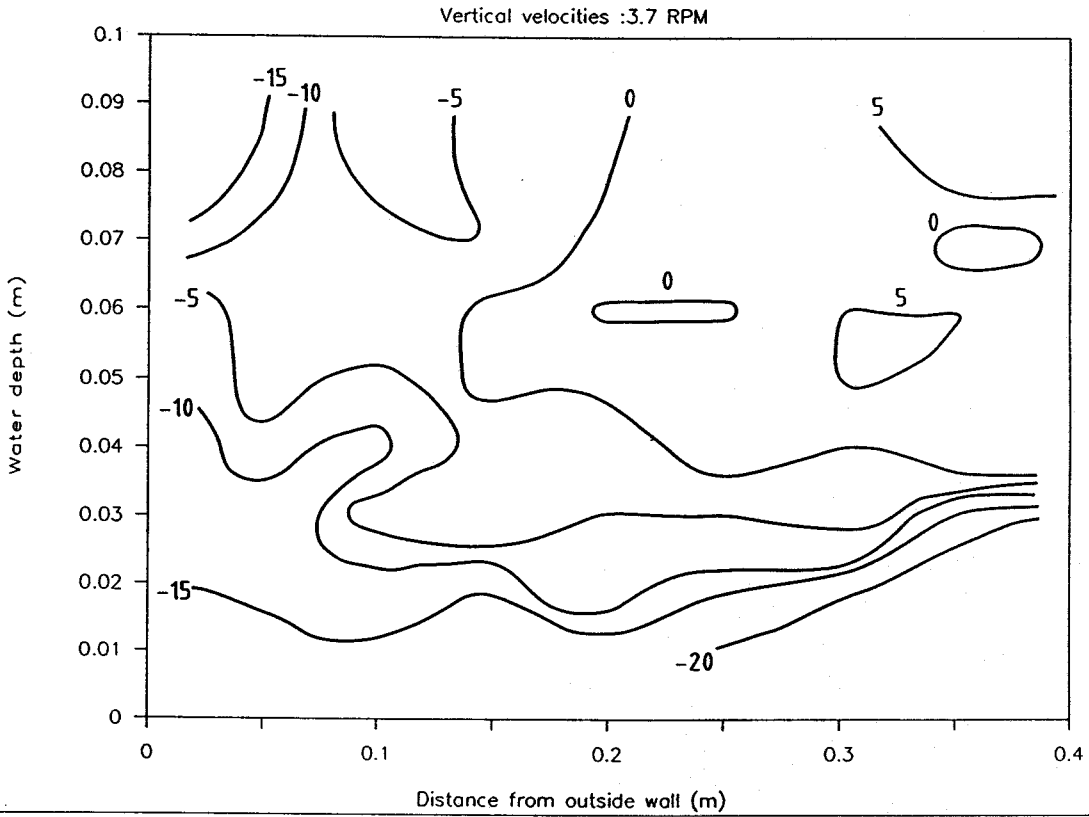
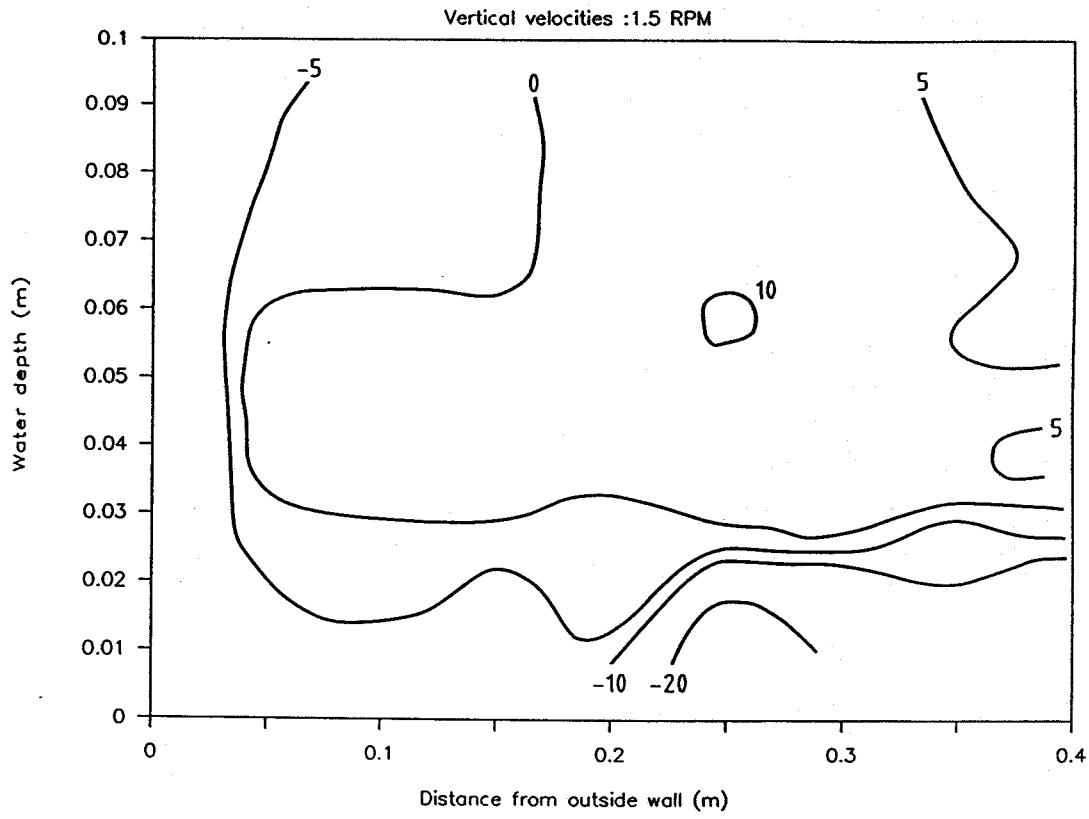


Fig 11 Plot showing typical vertical velocity isovels for roof rotation rate indicated and a fluid depth of 0.1m.

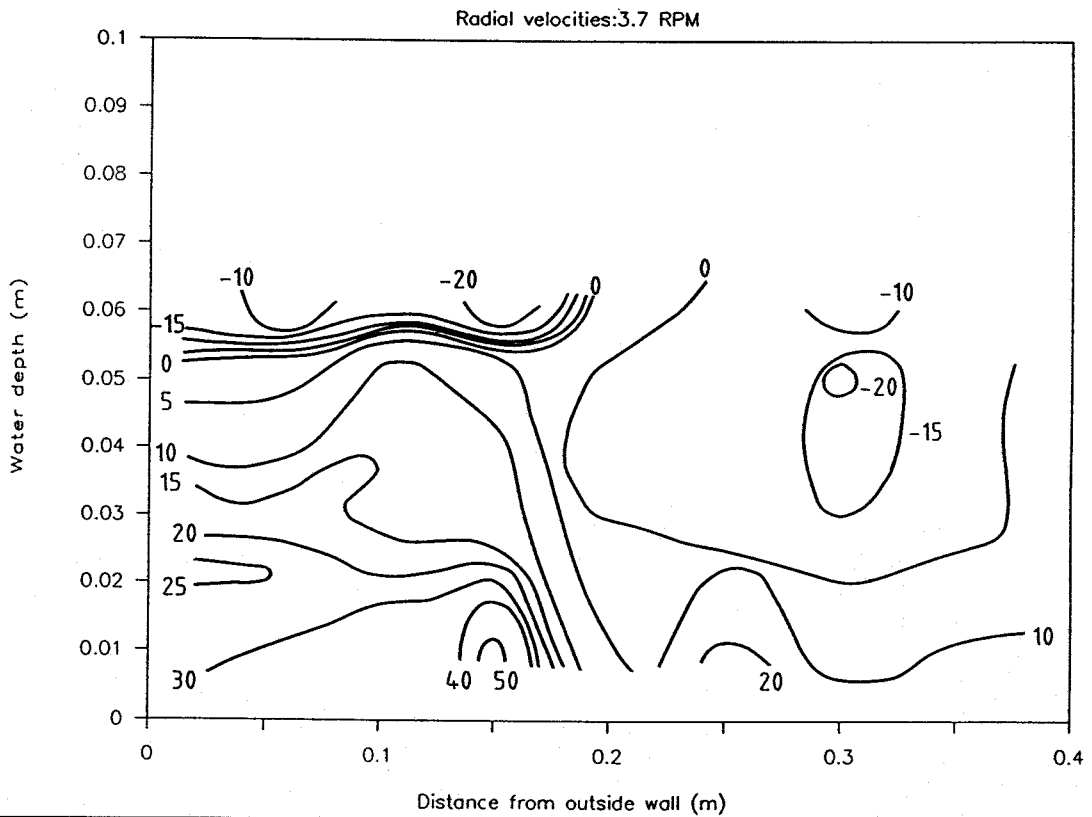
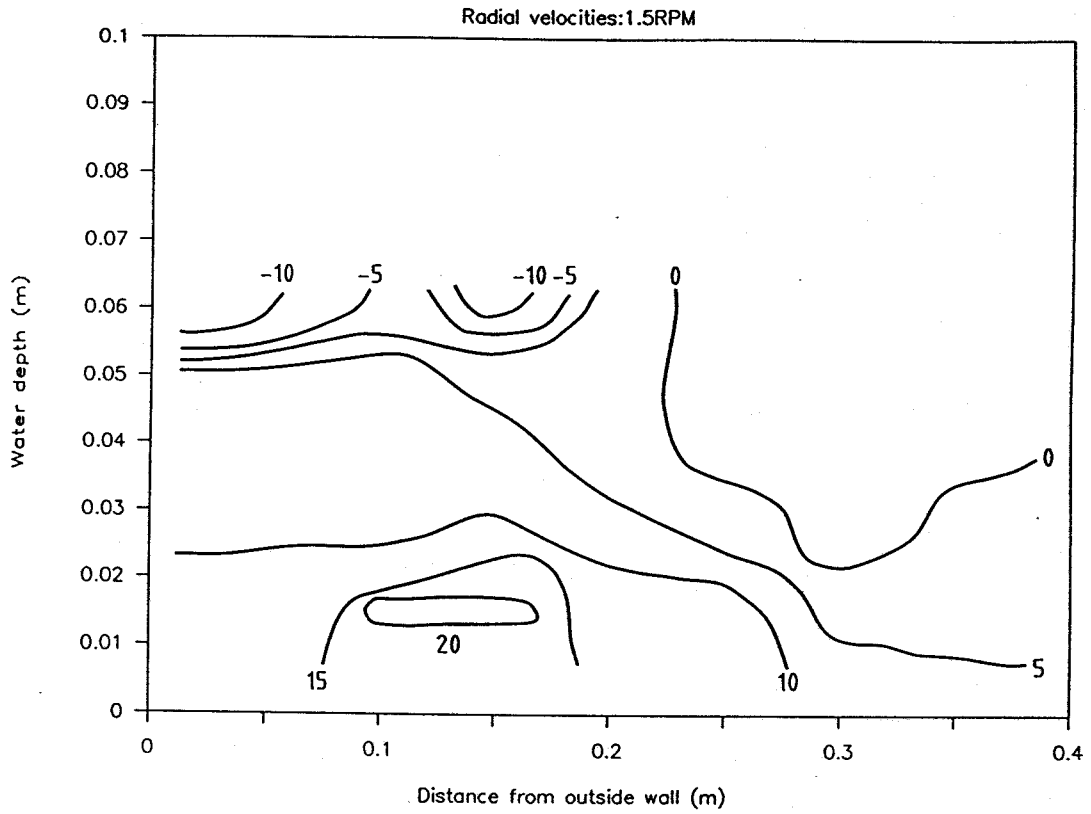


Fig 12. Plot showing typical radial velocity isovels for roof rotation rates indicated and a fluid depth of 0.1m.

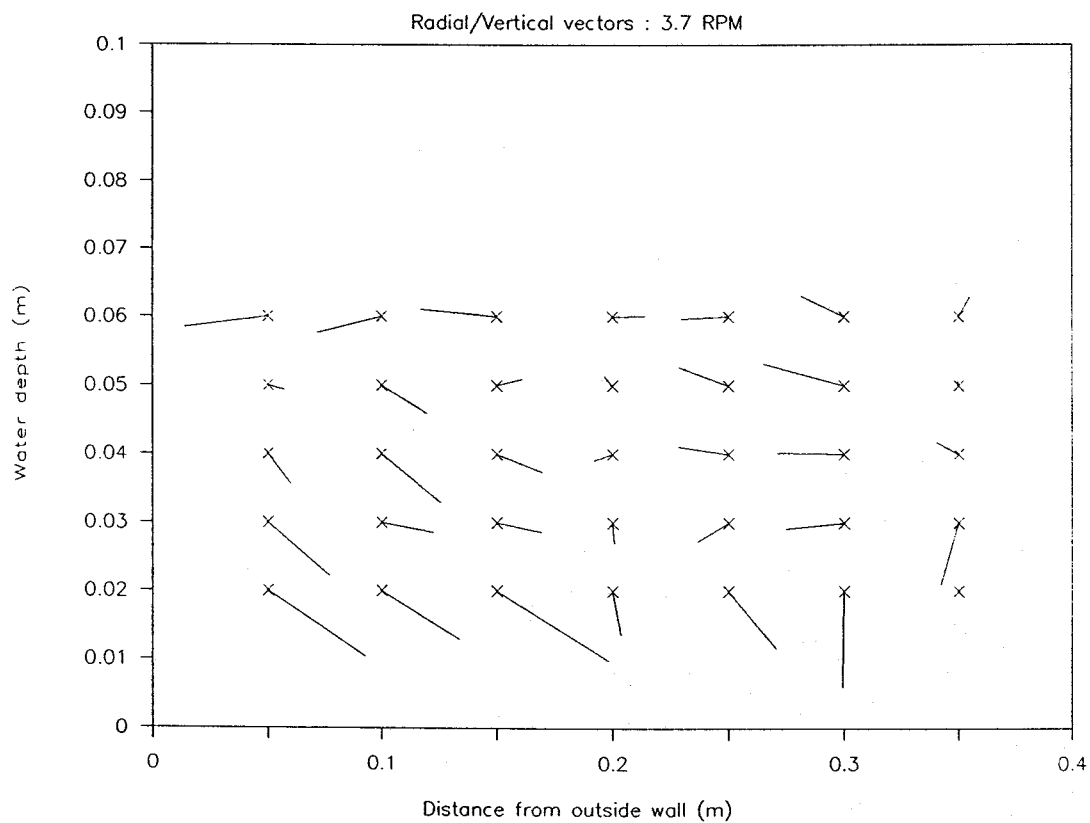
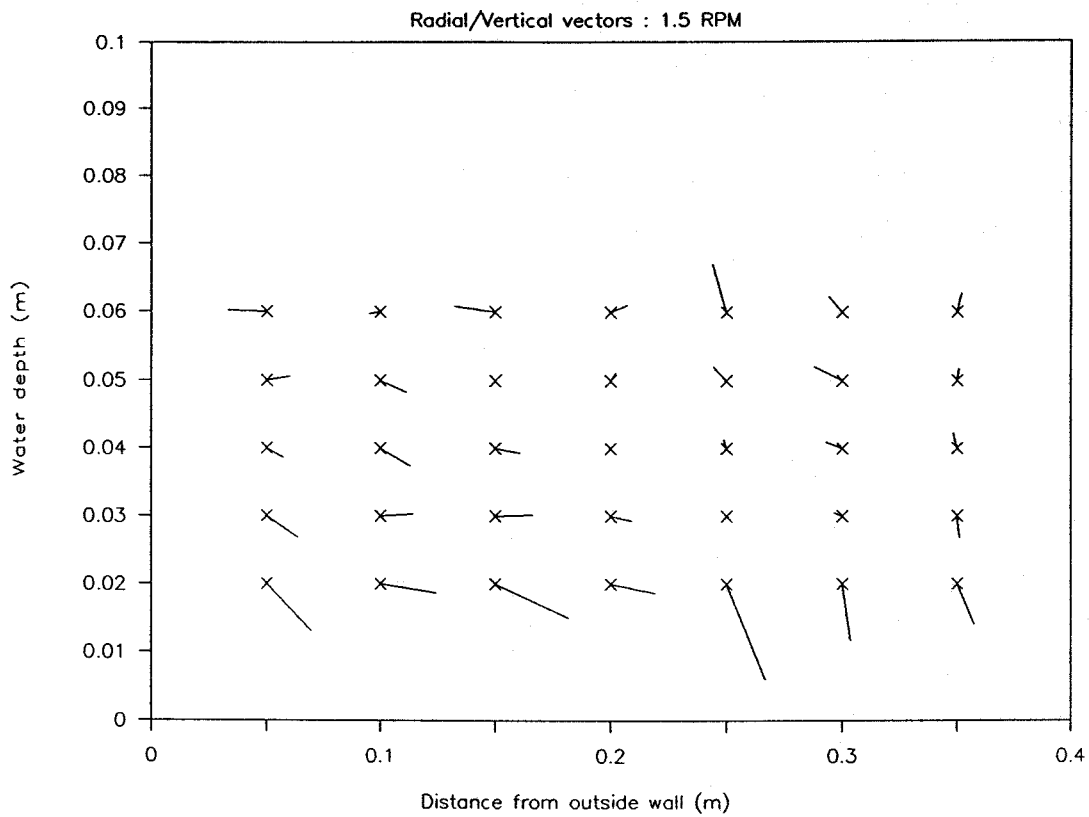


Fig 13 Flume cross sections showing typical vertical/radial velocity vector diagrams for a fluid depth of 0.1m and roof rotation rates indicated.

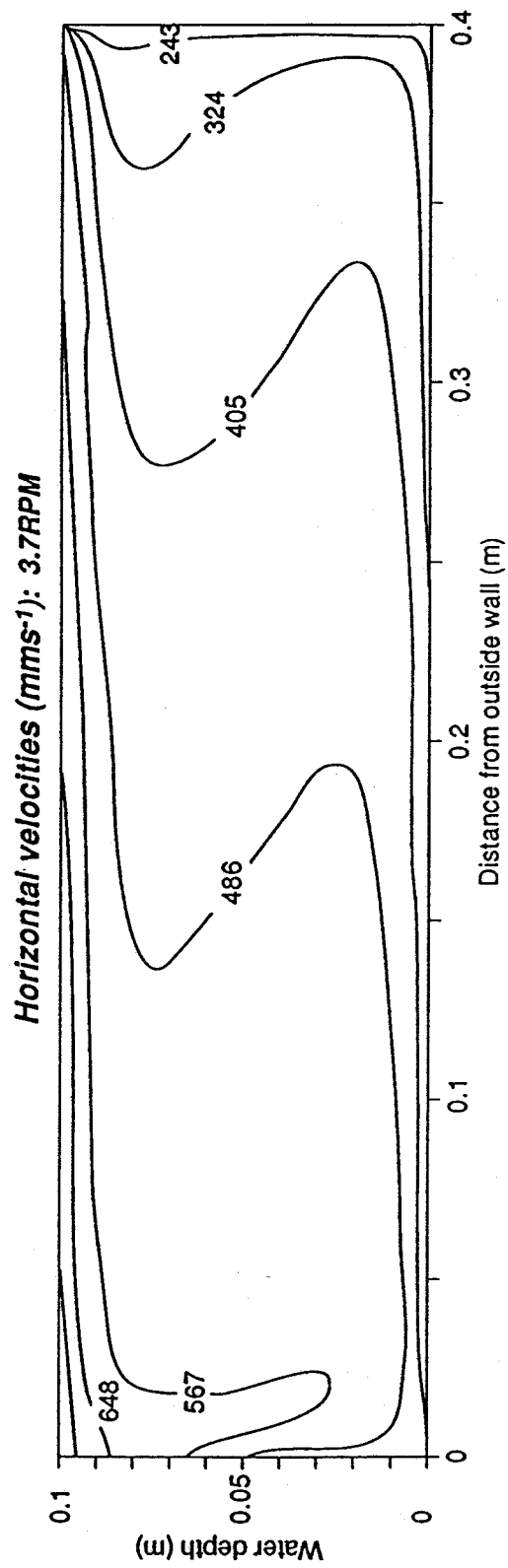


Fig 14 Typical PSW isovel pattern

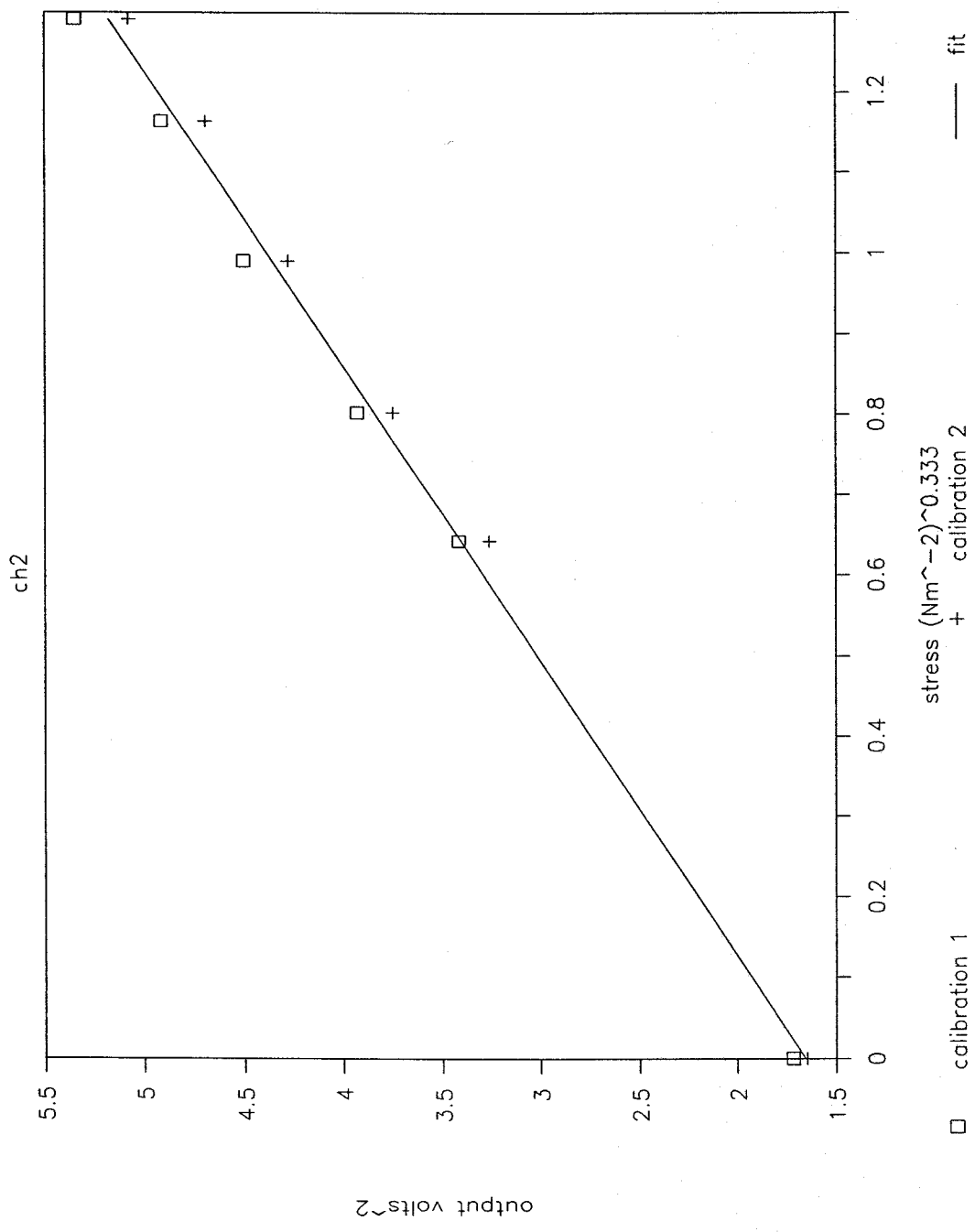


Fig 15 Typical shear stress probe calibration curve

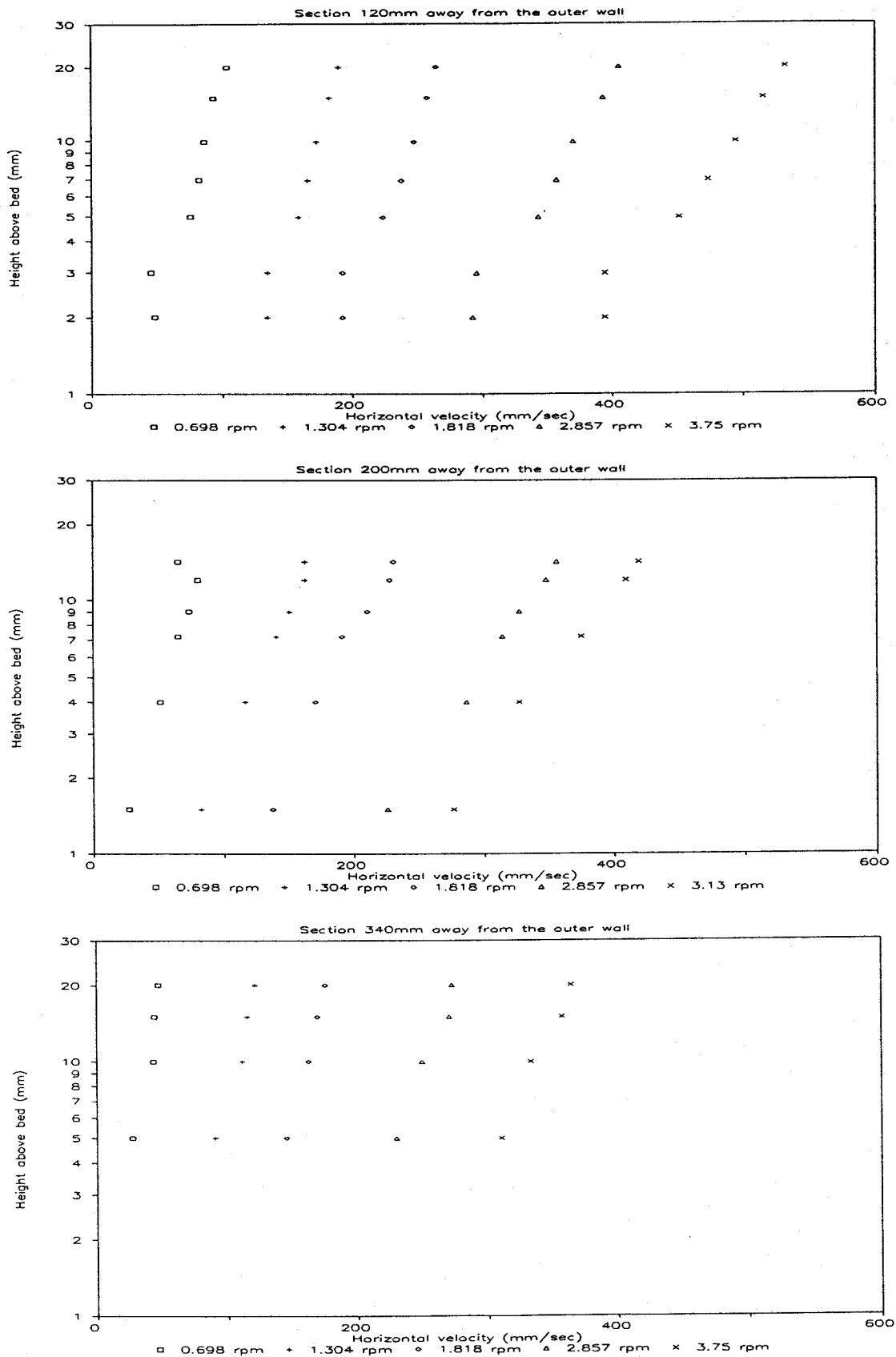


Fig 16 Graph showing near bed velocity profiles for three cross-flume positions for varying lid rotation rates.

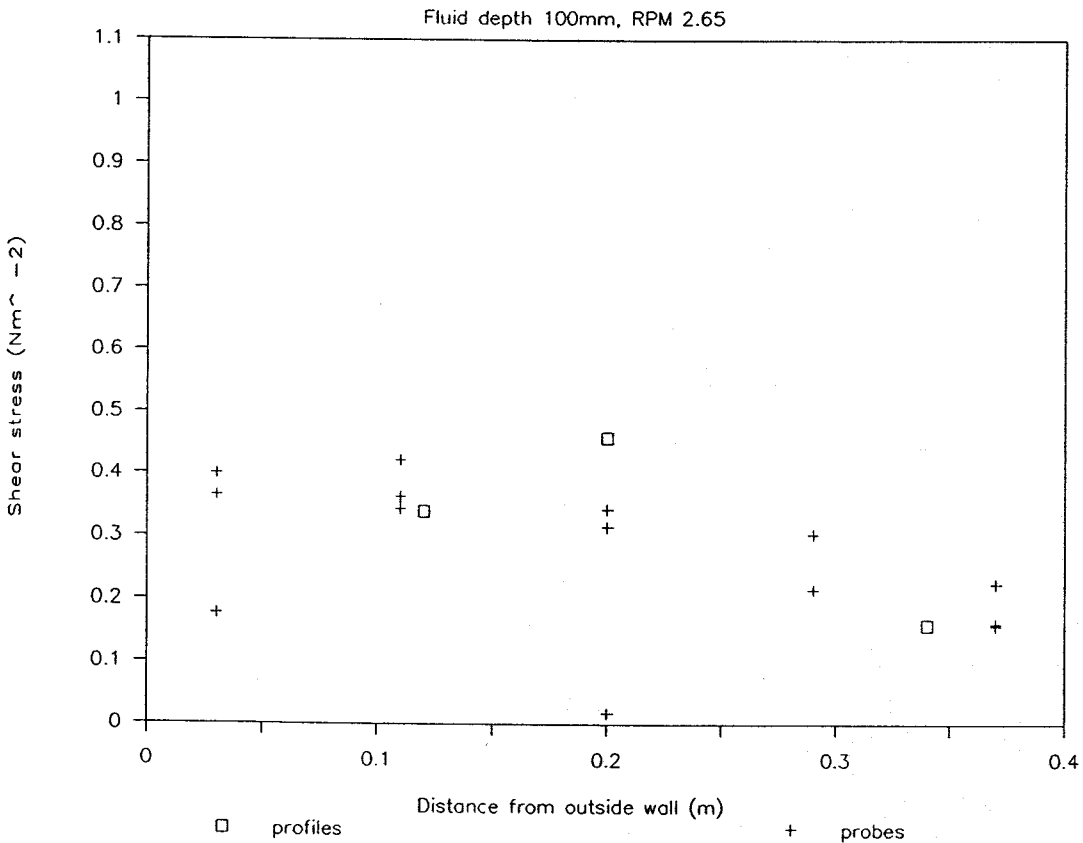
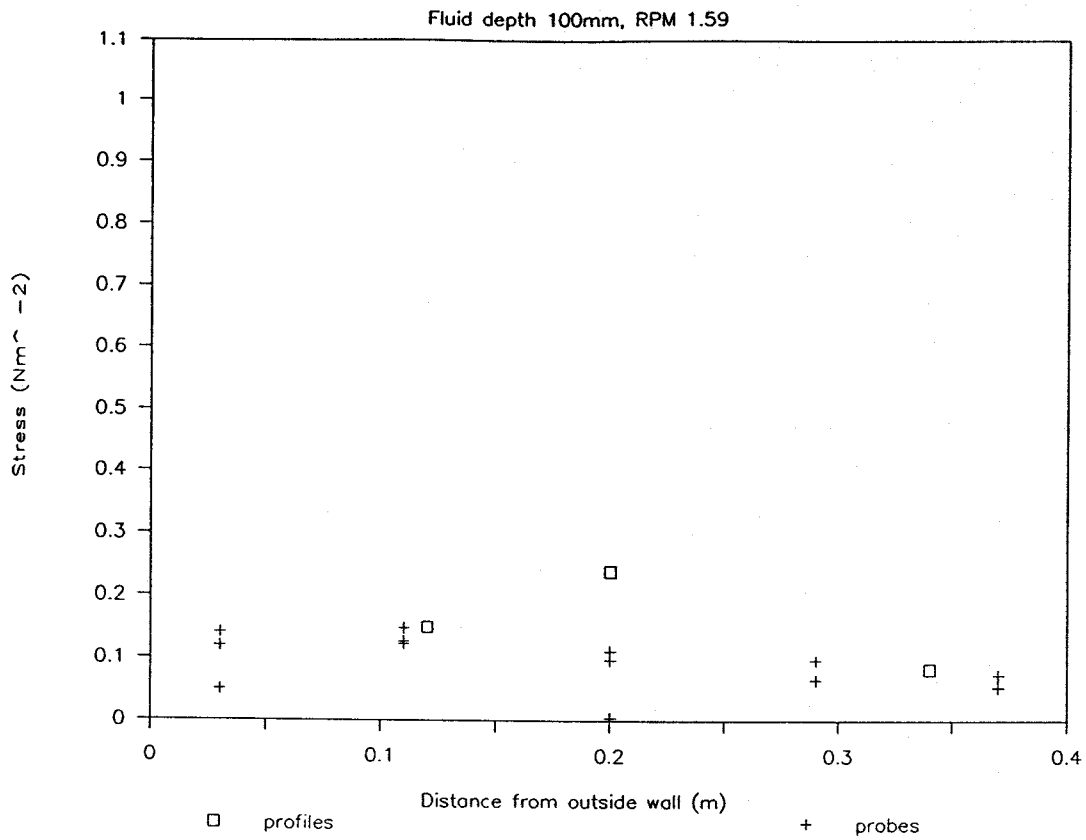


Fig 17 A comparison of shear stress measured by the probes and derived from near bed velocity profiles.

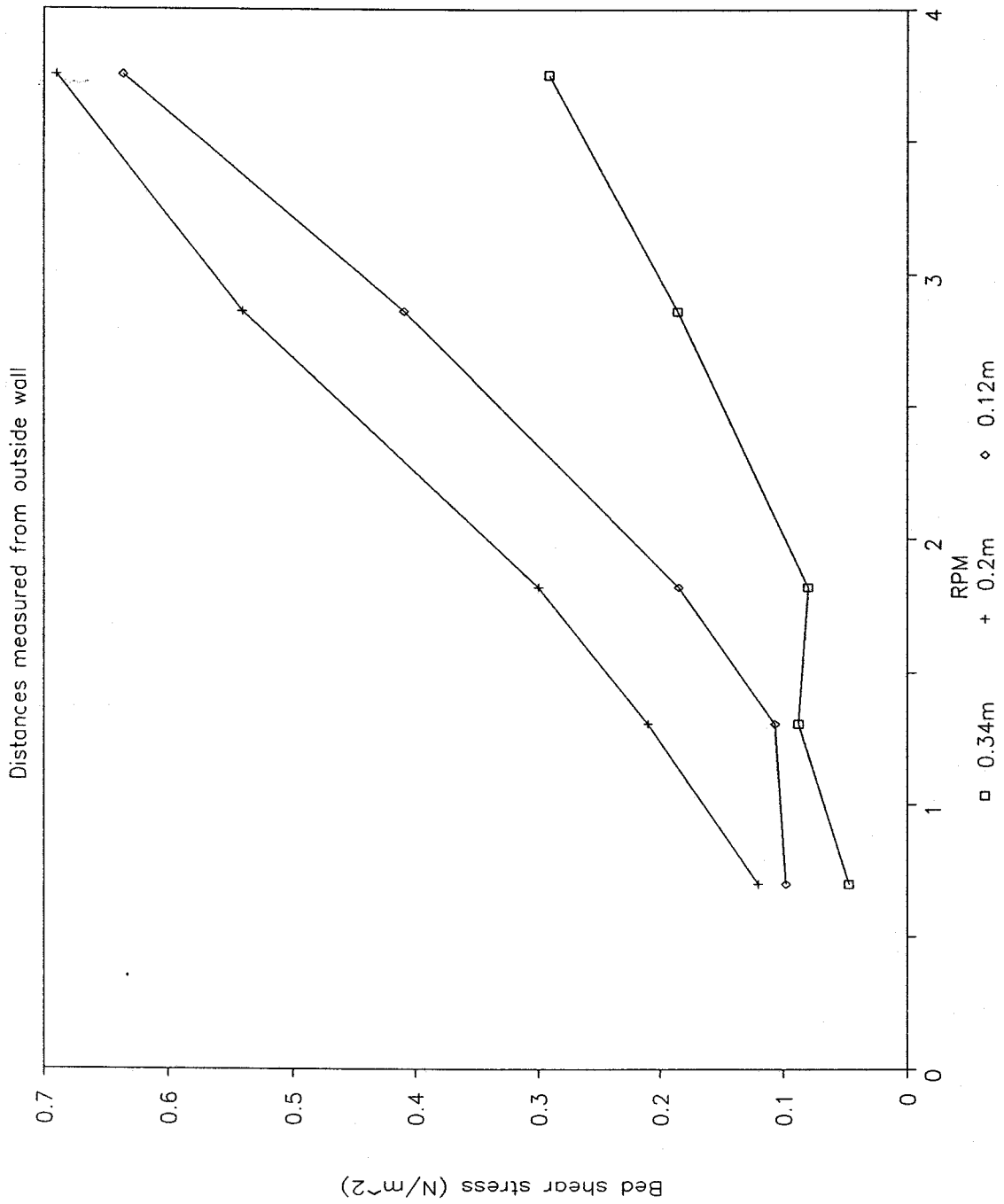


Fig 18 Bed shear stress values versus roof speed for three cross flume positions. Stress values derived from laser velocity profiles.

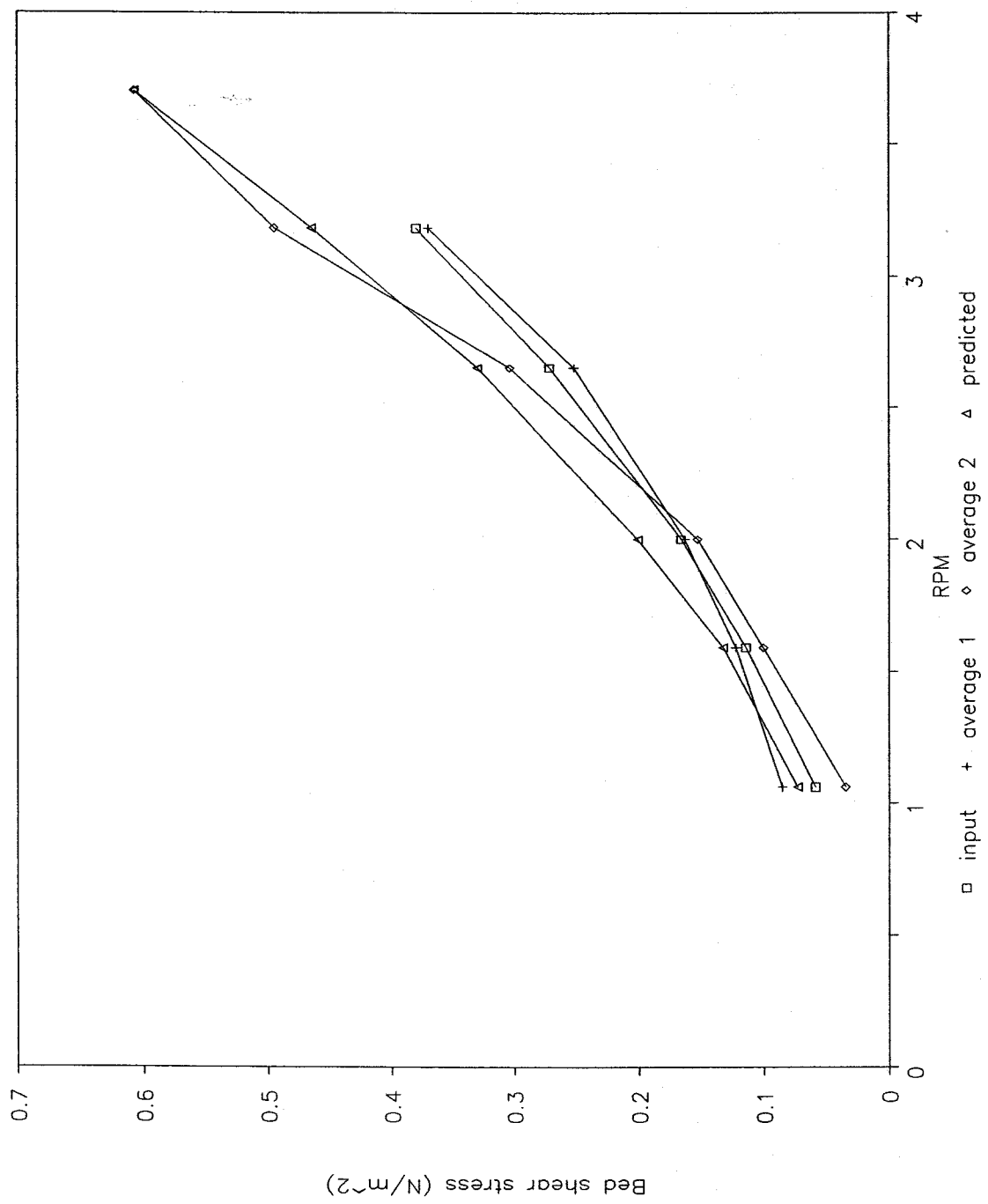


Fig 19 Average bed shear stress values against roof speed

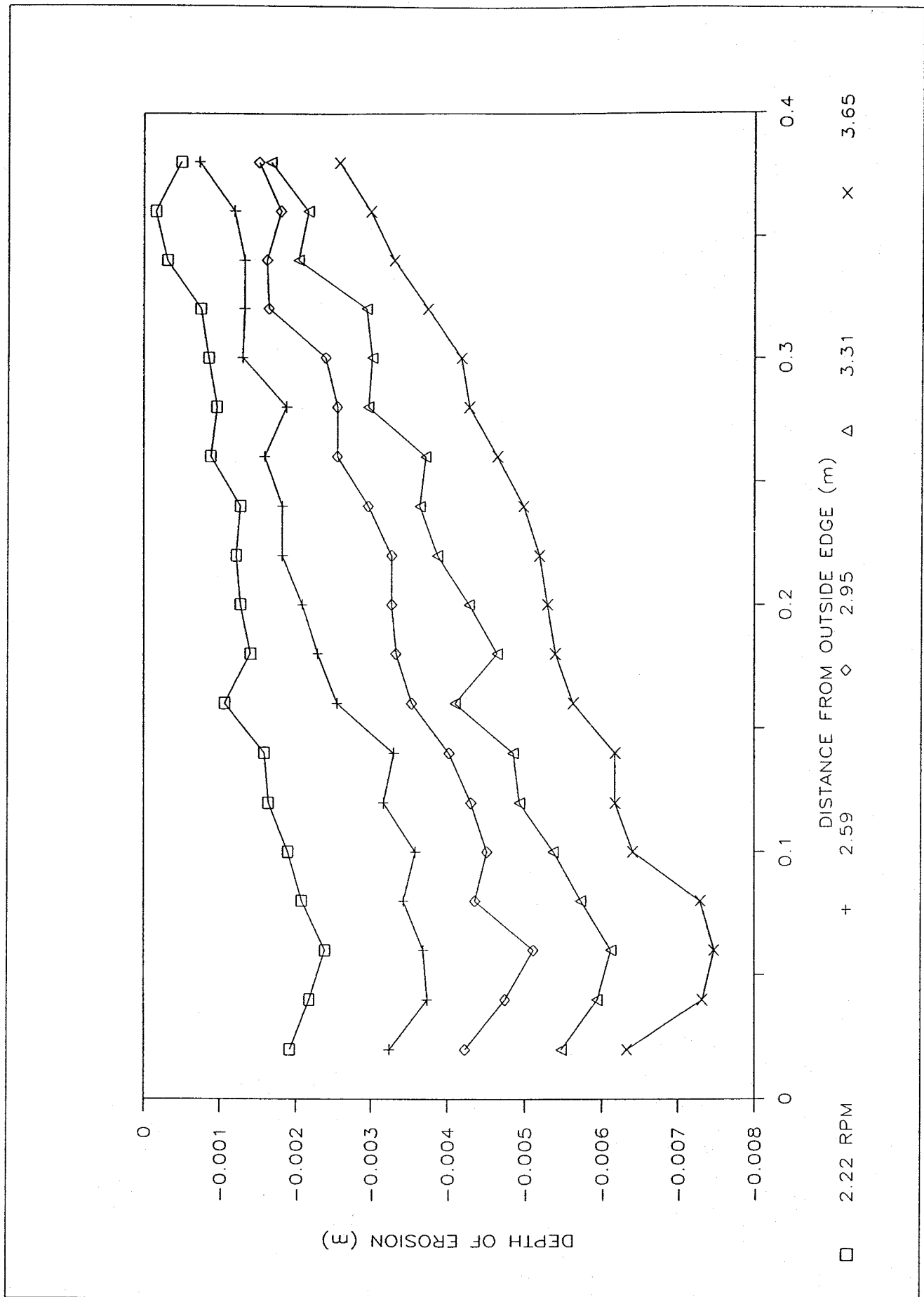


Fig 20a Graph showing typical erosion profiles across the flume for a number of lid rotation rates indicated.

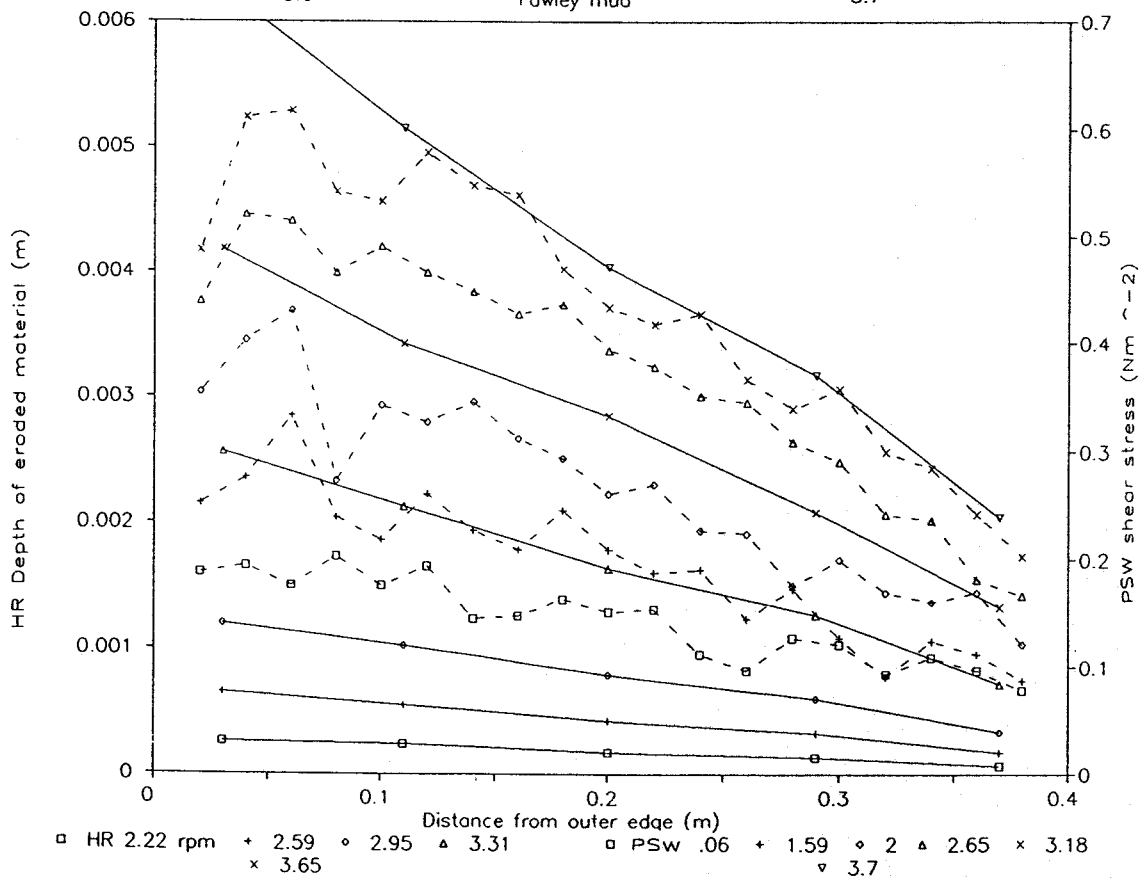
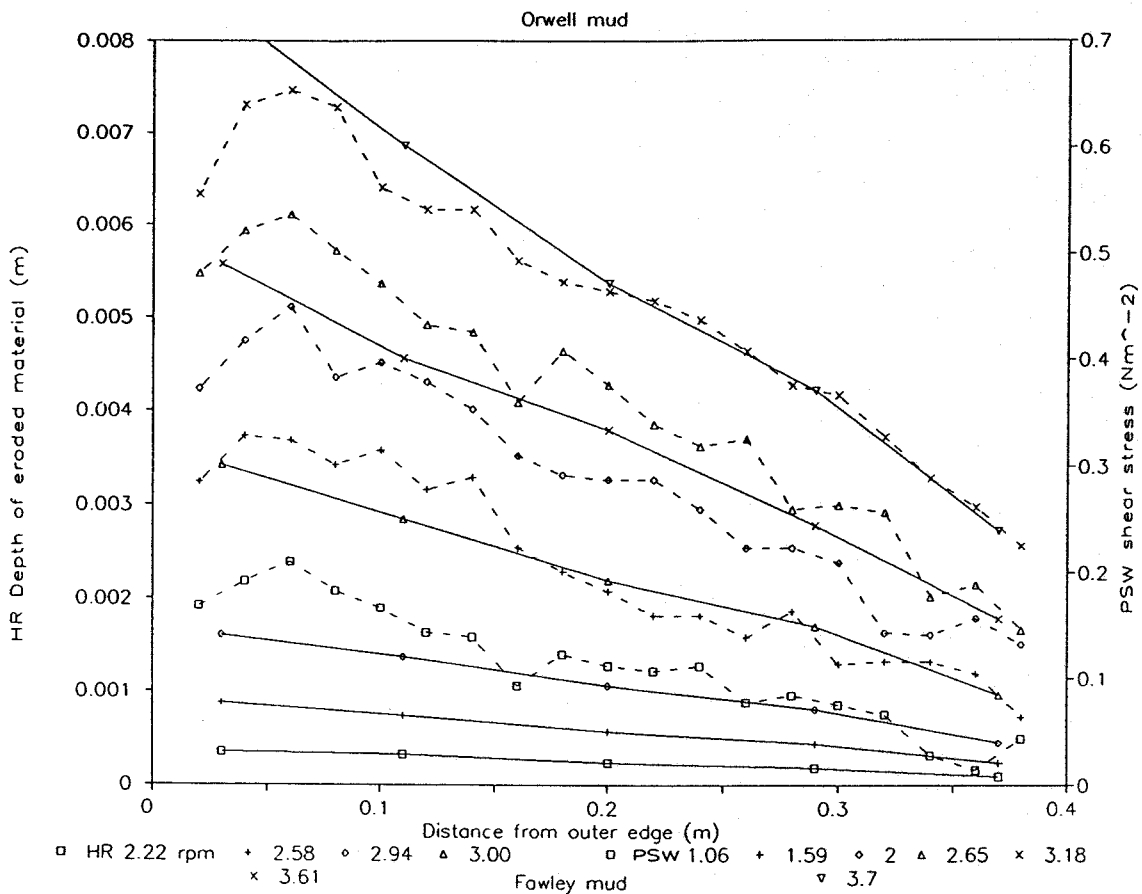


Fig 20b Graphs showing the relationship between depth of erosion and bed shear stress predicted by the PSW numerical model.

# Plymouth stress determinations

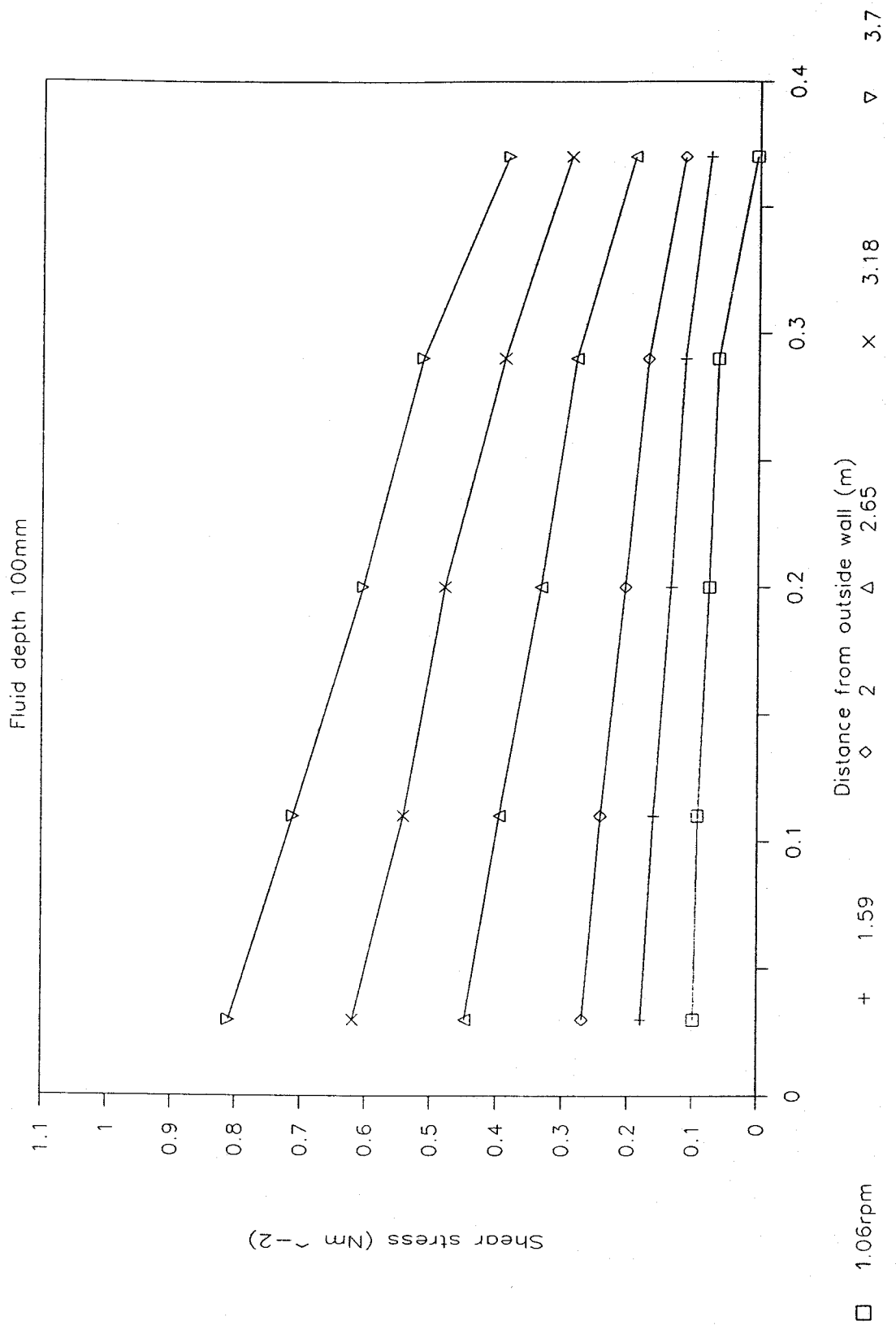


Fig 21 A composite plot summarizing PSW bed shear stress results.

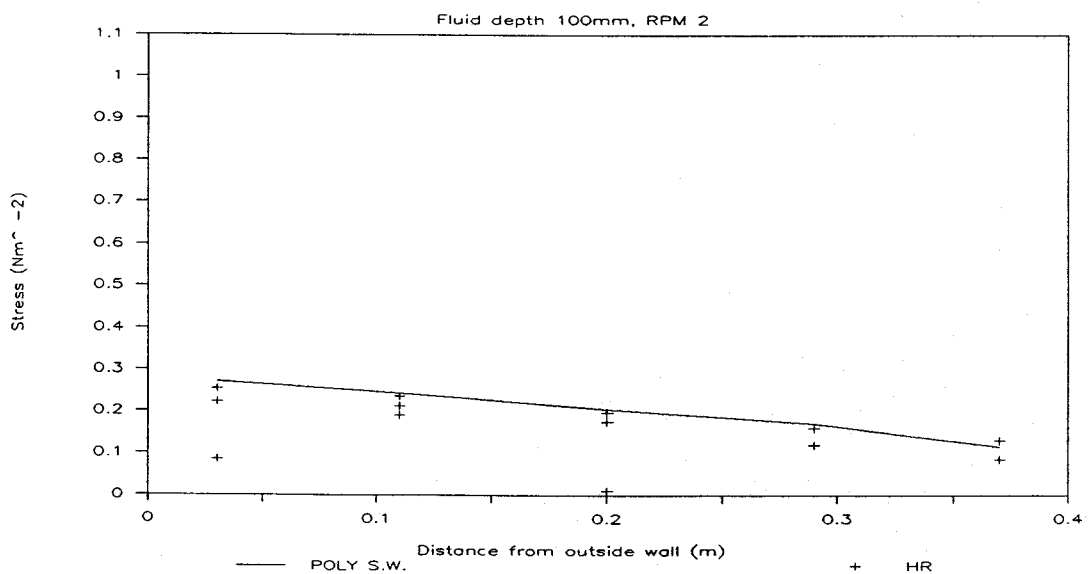
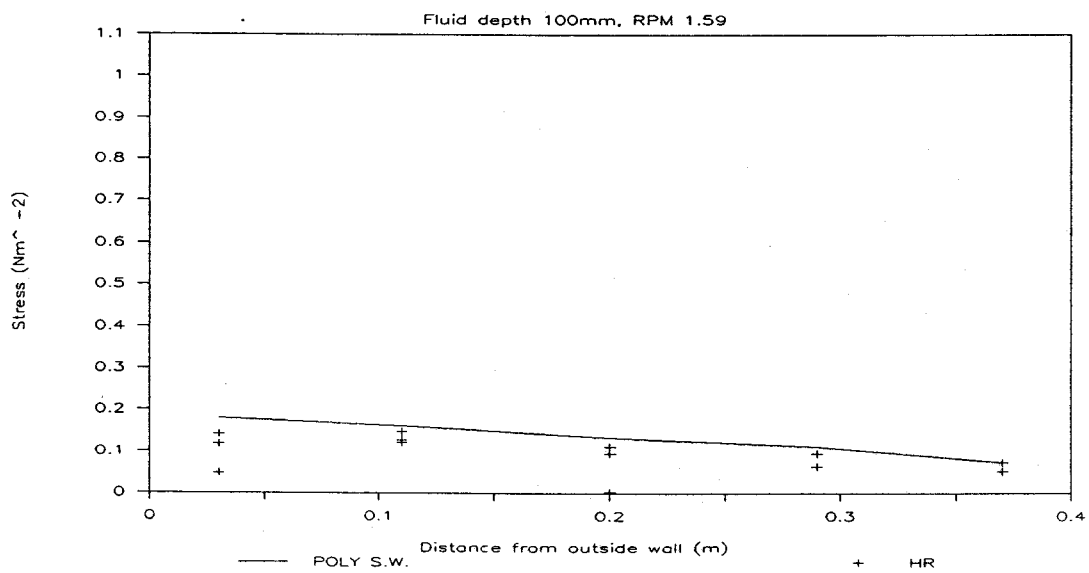
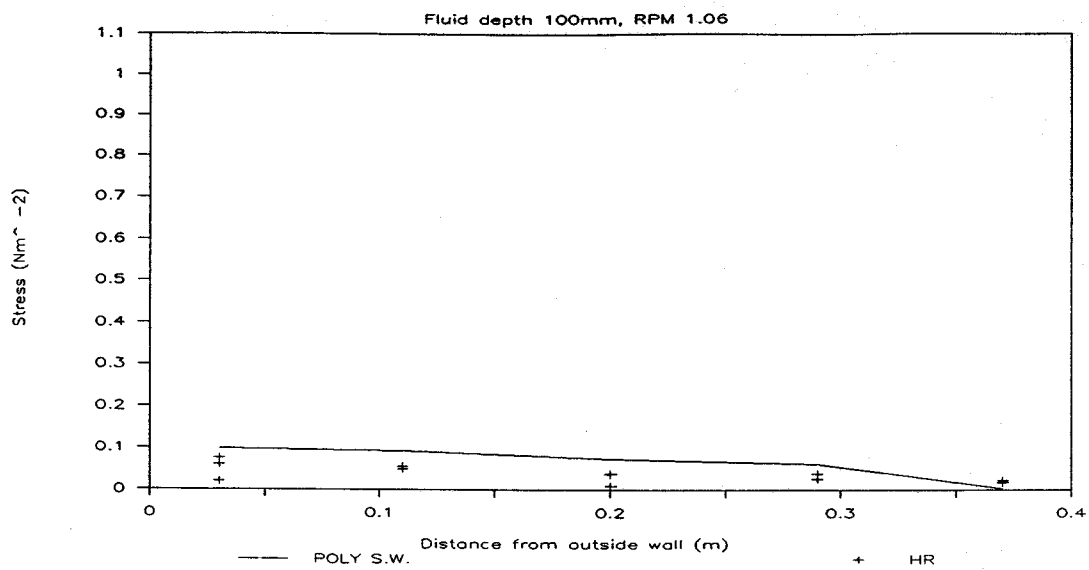


Fig 22 Graphs comparing carousel bed shear stress data with PSW mathematical model results for a fluid depth of 0.1m.

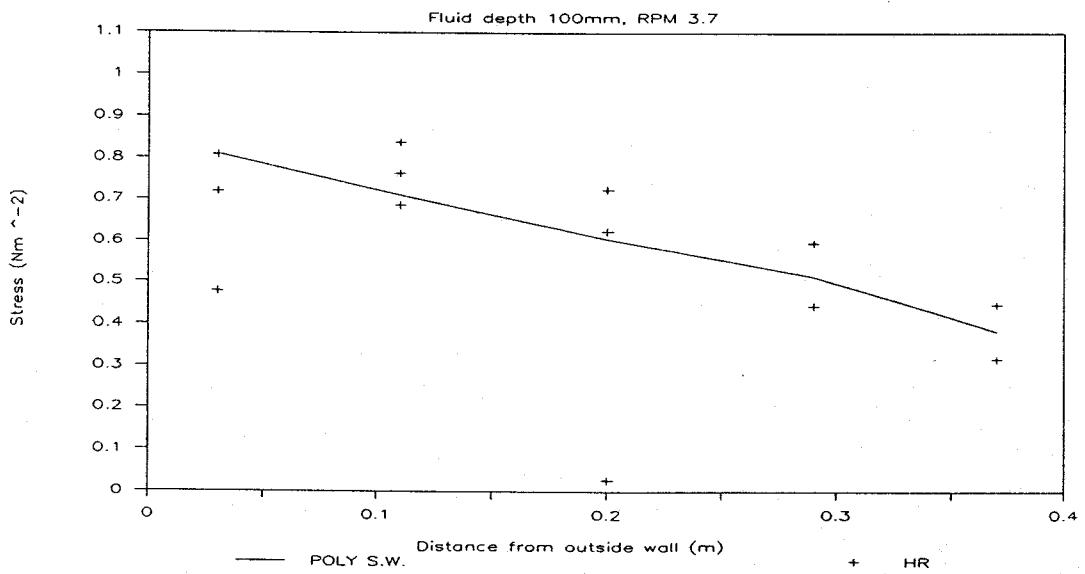
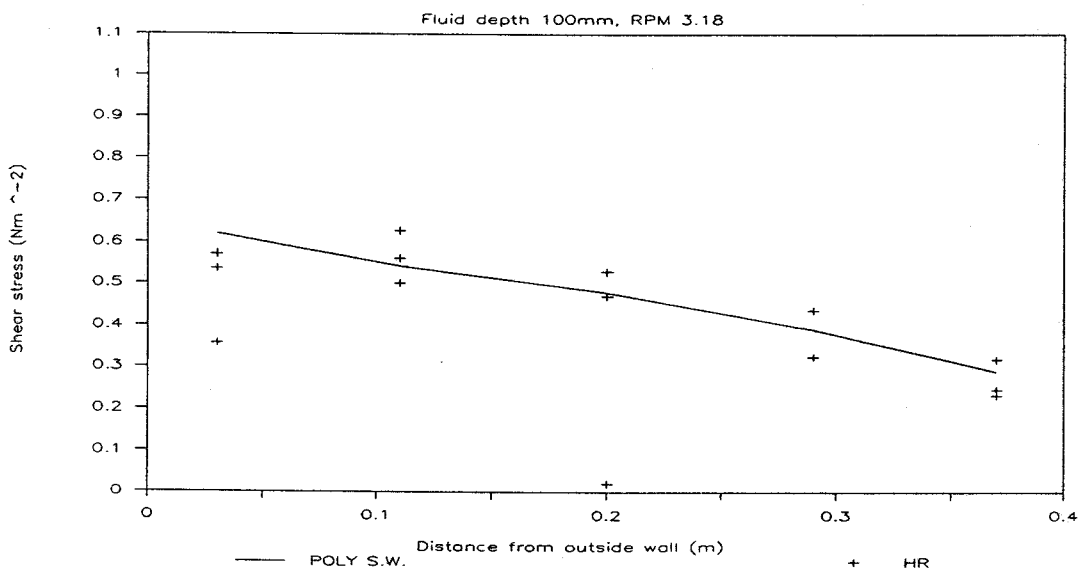
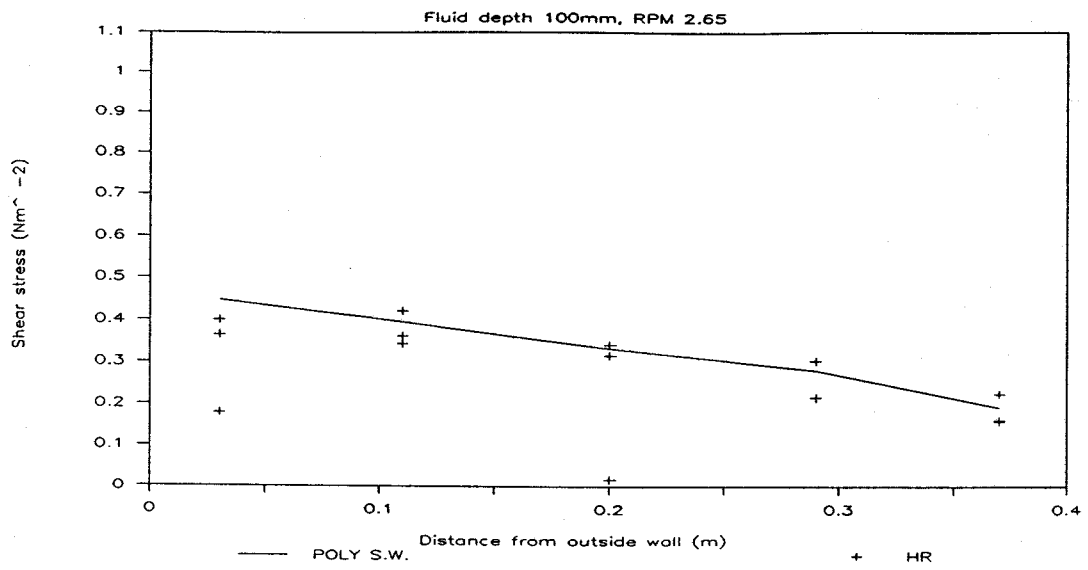


Fig 22 continued

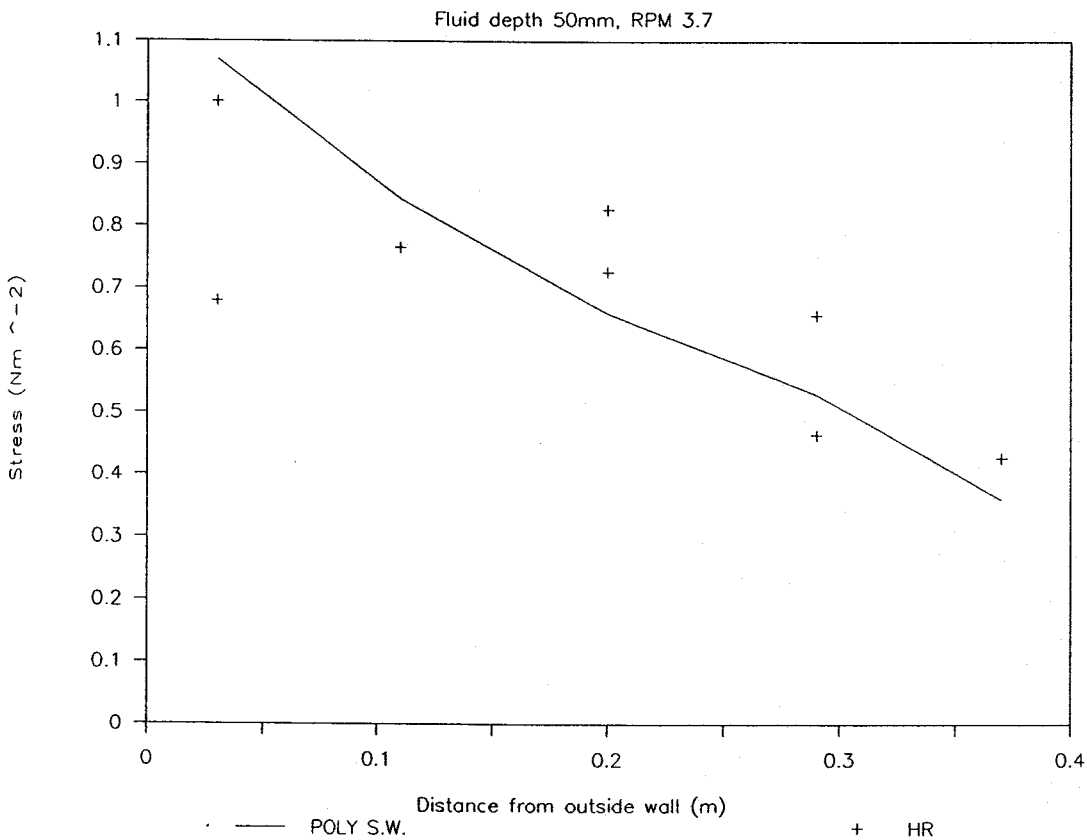
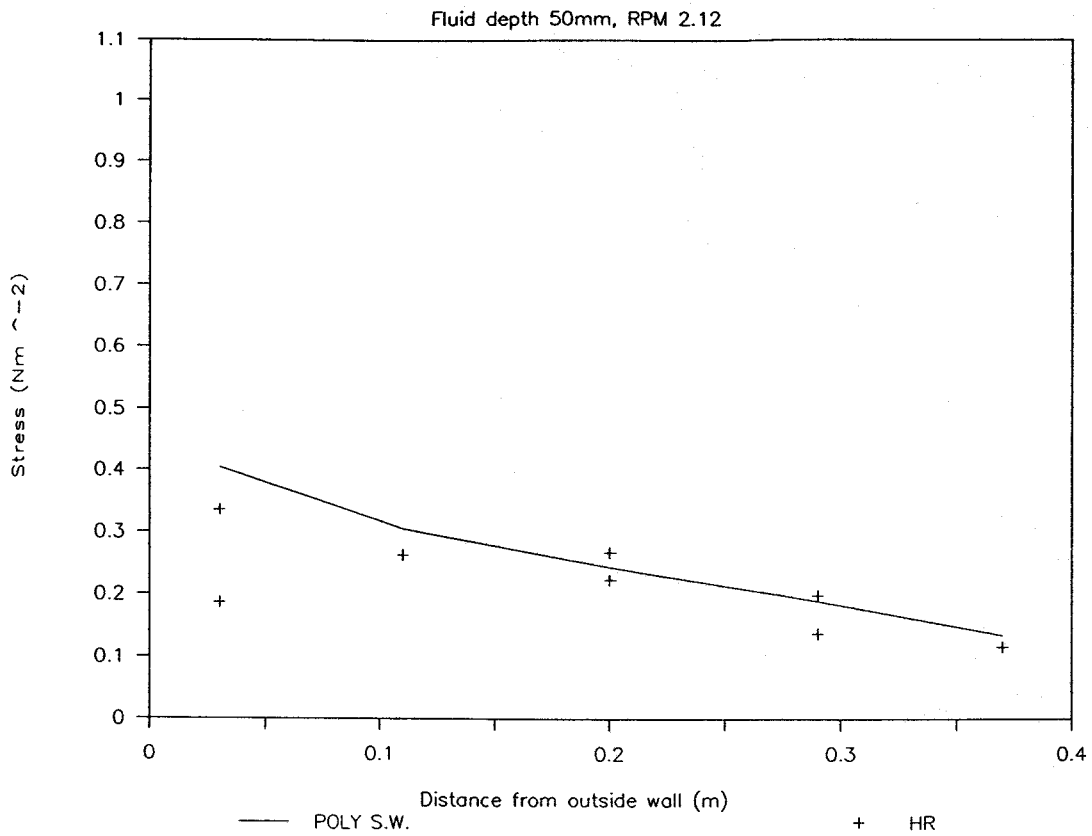


Fig 23 Two graphs comparing carousel bed shear stress data with PSW mathematical model results for a fluid depth of 0.05m.

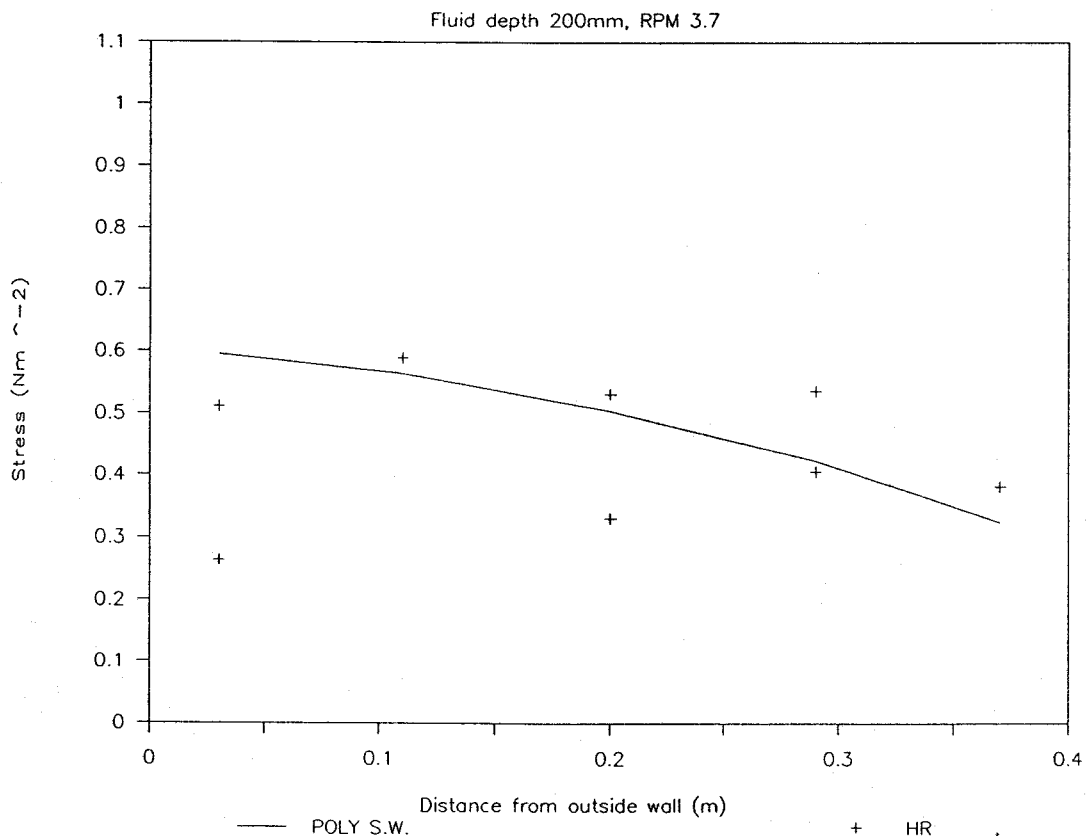
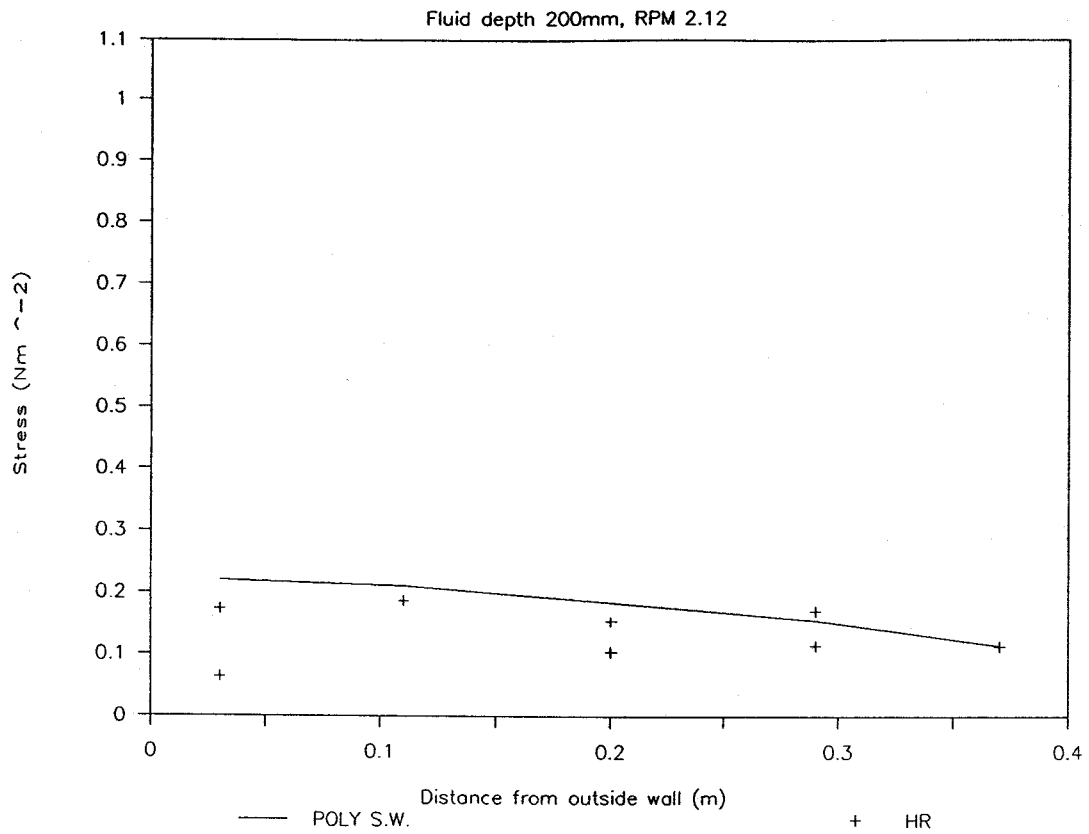


Fig 24 Two graphs comparing carousel bed shear stress data with PSW mathematical model results for a fluid depth of 0.2m.

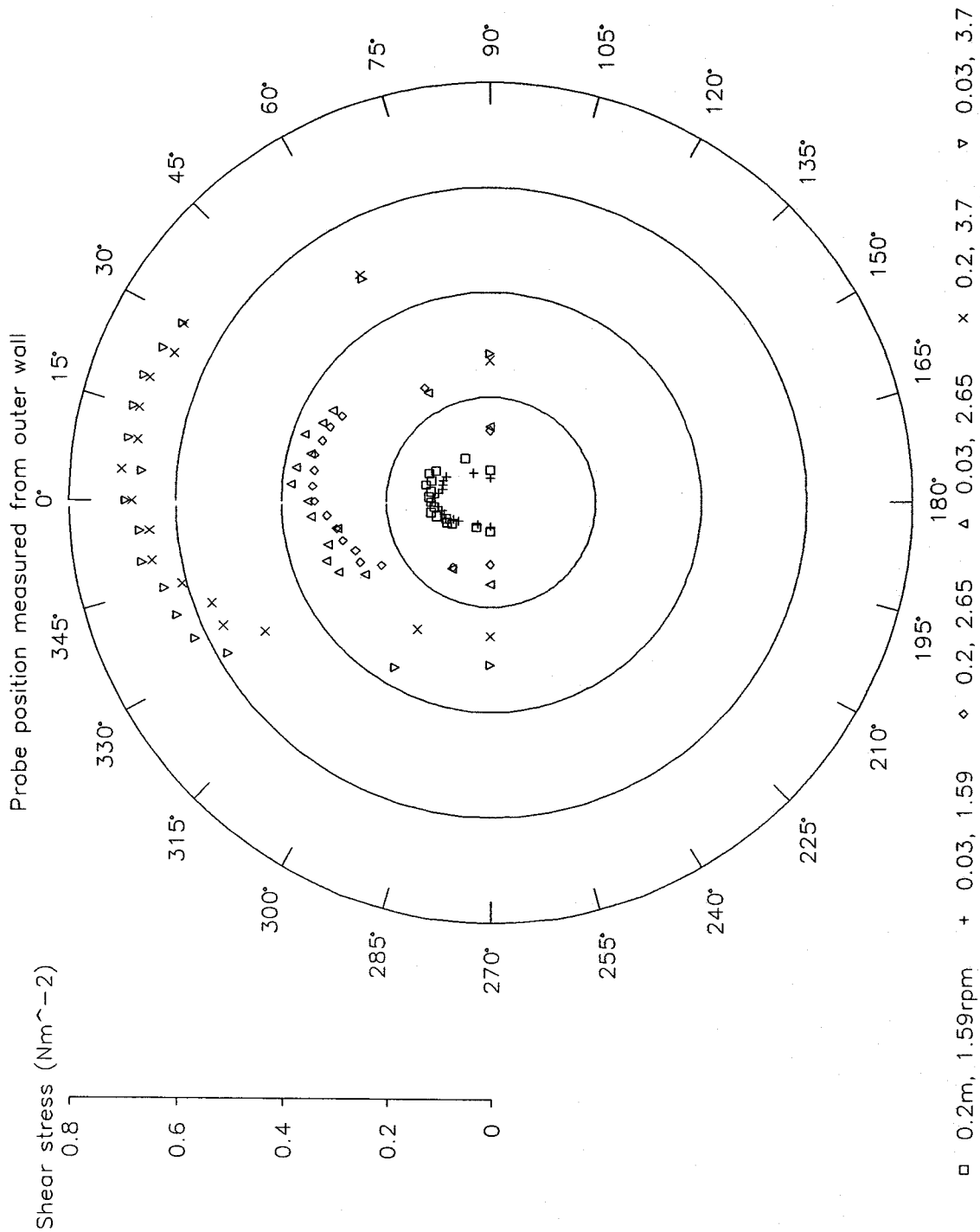


Fig 25 Composite plot showing the magnitude and direction of the bed shear stress. Probe positions and roof rotation rates are indicated

# Roof rotation rate 1.59rpm

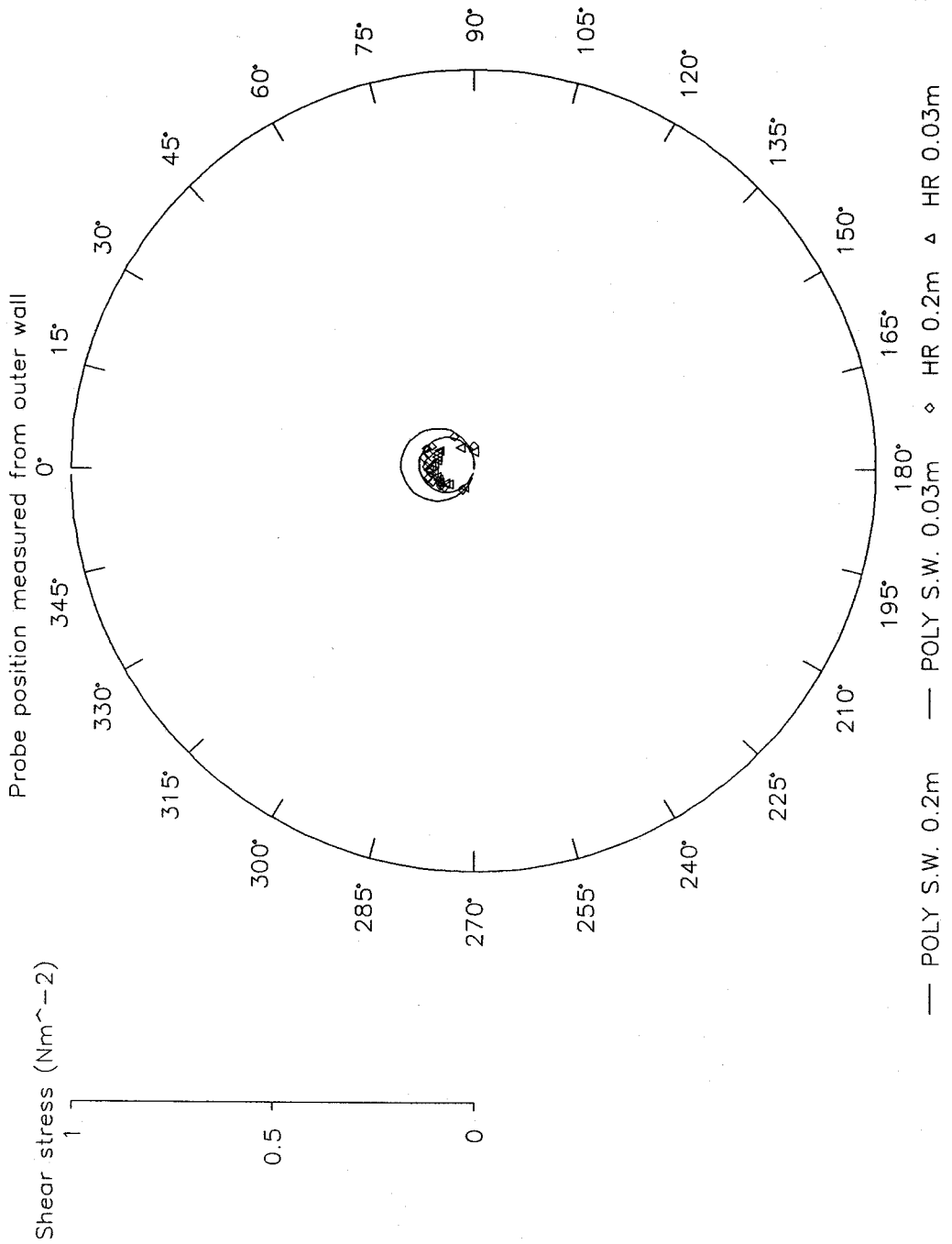


Fig 26a Composite plot comparing laboratory with predicted numerical data for the direction and magnitude of the bed shear stress

# Roof rotation rate 2.65rpm

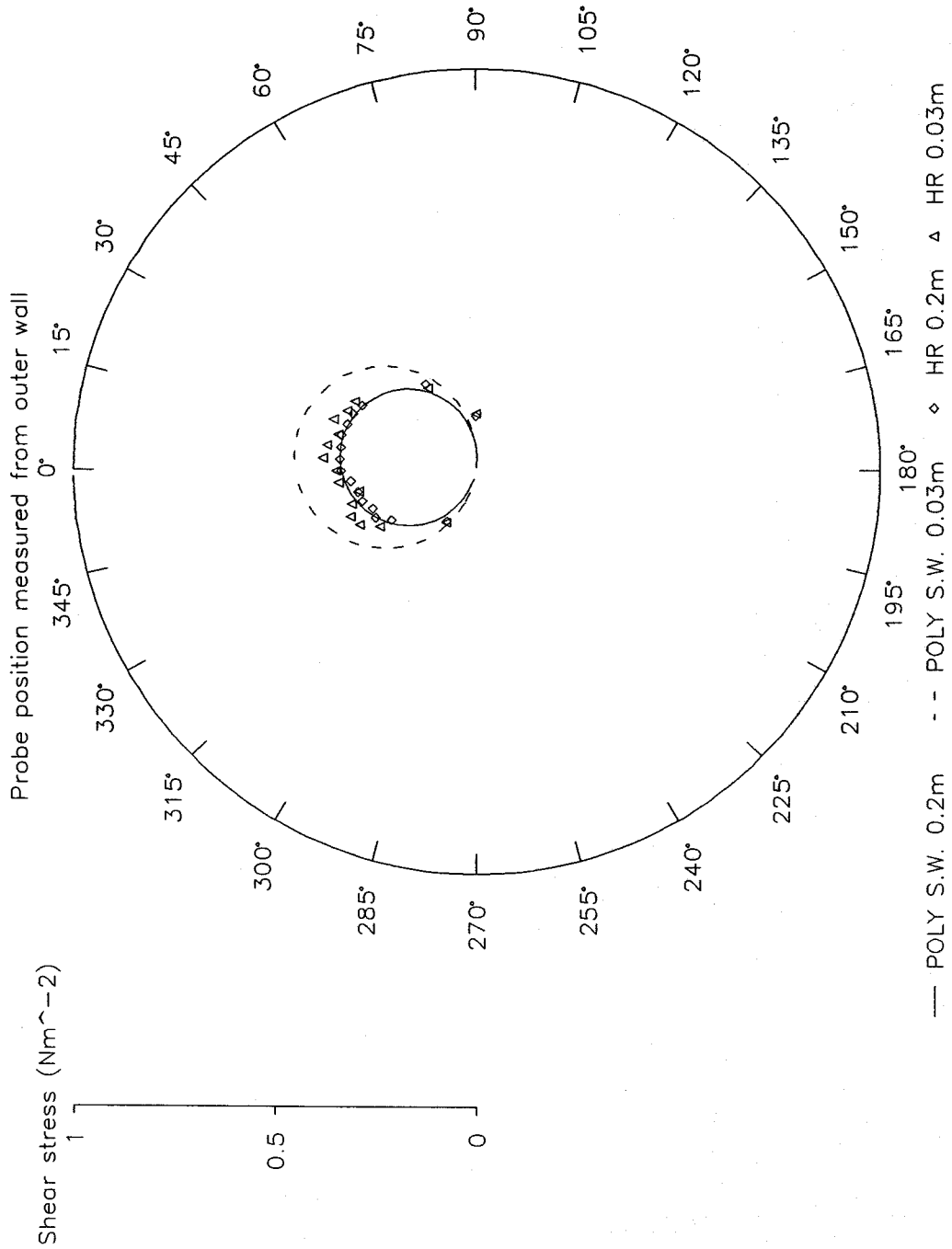


Fig 26b Composite plot comparing laboratory with predicted numerical data for the direction and magnitude of the bed shear stress

# Roof rotation rate 3.7rpm

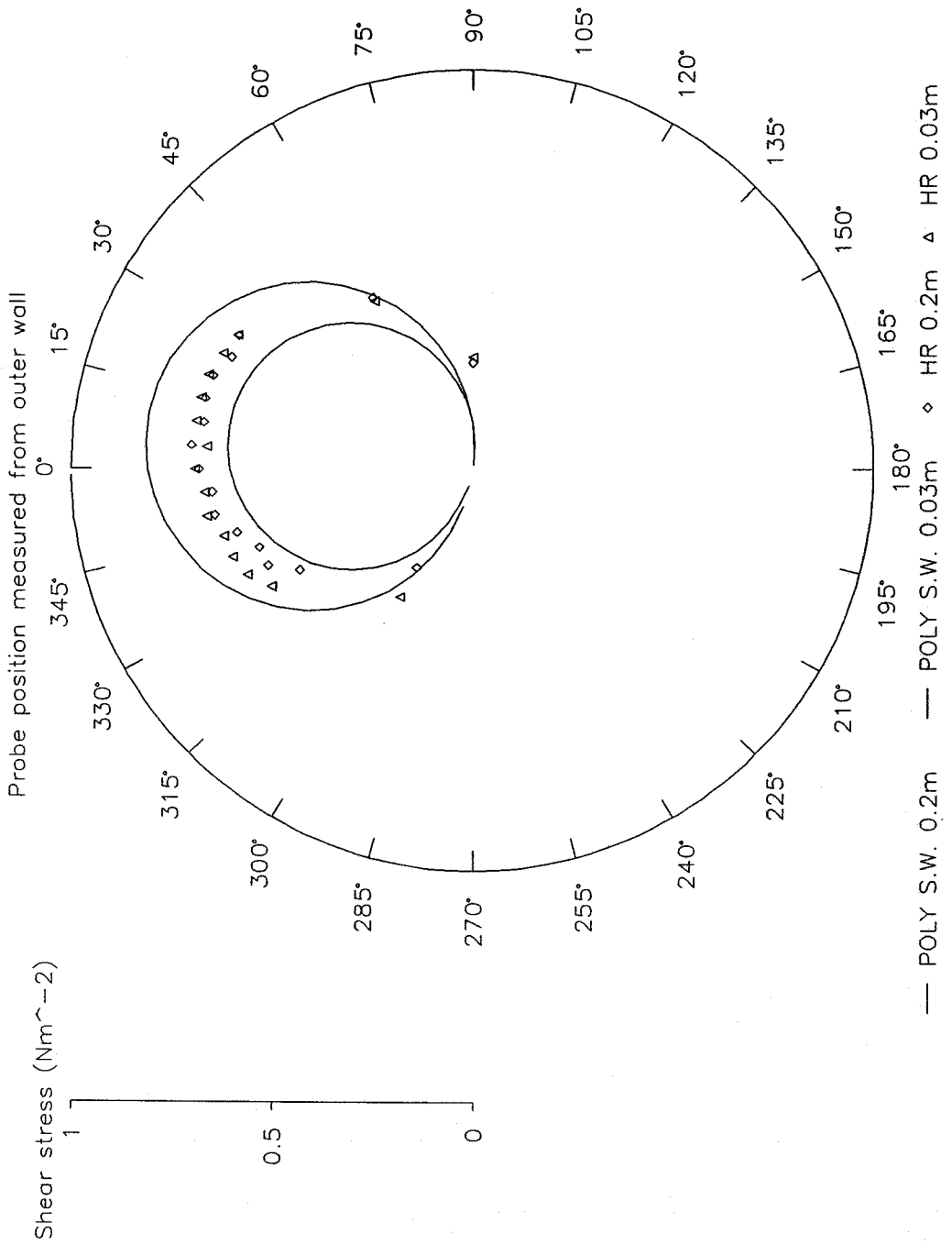


Fig 26c Composite plot comparing laboratory with predicted numerical data for the direction and magnitude of the bed shear stress.

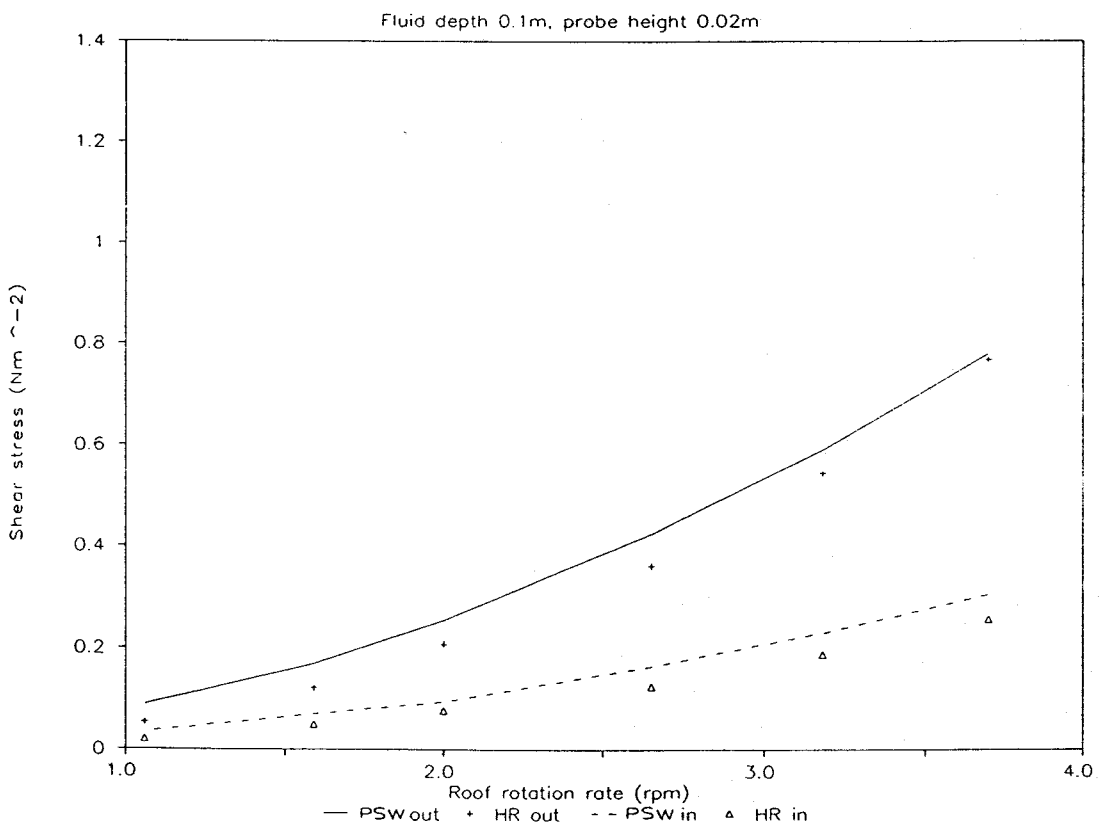
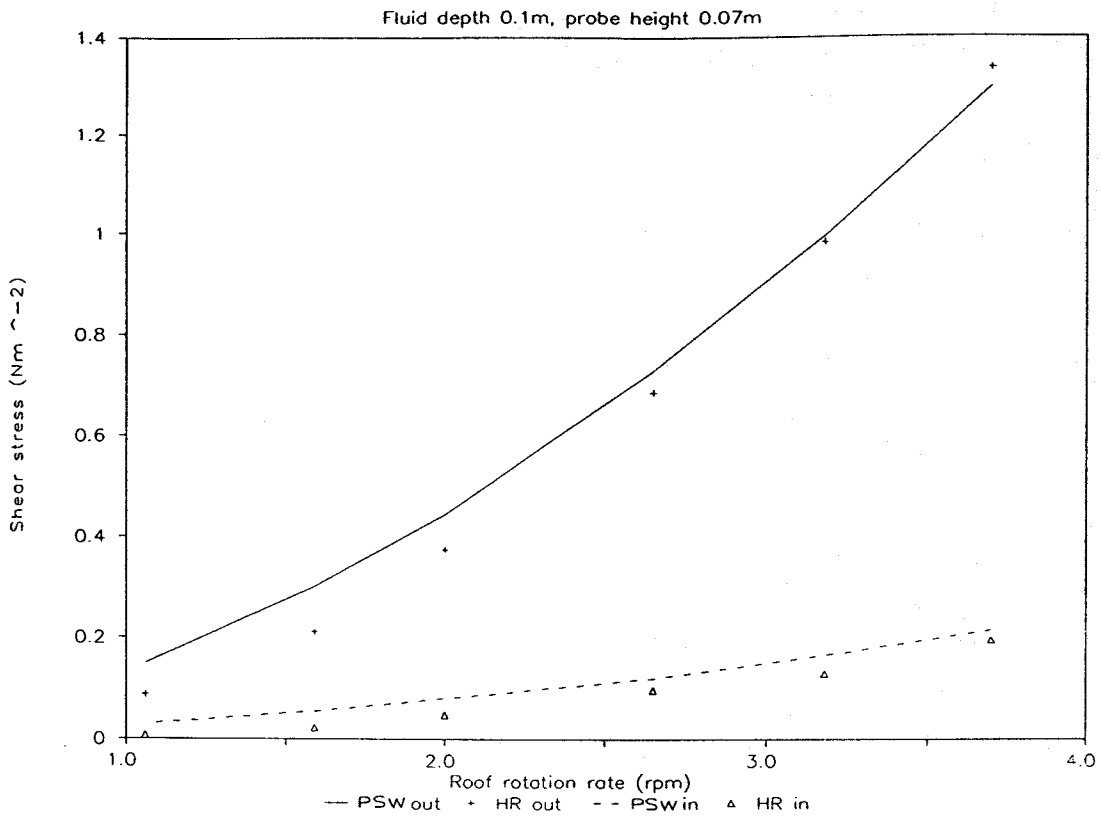


Fig 27 Graph comparing carousel side-wall shear stress with PSW mathematical model for 0.1m fluid depth and probe heights indicated.

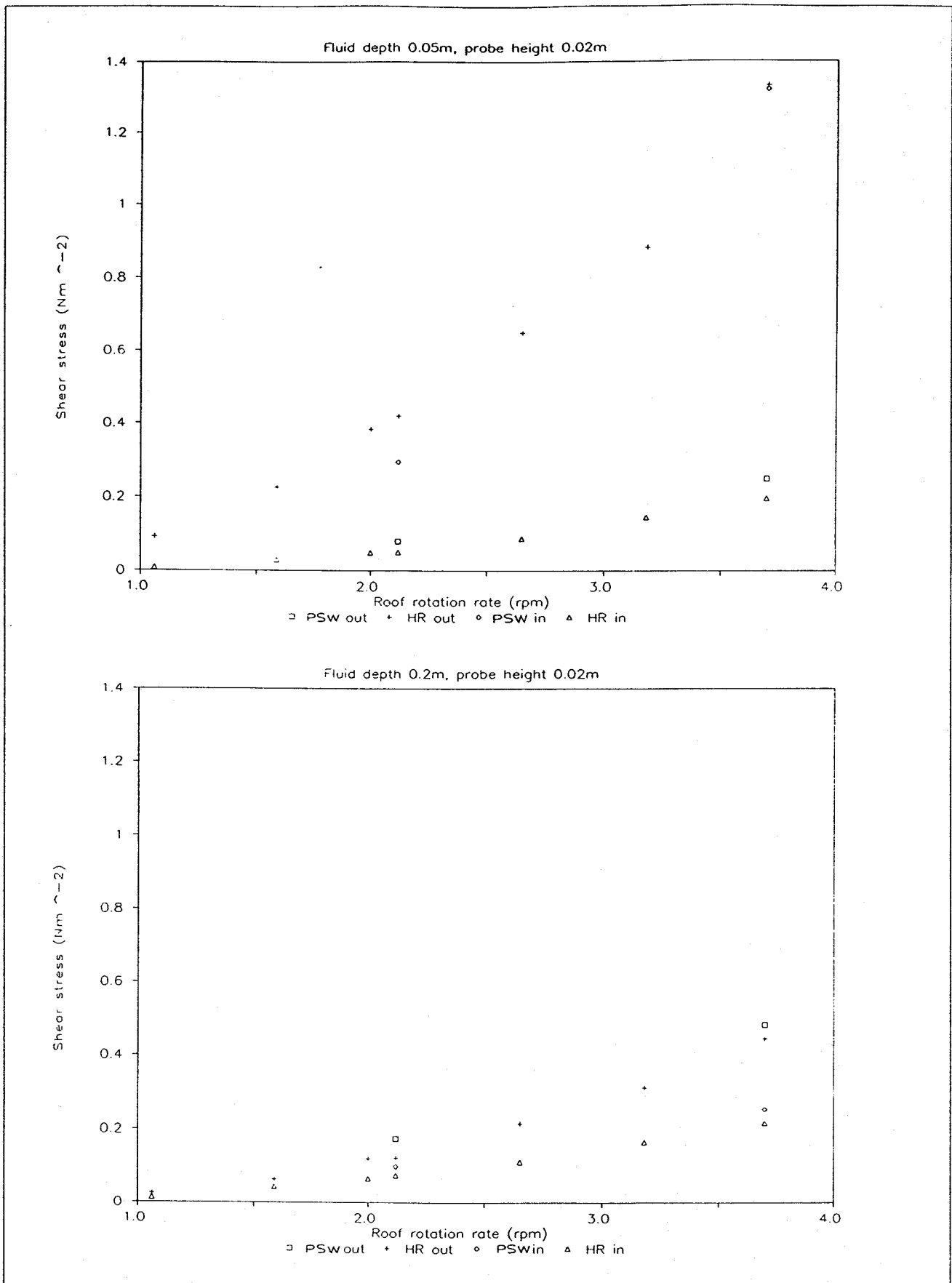
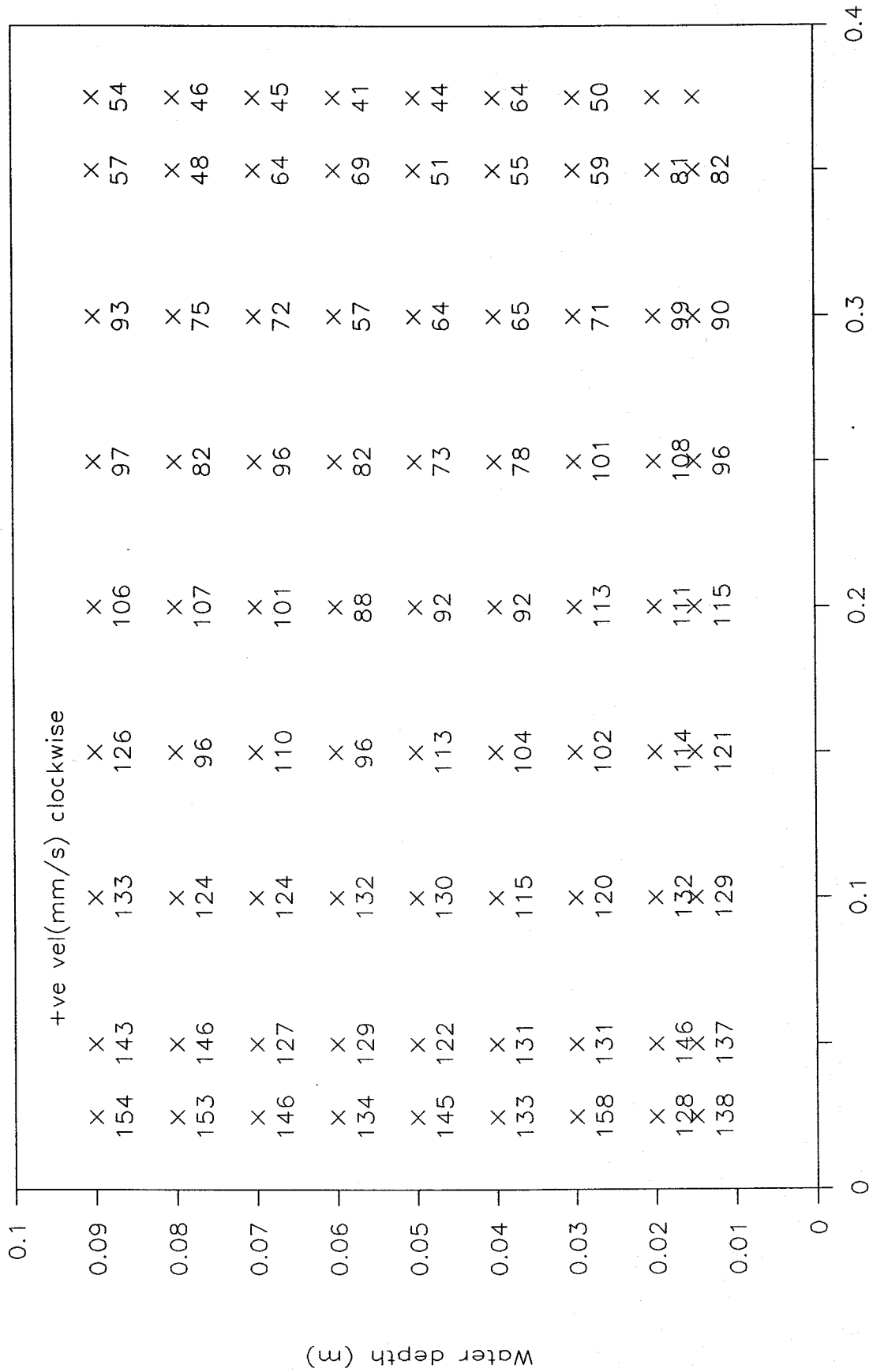


Fig 28 Graph comparing carousel side-wall shear stress with PSW mathematical model for 0.02m probe height and fluid depth indicated.

## ***Appendix***

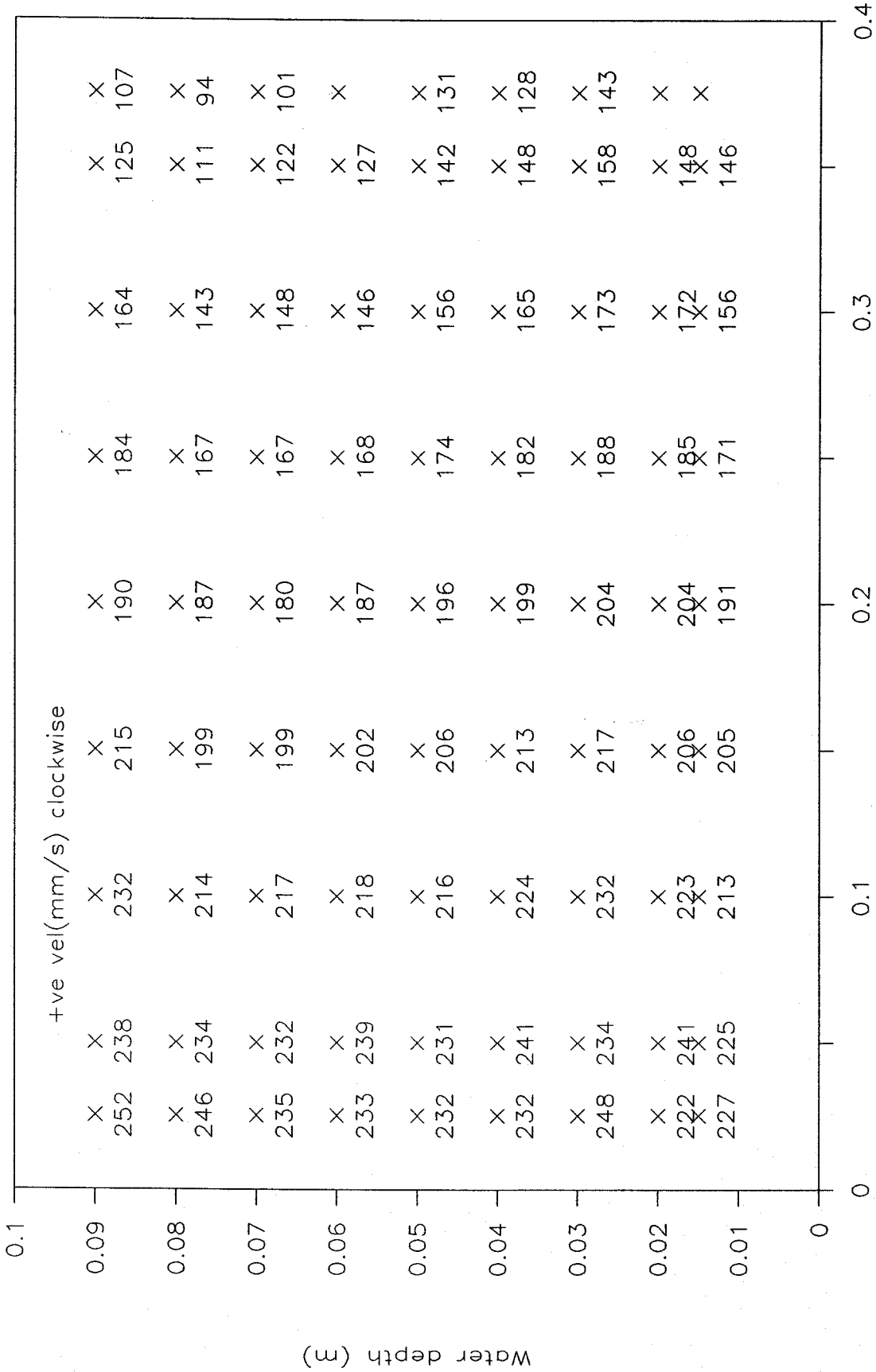


Horizontal velocities: 1 RPM



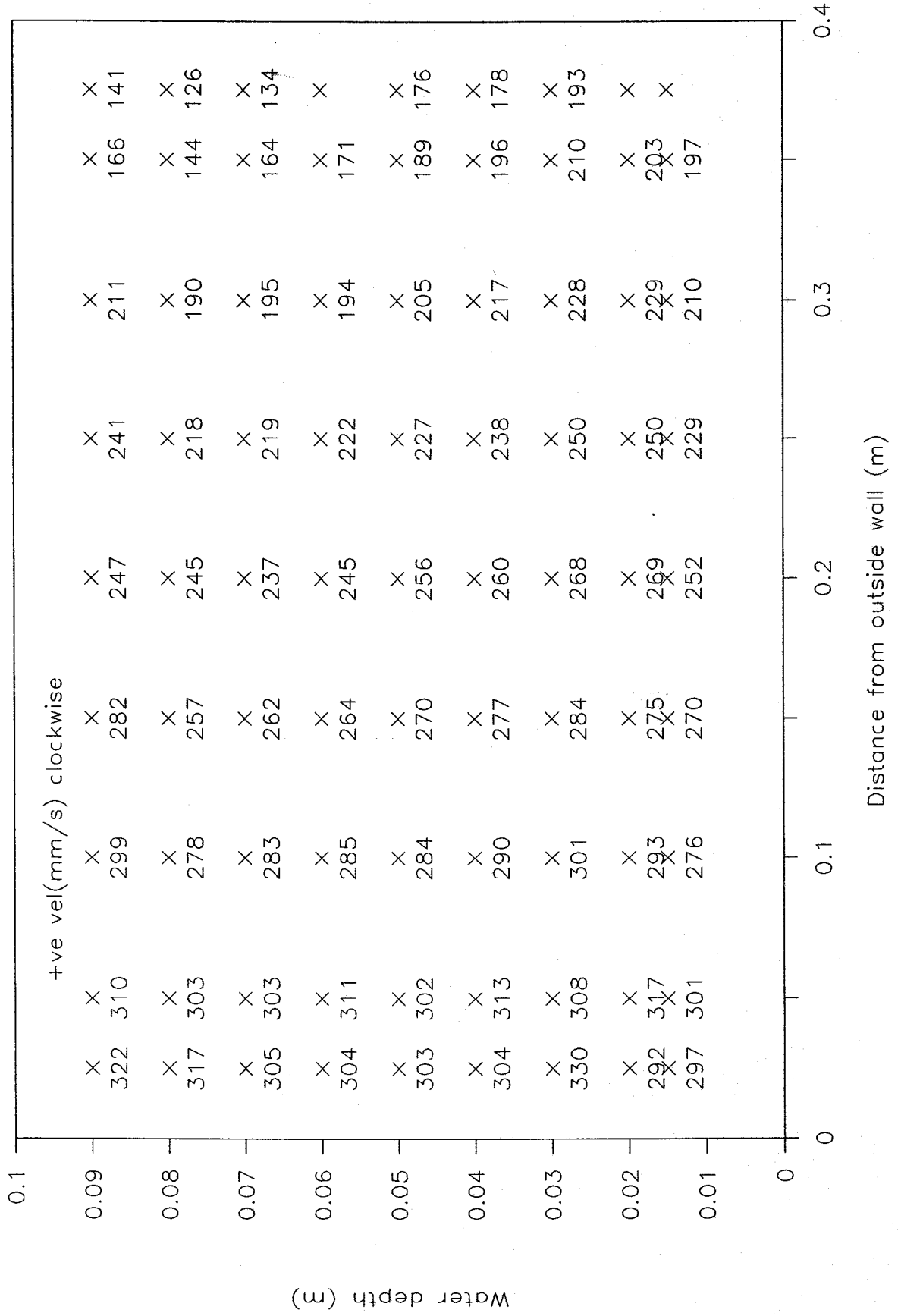
Distance from outside wall (m)

Horizontal velocities: 1.5 RPM

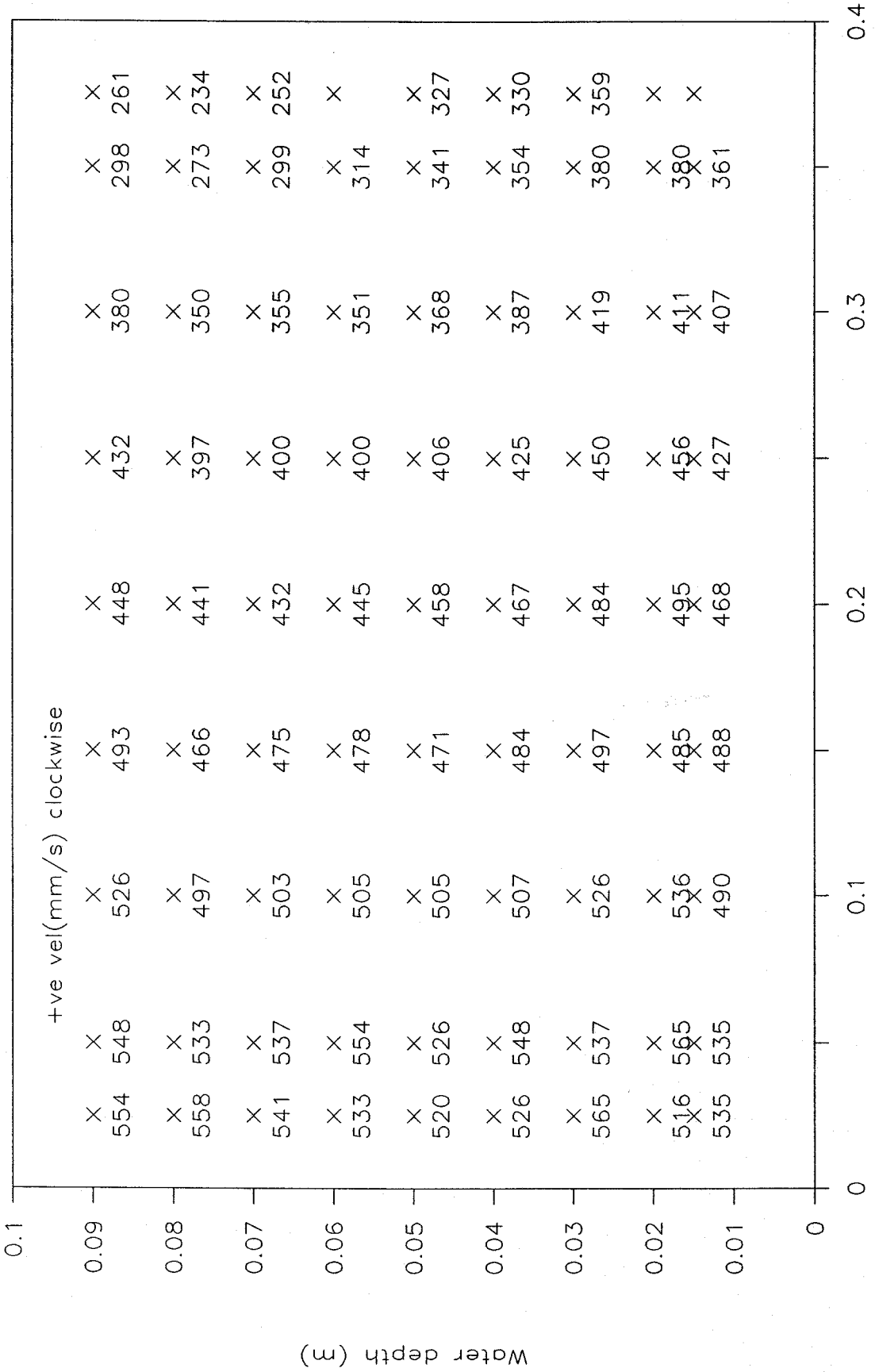


Distance from outside wall (m)

Horizontal velocities: 2 RPM

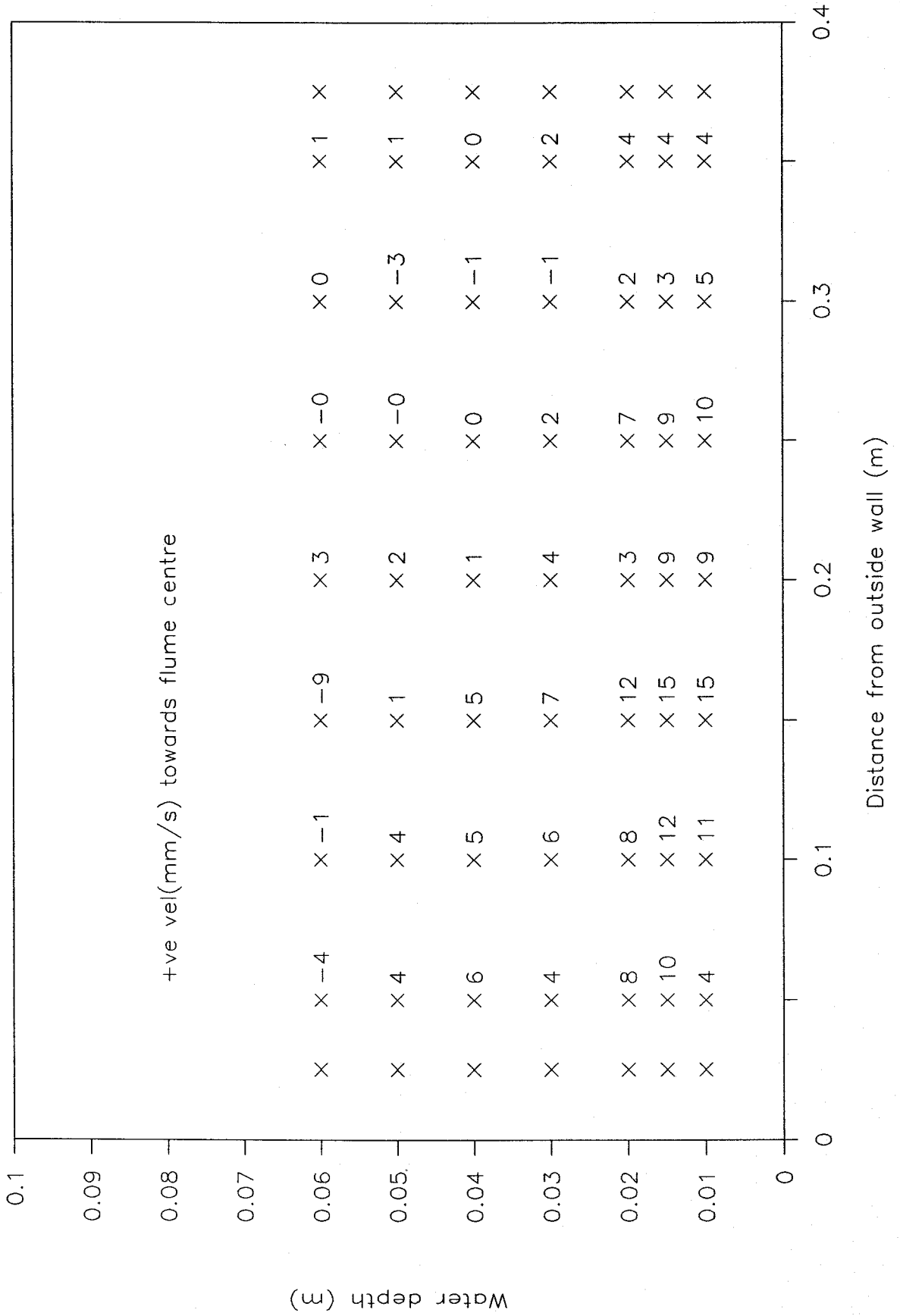


Horizontal velocities: 3.7 RPM



Distance from outside wall (m)

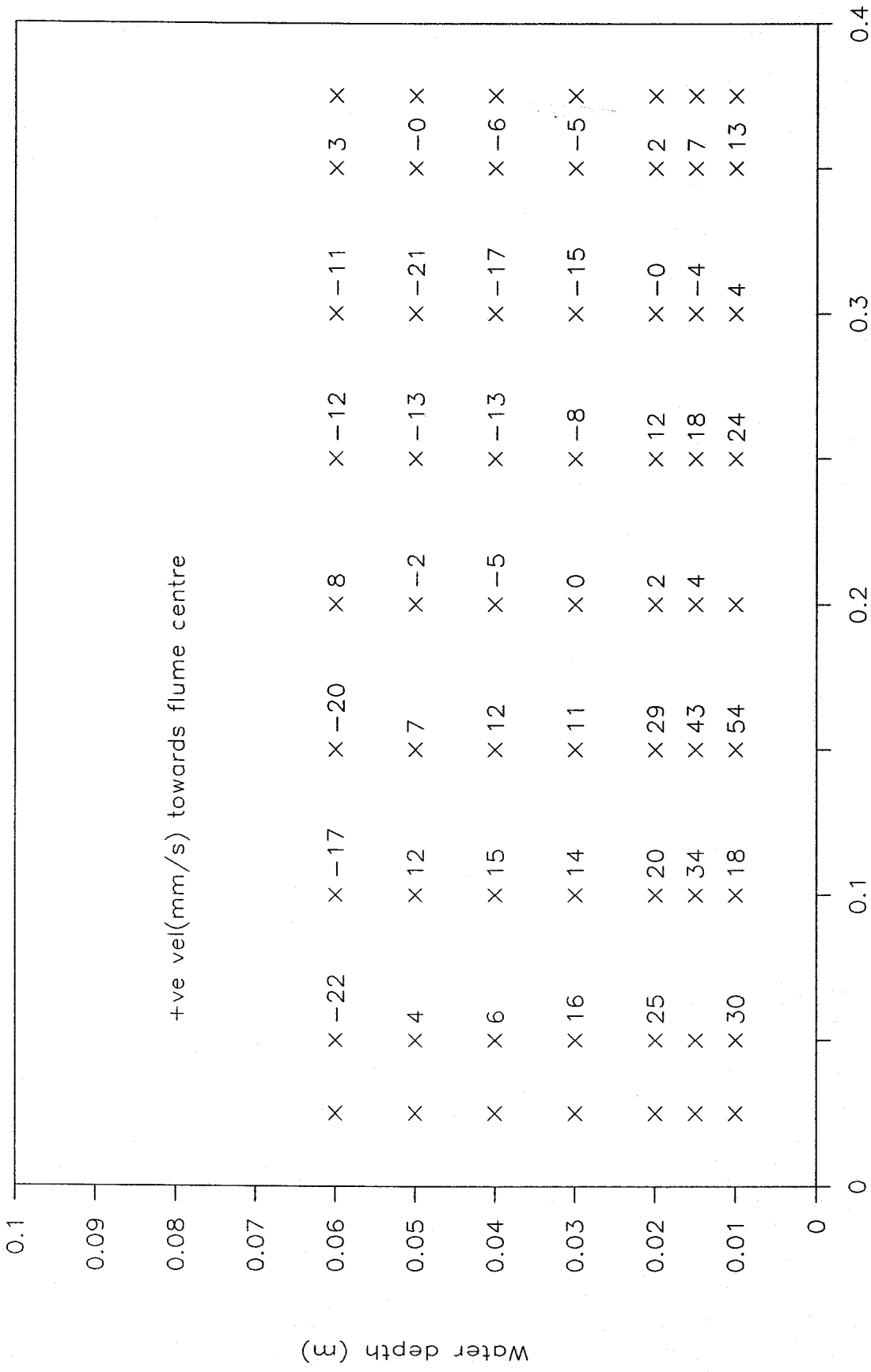
Radial velocities: 1 RPM





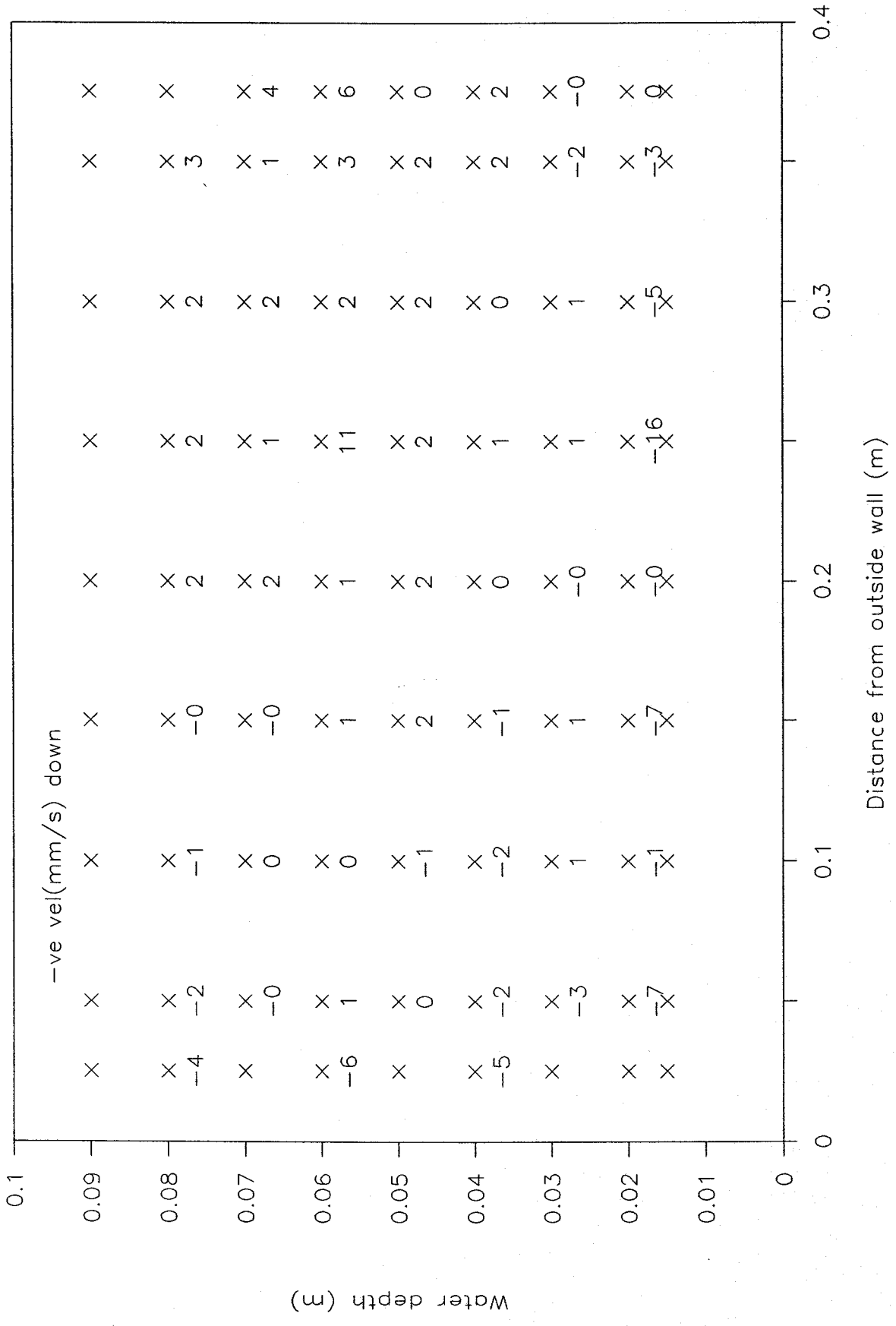


Radial velocities: 3.7 RPM

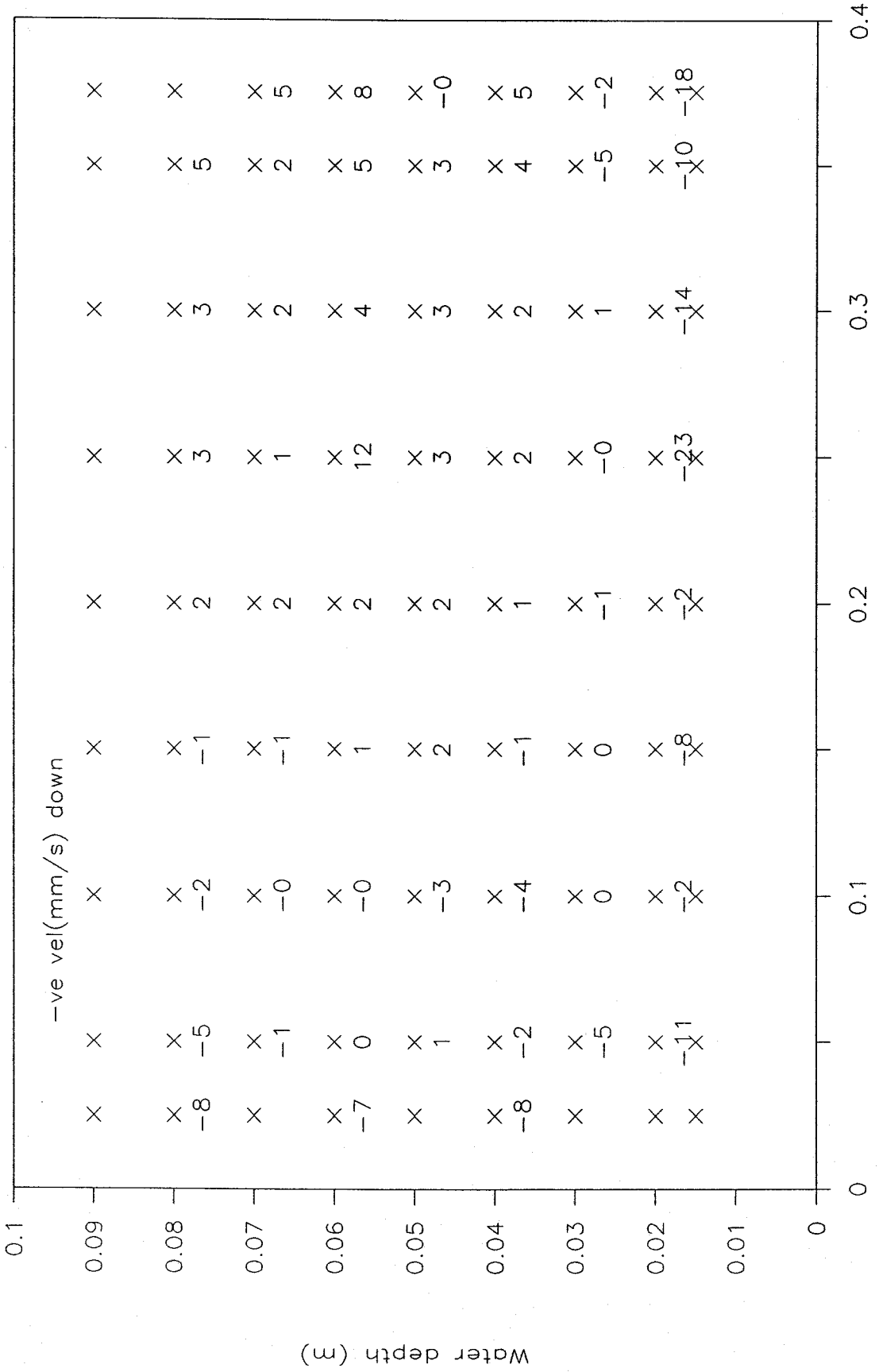


Distance from outside wall (m)

Vertical velocities : 1 RPM

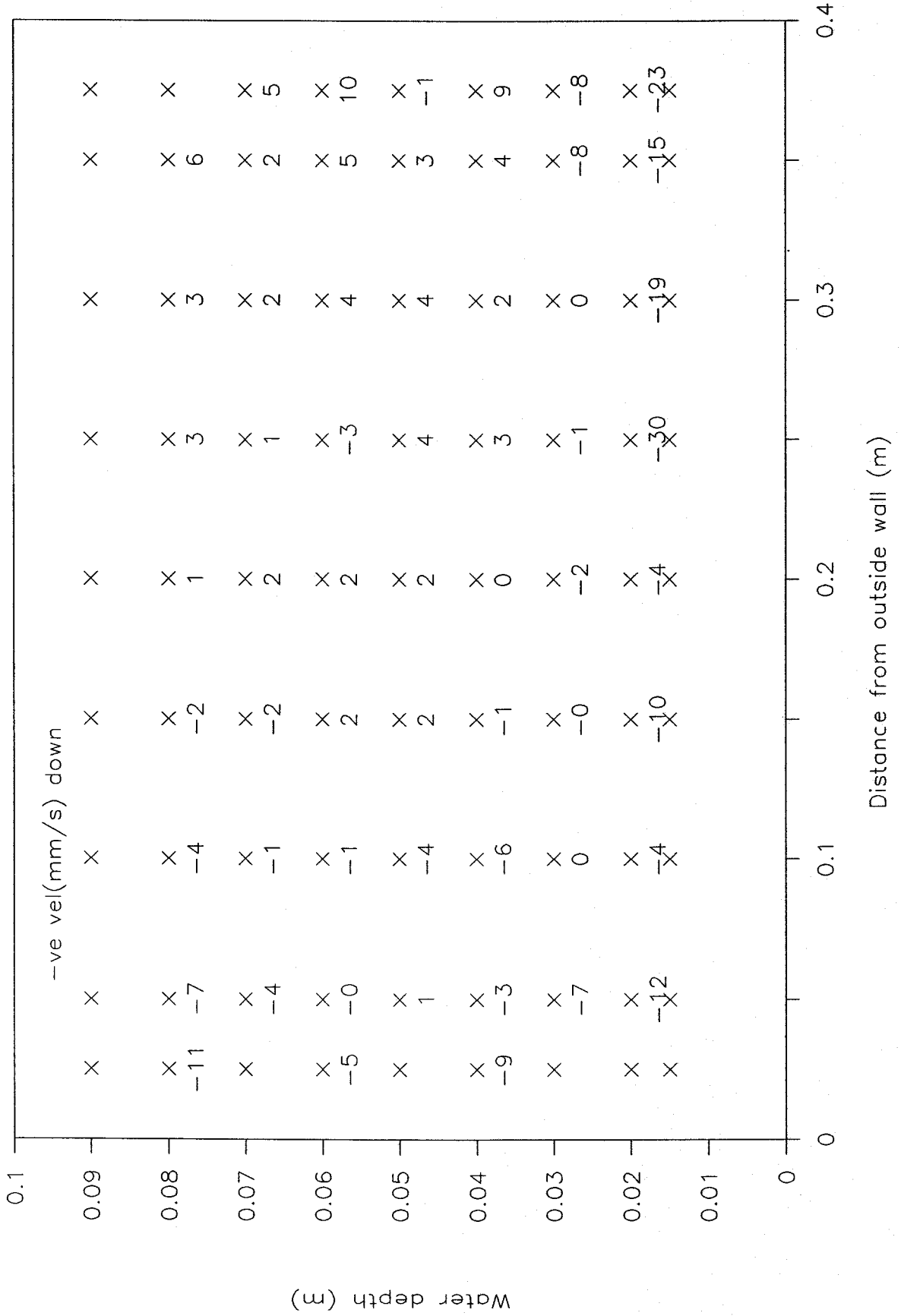


Vertical velocities : 1.5 RPM

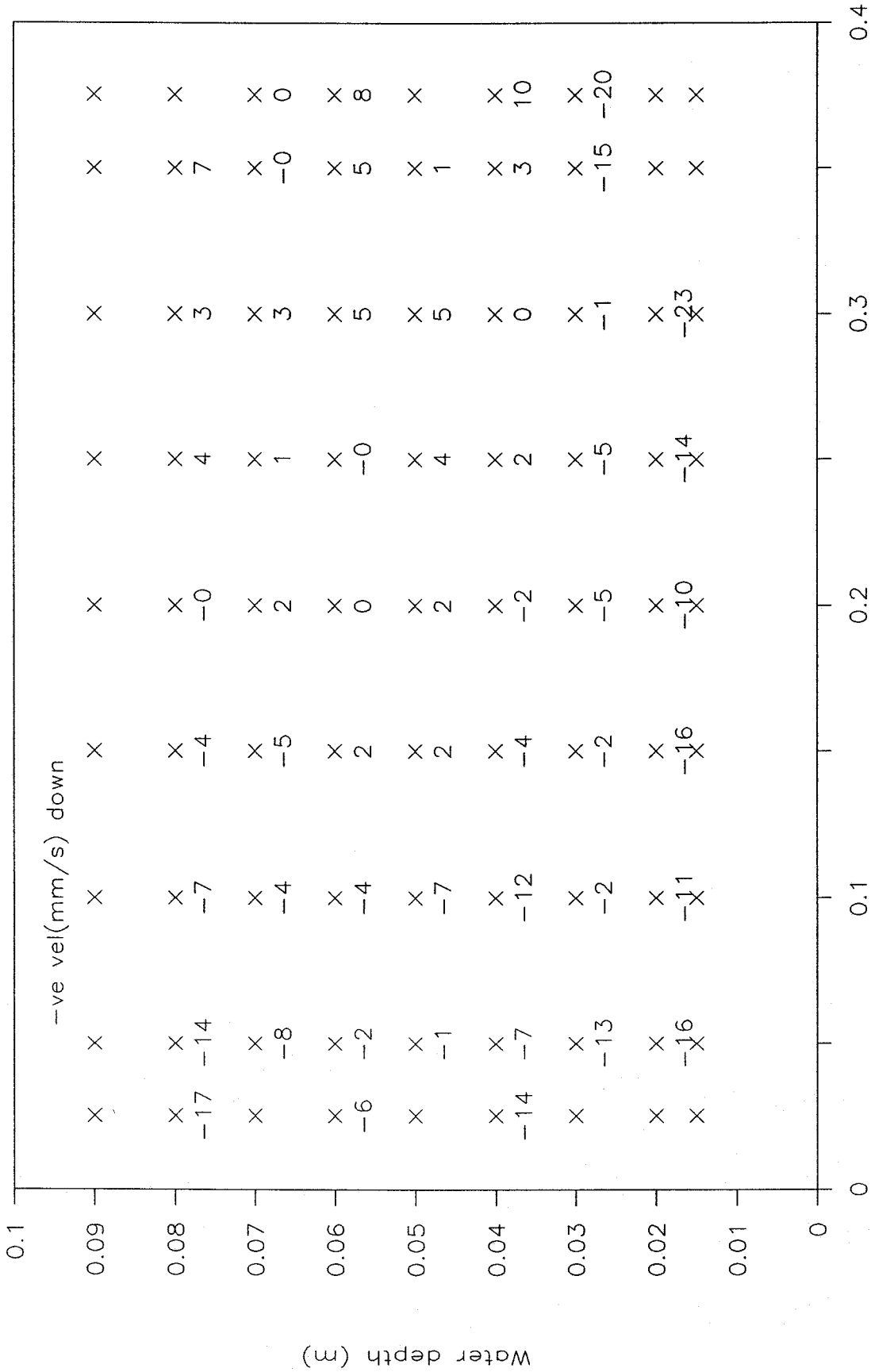


Distance from outside wall (m)

Vertical velocities :2 RPM

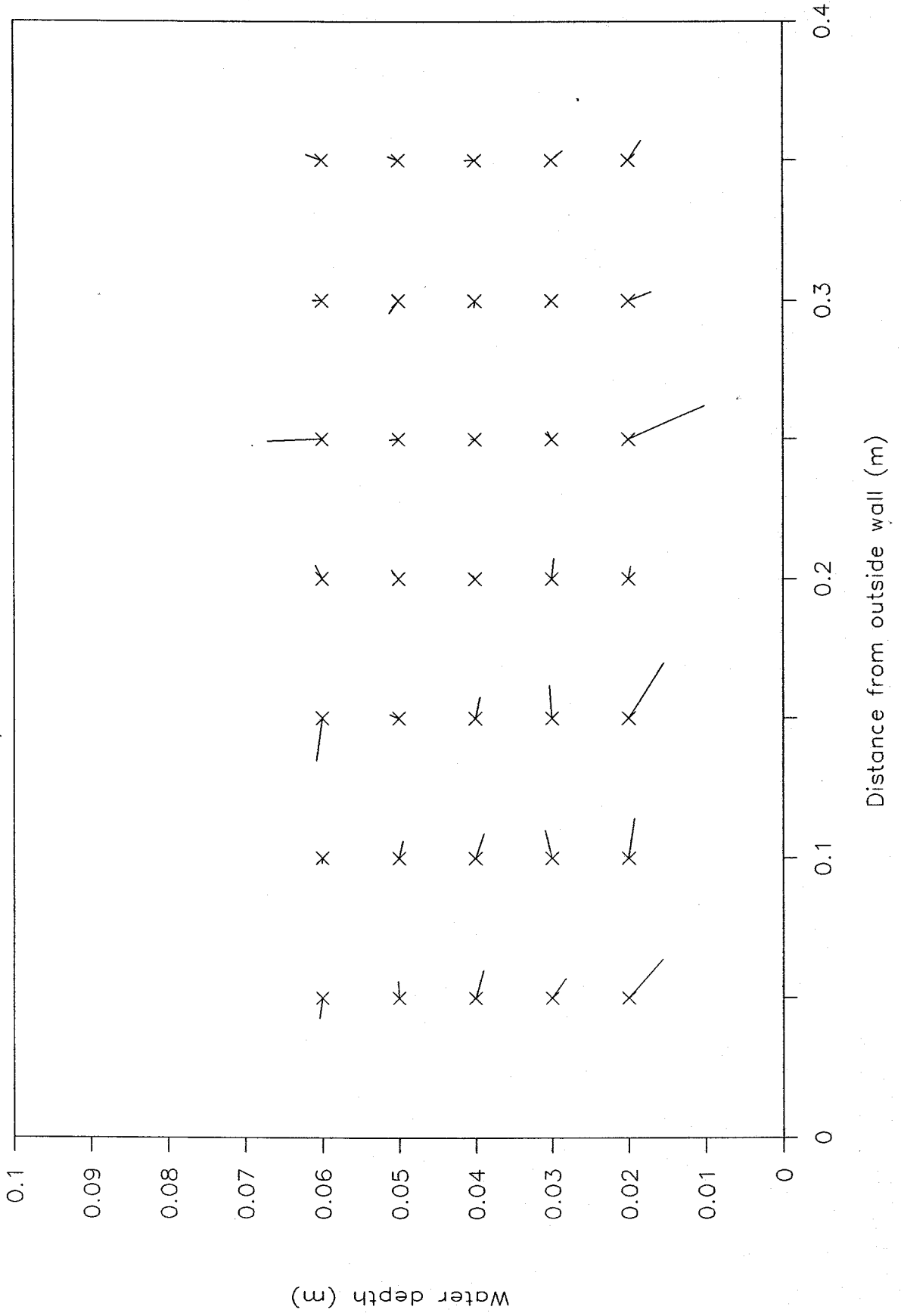


Vertical velocities :3.7 RPM

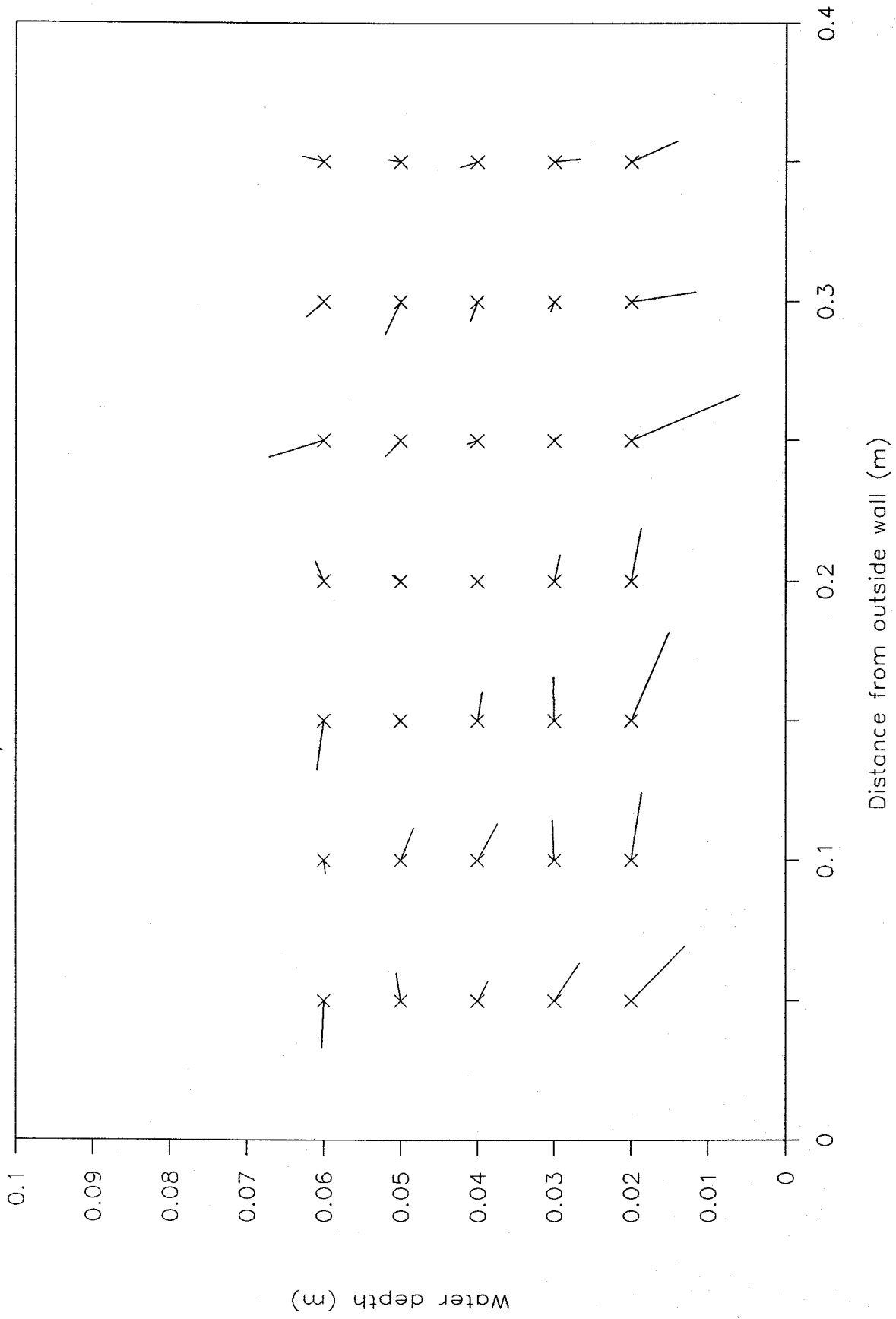


Distance from outside wall (m)

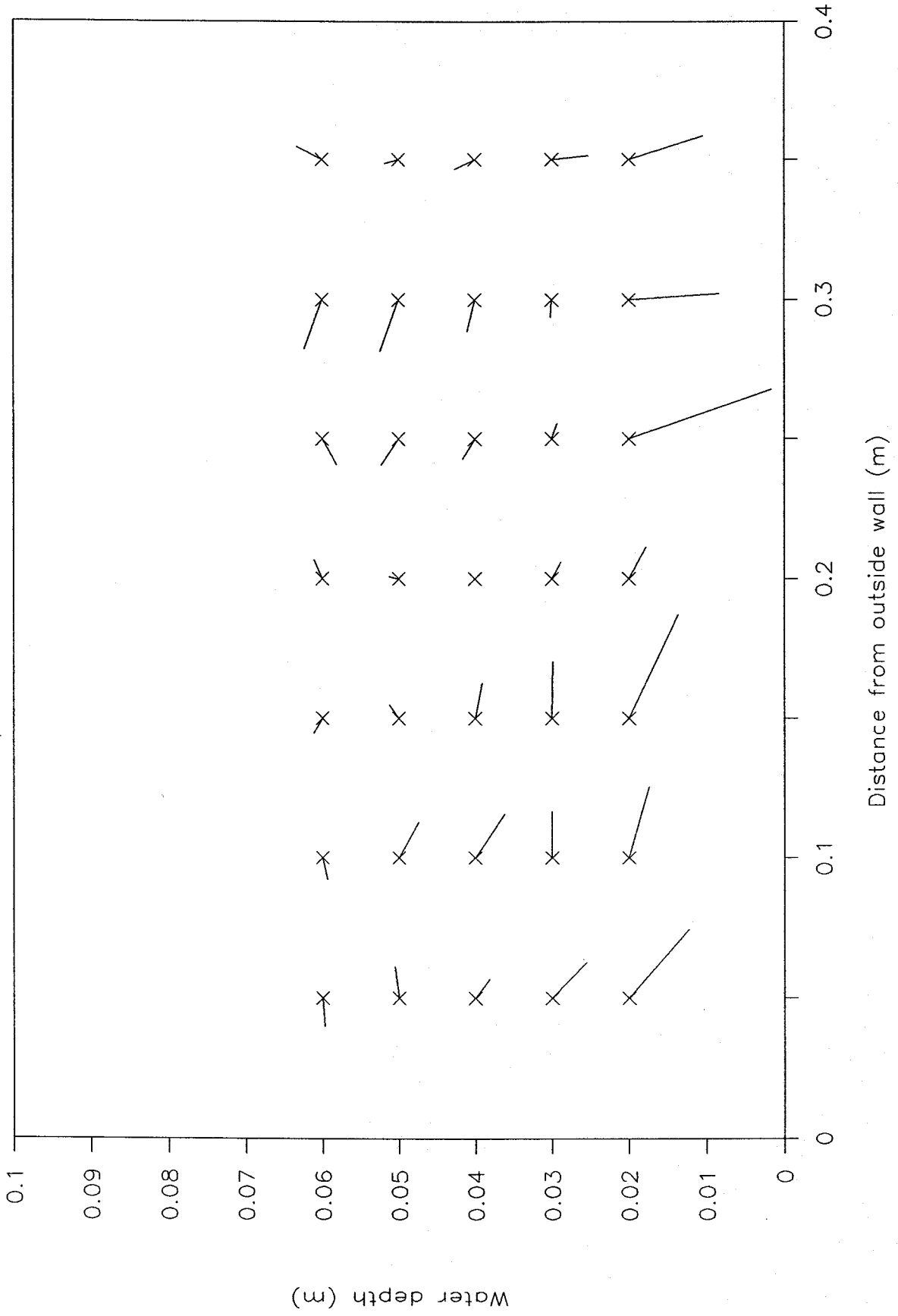
Radial/Vertical vectors : 1 RPM



Radial/Vertical vectors : 1.5 RPM



Radial/Vertical vectors : 2 RPM



Radial/Vertical vectors : 3.7 RPM

